The Effect of Cosmic Web Filaments on Quenching in Galaxy Clusters

THE EFFECT OF COSMIC WEB FILAMENTS ON QUENCHING IN GALAXY CLUSTERS

By Sachin KOTECHA, BMath

A Thesis Submitted to the School of Graduate Studies in the Partial Fulfillment of the Requirements for the Degree Master of Science

McMaster University

Master of Science (2020)

Hamilton, Ontario (Department of Physics and Astronomy)

TITLE: The Effect of Cosmic Web Filaments on Quenching in Galaxy Clusters

AUTHOR: Sachin KOTECHA, BMath (University of Waterloo)

SUPERVISORS: Dr. James WADSLEY and Dr. Charlotte WELKER

NUMBER OF PAGES: x, 109

Abstract

Environment plays an important role in the evolution of galaxies. In particular, denser environments, such as galaxy clusters and large-scale field filaments of the cosmic web have been found to reduce star formation in galaxies. The intersection of these environments provides an interesting regime of study. We investigate how cosmic filaments impact the quenching of galaxies within one virial radius of 324 simulated clusters. We use hydrodynamic runs from The Three Hundred Project along with the cosmic web extractor DisPerSE to track filaments and the structure finder VELOCIraptor to identify halos hosting galaxies. Limited by the resolution of the simulation, we examine star formation indirectly by way of galaxy colour and cold gas fraction. We find that cluster galaxies residing closer to filaments tend to be star-forming, bluer, and contain more cold gas than their counterparts further away from filaments. This is in stark contrast with galaxies residing outside of clusters, where galaxies close to filaments show clear signs of density related pre-processing. Careful examination of flows around and into cluster galaxies strongly suggests that the colder, dynamically coherent hydrodynamic streams along intra-cluster filaments partially shield galaxies close to them from strangulation by the hot, dense intra-cluster medium. These streams, in addition to the reduced density contrast of intra-cluster filaments with the intra-cluster medium, also limit the ram pressure stripping experienced by cluster galaxies. We further examine stripping in the context of gas disturbances in phase space to create a classification for wet and dry galaxies.

Acknowledgements

Just as with Tom Riddle's Horcruxes, the acknowledgements for this thesis are seven in number. **First**, to my parents. Thank you for raising me in the best way you knew how, for instilling in me the morals and values with which I live my life. Although you no longer have any idea what it is I'm studying, you're always there for me. **Second**, to Mrs. White, my Grade 6 teacher. You are *that* educator to me. From spearheading the enrichment of my education, to forcing me to stop being such a tattle-tale, you changed my life for the better. **Third**, to Pri. You've been a great friend and support system during most of my time at Mac. Thank you for listening to my problems, and of course, for driving me to the ER at 5am. **Fourth**, to my HSA family, especially Divya and Roshni. Being involved with HSA and getting to know you all is easily one of the highlights of my time at Mac, and was the best possible extracurricular. Thank you for letting me be a part of the team. **Fifth**, to any student I've ever TAed and every audience member at one of my planetarium shows. Education and outreach are my passions, so thank you for indulging me. **Sixth**, as per tradition passed down through the ages, I must thank the academics in my life. Thank you James for directing me towards this project when all I knew coming in was that I liked astrophysics, and for the constant supply of cookies. Thank you Charlotte for the human touch throughout this work, you have been a wonderful mentor and a great source of encouragement. As for the **seventh**, unintended split, I hope anyone who has made the mistake of looking at this work finds that a piece of the knowledge within attaches itself to them. Thank you for reading. ⚡

Contents

List of Figures

viii

List of Acronyms

AGN active galactic nucleus

BCGs brightest cluster galaxies

CMB cosmic microwave background

ICM intra-cluster medium

ISM interstellar medium

RPS ram pressure stripping

SDSS Sloan Digital Sky Survey

SFR star formation rate

SPH smoothed particle hydrodynamics

sSFR specific star formation rate

UV ultraviolet

Declaration of Authorship

This thesis contains one article in preparation for submission to the *Monthly Notices of the Royal Astronomical Society* presented in Chapter 2, as well as other original research presented in Chapters 3 and 4.

The article presented in Chapter 2 was written by myself, Sachin Kotecha, with Charlotte Welker as second author. I, Sachin Kotecha, conducted all data analysis and created all plots for this Chapter, with the exception of data production and analysis related to galaxy colours conducted by Zihan Zhou, and illustrative diagrams created by Charlotte Welker. James Wadsley provided scientific guidance. Pascal Elahi provided the halo catalogues. Gustavo Yepes ran the simulations.

The original research in Chapters 3 and 4 was conducted and written up by myself, Sachin Kotecha.

Chapter 1

Introduction

1.1 The Cosmic Web

Beautiful structure pervades the cosmos. These structures we see on the largest scales of the Universe today were seeded from the smallest scales shortly after the Big Bang. Around 10^{-36} seconds into its birth, the Universe underwent a rapid expansion period, known as the epoch of inflation (Guth 1981), whereby primordial quantum fluctuations resulted in tiny density perturbations in an otherwise homogeneous field post-inflation. Evidence of early Universe density perturbations are imprinted on the cosmic microwave background (CMB) as temperature fluctuations (COBE (Smoot et al. 1992), WMAP (Bennett et al. 2003), Planck (Ade et al. 2014)). Figure 1.1 shows these temperature fluctuations in the CMB, imaged by Planck in 2013. At the time of photon decoupling, around 370000 years after the Big Bang, those photons in overdense regions spend more of their energy budget moving out of this region and hence are colder than the average photon, and those in underdense regions spend less than average, appearing slightly warmer. Over the following 13.7 billion years, these small perturbations grew to form the structures we see today in part thanks to gravitational collapse (e.g. Peebles 1980).

Gravity drives the large-scale flows of material in the Universe: the overdense peaks in
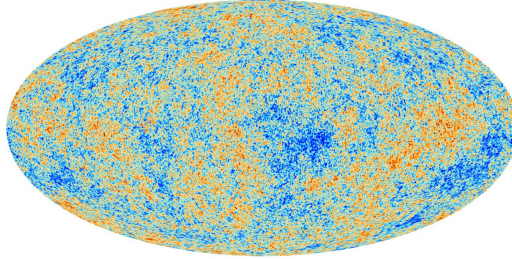
FIGURE 1.1: Temperature fluctuations imprinted on the CMB, from Planck in 2013. The deepest red correspond to $300\mu K$ above the average and the deepest blue to $300\mu K$ below the average. These temperature fluctuations correspond to the early Universe density fluctuations that seeded structure. (Credit: ESA, Planck Collaboration)

the early Universe collapse, drawing in matter from their surroundings, while underdense valleys see matter flow out. The increasingly dense structures are called filaments and walls, while the emptying regions are called voids. The densest gravitationally collapsed regions occur at the intersection point of filaments, called nodes. The vast network of filaments intersecting at nodes, form a spider-web around the voids encapsulated by walls, earning the large-scale structure of the Universe its name: the cosmic web.

A key aspect of understanding this structure is the nature in which it formed. Historically, there were two views of structure formation which initially seemed incompatible: top-down and bottom-up. Zel'Dovich (1970) proposed a framework of anisotropic collapse leading to the creation of filaments, walls, and clusters based on potential cosmic flows. A direct consequence of this approach is that in order to achieve smaller structures, the matter which first formed into so-called pancakes would then need to fragment, thereby earning the moniker top-down. Peebles (1980) was a proponent of hierarchical clustering where smaller structures (small halos) created through spherical collapse of density peaks merge to form larger bodies (larger halos), a bottom-up evolution. Bond et al. (1996) reconciled these two views, presenting our current understanding that the two scenarios occur simultaneously on vastly different scales. The top-down model governs the largest spatial scales, in the linear regime, whereas the bottom-up model governs the

smaller spatial scales, in the non-linear regime. Thus we end up with galaxies embedded in the filamentary structures of matter. At the nodes of the large-scale cosmic web created in the top-down methodology of Zeldovich, clusters formed through a bottom-up process whereby galaxy halos form first, which eventually coalesce to form groups, which further merge to form clusters (e.g. Press and Schechter (1974), Gott and Rees (1975), White and Rees (1978), Bond and Myers (1996)).

The cosmic web is an obvious feature in both astrophysical simulations (see left panel Figure 1.2, from the Millenium simulation of Springel et al. (2005)) and observations (see right panel Figure 1.2, from the Sloan Digital Sky Survey (SDSS)). In large-scale spectroscopic surveys, like the SDSS, galaxies trace the branching filaments of the web, with clusters highlighting its nodes. Robust filament extractors, such as DisPerSE (Sousbie 2011) which is used in this work, have been utilized extensively to create filament networks from simulation data (e.g. Laigle et al. (2014), Codis et al. (2018), Kraljic et al. (2018)) as well as from observations (e.g. Laigle et al. (2017), Bird et al. (2019), Welker et al. (2019)). However due to the lower density of these cosmic filaments, only recently has work by Umehata et al. (2019) provided us with our first direct observations of a filament of the cosmic web. Their work specifically highlights the idea that cosmic filaments may funnel cold gas towards galaxies.

1.2   Galaxies

Within the context of the structure formation model described in the previous section, the halos that initially form have gas collapse inwards due to gravity. A portion of the hot gas cools and eventually forms into dense clouds, and in these regions stars form. These blobs of collapsed gas within halos which contain stars are what we call galaxies.

It has long been evident that there are broad categories that galaxies fall into based on their appearance. The famous Hubble Tuning Fork (Figure 1.3) (Hubble 1926) shows
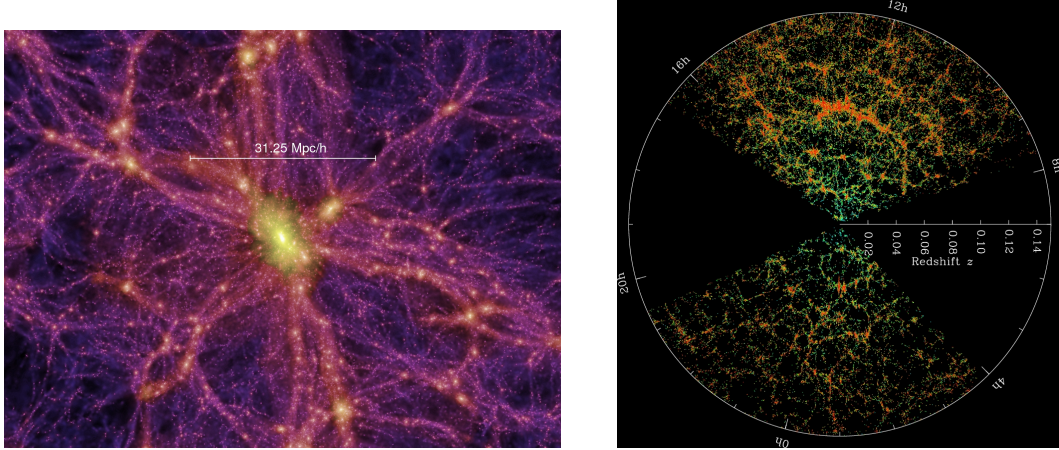
FIGURE 1.2: **Left panel:** Dark matter traces the cosmic web in the Millenium simulation in this 15 Mpc/h thick slice. Reproduced from Springel et al. (2005) with permission. **Right panel:** The galaxy distribution traces the cosmic web in the Sloan Digital Sky Survey. Each dot is a galaxy, the colour is the $g - r$ colour. (Credit: M. Blanton and SDSS)

Hubble's attempt at classifying galaxies based on their morphologies alone. His classifications for galaxies were elliptical (E), normal spirals (S), barred spirals (Sb), and irregulars (Ir). This tuning fork could be seen as an evolutionary sequence where the ellipticals on the left were 'early-type' and progressively moving towards the right becoming 'late-type' spirals. While we know this picture of evolution to be inaccurate now, the classification system is still used today as a tool to visually classify morphology.

As the ability to examine galaxies in more detail progressed, key properties of these elliptical and spiral galaxies were established. In terms of physical properties at $z = 0$, the mass of ellipticals varies from around $10^7 M_\odot$ up to more than $10^{13} M_\odot$ and with effective radii as large as tens of kiloparsecs (Carroll and Ostlie 2007). In this work we focus on massive ellipticals, above $10^{10} M_\odot$, rather than lower mass dwarf ellipticals. In comparison, spirals have typical masses between $10^8 M_\odot$ and $10^{11} M_\odot$ and stellar diameters up to tens of kiloparsecs (Carroll and Ostlie 2007). The morphology-density relation suggests that ellipticals are more likely to be found in denser environments such as clusters and spirals are more likely to be found in less dense environments such as the
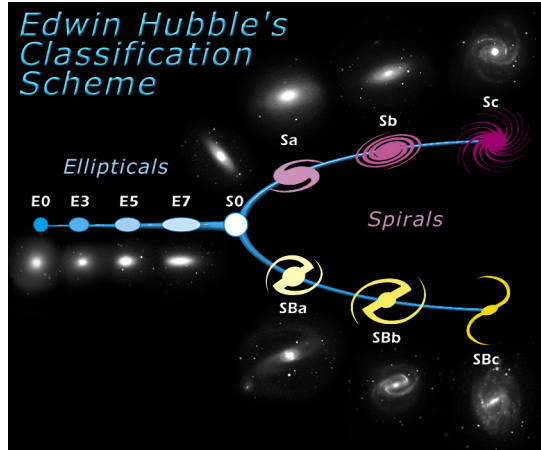
FIGURE 1.3: The Hubble tuning fork, with 'early-type' ellipticals on the left and 'late-type' spirals on the right, split between barred and unbarred. (Credit: NASA & ESA)

field or in small groups (e.g. Dressler (1980), Postman and Geller (1984)).

Notably, ellipticals tend to be redder and spirals tend to be bluer (Strateva et al. 2001). Galaxy colours are given by the magnitude difference between two colour filters, usually one 'red' and one 'blue'. Overall, the galaxy colour distribution is bimodal (e.g. Strateva et al. (2001), Balogh et al. (2004), Baldry et al. (2004)). From their appearance on colour-mass diagrams, the two peaks of the distribution are commonly known as the red sequence and blue cloud, while the dip in between is called the green valley (see Figure 1.4 which shows the colour-mass diagram from Galaxy Zoo (Schawinski et al. 2014)). It is important to note that recent research has highlighted the fact that the colour-morphology split is not necessarily strict, with citizen science project Galaxy Zoo bringing red spirals and blue ellipticals to the forefront in Schawinski et al. (2009), Masters et al. (2010), and Schawinski et al. (2014). Research from Galaxy Zoo has also offered insight on how colour depends on environment and how this is distinct from the morphology relationship with environment, finding that colour is more environmentally-dependent than morphology (Bamford et al. 2009). The colour of a galaxy tells us of its constituents; redder galaxies contain older stellar populations whereas bluer galaxies

tend to be made up of younger stellar populations.
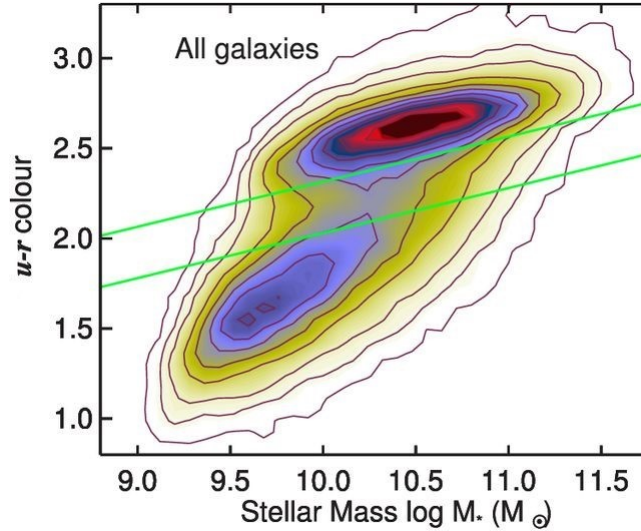
FIGURE 1.4: The galaxy colour-mass relation from Galaxy Zoo. The blue cloud is bottom left, the green valley between the lines, and the red sequence top right. Reproduced with permission from MNRAS Volume 440, Issue 1, Schawinski et al. (2014) Figure 2.

The other key component of the picture is the gas content of a galaxy: bluer galaxies tend to have more cold gas than their redder counterparts (e.g. Young and Scoville (1991), Saintonge et al. (2011), Saintonge et al. (2017)). Some portion of the atomic gas in galaxies will form into dense, cold, molecular clouds. Stars form from the collapse of these clouds of cold molecular gas in galaxies. Thus the blue galaxies, rich with gas, have higher star formation rates (measured in $M_\odot/yr$) than those red galaxies with minimal gas content. The removal or exhaustion of this gas without replenishment can lead a galaxy to cease to be star forming. This phenomenon is known as quenching. Analysis of galaxy colours and cold gas content, such as is done in this thesis, is therefore useful in understanding quenching.

In the context of galaxy-scale filaments, a great deal of work has focused on their ability to funnel cold gas into the cores of galaxies, known as the cold-flow or cold mode accretion model of galaxy formation (e.g. Katz and White (1993), Keres et al. (2005),

Dekel et al. (2009), Brooks et al. (2009), Kleiner et al. (2016)). These cold flows arise from density anisotropies in the gas being accreted onto halos and present as collimated, thin streams plunging into the halos. The classical picture of galaxy formation (e.g. Rees and Ostriker (1977), Silk (1977), Fall and Efstathiou (1980)) posits that as gas collapses into a dark matter halo it shock-heats to the virial temperature of the halo, after which in the densest regions a fraction of it radiatively cools, creating a steady supply of cold gas for star formation. However, problems arose with this picture when work with simulations found that the majority of gas accreted onto these halos never shock-heats up to the virial temperature (e.g. Birnboim and Dekel (2003), Kereš et al. (2009)). The cold flow model is largely considered the solution to this issue and is dominant at high redshift. It is important to emphasize that cold flow work has focused on galaxy-scale filaments feeding centrals.

In the context of larger scale halos such as clusters and the filaments branching into them, Figure 1.5 taken from Cornuault et al. (2018) highlights an illuminating point. The figure shows the filament overdensity f against halo mass coloured by the ratio of cooling time to the dynamical time. The figure shows that for massive halos of order $10^{12.5} M_\odot$ at $z = 2$ (those that represent clusters at $z = 0$), dense filaments ($\log(f) = 2$) persist as regions of multiphase accretion. Thus, at $z = 0$, even if filaments deep into clusters are fragmented by mechanisms such as virial shocks, streaming instabilities, or AGN feedback, they may persist as regions of increased coherence and accretion within the cluster environment. Thus there may be effects by such filaments on satellite halos in cluster environments.

1.3   Galaxy Clusters

Galaxy clusters are the largest gravitationally bound objects in the Universe, home to hundreds to thousands of galaxies, and tend to be several megaparsecs across. They are
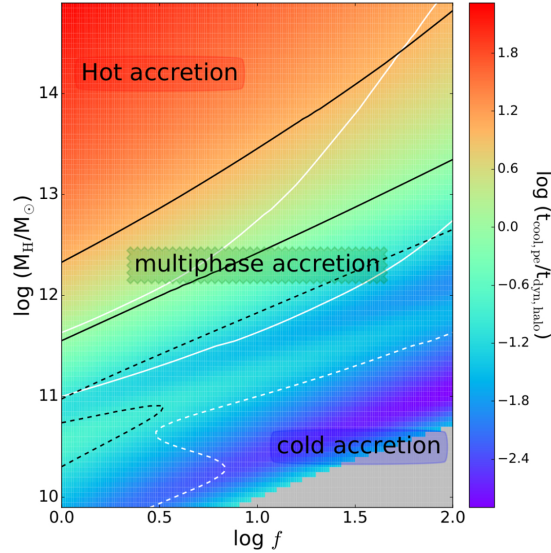
FIGURE 1.5: Ratio of the post-expansion cooling and halo dynamical timescales as a function of halo mass, and filament overdensity f, at $z = 2$. The colors represent $\log(t_{\rm cool}/t_{\rm dyn})$. Notably, the densest filaments ($f = 2$) in halos of masses on the order of $10^{12.5} M_\odot$ at $z = 2$, those which would represent clusters at $z = 0$, show multiphase accretion. Reproduced with permission from Cornuault et al. (2018) Figure 3.

an environment rich with complex dynamics and galaxy interactions. These structures provide valuable information on galaxy evolution and can act as cosmological probes. Perhaps the most famous example of galaxy clusters aiding our understanding of the Universe came courtesy of Fritz Zwicky (Zwicky (1933), Zwicky (1937)). Zwicky found that the mass he calculated for the Coma Cluster from the virial theorem using galaxy velocities greatly outweighed the mass from luminous matter alone, and suggested the existence of invisible dark matter as the missing mass.

While Zwicky was, as we know now, correct about dark matter, there is another component to the mass of a cluster other than galaxies (roughly 2% of a typical cluster mass) and dark matter (roughly 85% of a typical cluster mass) (Rudnick 2019). The remaining mass in clusters is the intra-cluster medium (ICM). The ICM is comprised of hot ($10^7 - 10^8$ K) (Mohr et al. 1999) gas emitting at X-ray energies (e.g. Meekins et al. (1971), Gursky et al. (1972)) via thermal bremsstrahlung. As an example, Figure 1.6

shows a composite optical (white, from SDSS) and X-ray (purple, from Chandra) image of the Coma cluster. The strong X-ray emission of the ICM allows for observations of clusters out to high redshift, with some work in this regime coming from Chandra (e.g. a massive cluster at $z = 1.24$ (Rosati et al. 2004), the ICM in $z > 1$ clusters (Stanford et al. 2001)). Furthermore, the ICM leads to distortions in the CMB of about $10^{-4} - 10^{-5}$ K, known as the Sunyaev-Zeldovich effect, caused by inverse Compton scattering of CMB photons to higher energies by ICM electrons (Sunyaev and Zeldovich (1970), Sunyaev and Zeldovich (1972), Sunyaev and Zeldovich (1980)). This effect, which is a redshift independent signal, allows for additional high redshift cluster observations (e.g. South Pole Telescope (Reichardt et al. 2013), Atacama Cosmology Telescope (Hasselfield et al. 2013), Planck (Ade et al. 2016)).

FIGURE 1.6: A composite optical (white, from SDSS) and X-ray (purple, from Chandra) image of the Coma cluster, highlighting the ICM. (X-ray: NASA/CXC/Univ. of Chicago, I. Zhuravleva et al, Optical: SDSS)

In the context of this thesis, the cluster environment's importance lies in its ability to impact the gas content of cluster galaxies. I highlight a few of these mechanisms below.

One such mechanism is tidal stripping. This is in essence caused by the tidal field of a cluster potential well (Merritt 1984). Beyond a certain galaxy-centric radius, galaxies cannot hold onto their material and will lose it to the cluster.

Given the increased proximity to neighbouring galaxies by virtue of being the cluster environment, harassment is another mechanism at play (Moore et al. 1996). This occurs when galaxies fly-by each other but do not coalesce. Harassment typically changes the morphology of galaxies (Moore et al. 1998).

A galaxy's motion through the hot, dense ICM on their orbit around the cluster centre causes a very important effect on cluster galaxies: ram pressure stripping. First proposed by Gunn and Gott (1972), this mechanism is highly effective at quickly stripping out gas from cluster galaxies. The mechanism relies on an imbalance of two things: a galaxy's gravitational potential and the ram pressure the galaxy feels as it moves through the ICM. The former simply increases with galaxy mass. The latter, can be expressed as $P_{\mathrm{ram}} = \rho v^2$, where ρ is the density of the surrounding ICM and v is the galaxy's velocity through it. If the ram pressure on a gas particle exceeds the gravitational potential it feels in the galaxy (dependent on its galaxy-centric distance and the density profile of the galaxy) it will be stripped out. This means that for more diffuse galaxies, there is a small radius beyond which gas can be easily stripped, whereas for more concentrated galaxies, the radius stripping can take place beyond is much larger.

Another important mechanism impacting the gas content of cluster galaxies, first suggested by Larson et al. (1980), is known as strangulation. Strangulation occurs when there is no refreshment of a galaxy's cold gas stores and a galaxy gradually ceases to form stars as it runs through what is left in its inventory. In the cluster context, strangulation is due to the hot ICM environment preventing accretion of cold gas. The timescales for strangulation are much longer than ram pressure stripping, typically taking several gigayears to achieve full quenching (e.g. Kawata and Mulchaey (2007), Peng et al. (2015)). Recent work of note was conducted by Peng et al. (2015) focusing on metallicity as a discriminator between ram pressure stripping and strangulation as quenching mechanisms. They argue that as star formation is continued over long timescales in a strangulation

situation, metallicity should continue to increase before a galaxy quenches, and therefore galaxies that have quenched through strangulation should have higher metallicities than those that quenched through ram pressure stripping.

Of these mechanisms, if filaments in clusters maintain coherent flows and are regions of preserved accretion, ram pressure stripping and strangulation would be most likely to be suppressed. Coherent flows would affect the relative velocity in ram pressure, and accretion could clearly play a role in affecting strangulation. An intra-cluster filament environment would likely have no discernable effect on tidal stripping nor harassment.

1.4   Quenching in Dense Environments

Considerable work has been done to understand how galaxies quench in dense environments such as clusters and filaments, the regimes where this thesis focuses. Studies have indicated that galaxies show signs of quenching progressively towards the centre of clusters using a variety of measures: star formation rate (SFR) (Balogh et al. 2000), the fraction of star-forming galaxies (Pintos-Castro et al. 2019), and the fraction of blue galaxies (Raichoor and Andreon 2012). The cluster environment increases in density towards the cluster centre, allowing for more opportunities for interactions as well as increased ram pressure stripping. Ram pressure stripping can rapidly quench galaxies in cases where it is efficiently stripping the gas content, on timescales under 1 Gyr (e.g. Abadi et al. (1999), Roediger and Hensler (2005)). One telltale visual sign that such stripping is taking place is the existence of long trails of gas extending from a galaxy (see Figure 1.7), more commonly referred to as 'jellyfish' galaxies (e.g. Ebeling et al. (2014), Poggianti et al. (2017)). The current picture for this situation, at least for low mass galaxies, is a slow-then-rapid model, where the ICM must reach some threshold density for ram pressure stripping to rapidly quench galaxies (Wetzel et al. (2013), Roberts et al. (2019), Maier et al. (2019)). The 'slow' portion of this model typically involves the

FIGURE 1.7: The Comet Galaxy is a jellyfish galaxy in galaxy cluster Abell 2667 which exhibits telltale signs of ram pressure stripping. Here, it is moving towards the top right of the frame. (Cropped from image with credit: NASA, ESA, Jean-Paul Kneib (Laboratoire d'Astrophysique de Marseille))

aforementioned strangulation mechanism.

The relationship between SFR and stellar mass is also particularly illuminating. We examine this in detail in the context of our simulation suite in Chapter 3, but present a brief example in Figure 1.8 taken from Roberts and Parker (2020). This figure shows the SFR-M_{star} relationship for both field galaxies (taken from the SDSS, in the background in grayscale), and cluster galaxies (from the Coma cluster, coloured foreground dots). The so-called main sequence of star formation where SFR increases with stellar mass is clearly visible, as is the secondary population of low SFR, high mass galaxies. These are the red and dead quenched population.

We have also more recently begun to understand how galaxies quench in relation to the cosmic web, specifically in non-cluster (field) environments. Kraljic et al. (2017) and Laigle et al. (2017) both find that star formation decreases with filament proximity. Figure 1.9 taken from Kraljic et al. (2017) uses both galaxy colour and specific
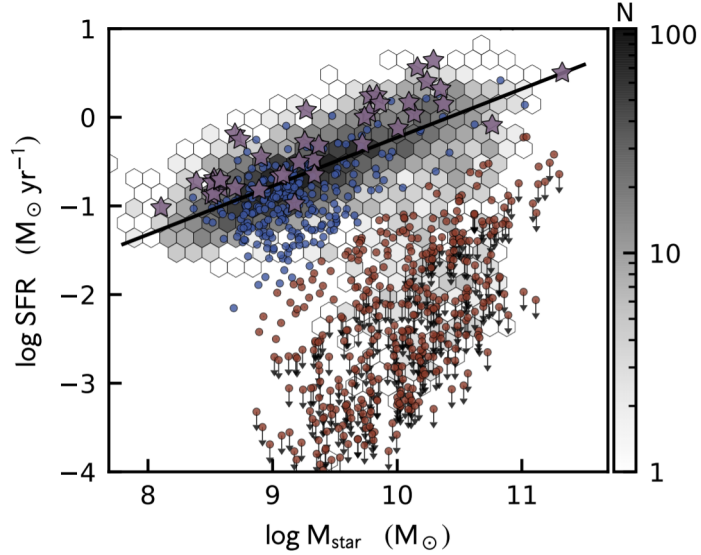
FIGURE 1.8: SFR versus stellar mass. Background greyscale shows distribution for galaxies from an isolated field sample from the SDSS and the trend line shows the best-fit to star-forming (sSFR $> 10^{11} yr^1$) field galaxies. Blue points correspond to normal star forming Coma galaxies, red points show passive Coma galaxies, and purple stars denote Coma ram pressure stripping candidates. Reproduced with permission from Roberts and Parker (2020) Figure 7.

star formation rate (star formation rate divided by stellar mass) to demonstrate this. Sarron et al. (2019) examined galaxies near filaments extending out of clusters from the AMASCFI Canada-France-Hawaii Telescope Legacy Survey. They found that passive galaxies are found closer to clusters than star-forming ones, and that filament galaxies are more passive than field galaxies. A phenomenon called 'pre-processing' is considered to be at play in these situations. In the field, galaxies are in less dense environments and are less likely to interact, but field filaments are a realm of marked density increase meaning galaxies will interact with one another close to filaments. Theory suggests that blue star-forming galaxies are merging and forming red passive galaxies along filaments as they migrate towards the dense nodes (as in Dubois et al. (2014)). While this increase in quenching towards filaments is relatively well-established for the field, it is unclear if it persists for filaments and galaxies deep within the virial radius of clusters, given the difference in environment and that intra-cluster filaments may not persist as strong

streams.
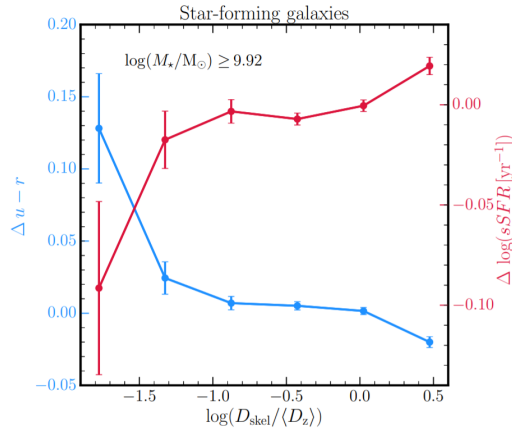
FIGURE 1.9: $\Delta u - r$ colour (blue line) and $\Delta \log(\text{sSFR})$ (red line) of star-forming galaxies as a function of distance to filament (D_{skel}). The y-axes indicate the amount by which $u - r$ colour and specific star formation rate differ from the median values at given mass. Star-forming galaxies tend be redder and have lower specific star formation rates when they get closer to the filaments. Reproduced with permission from MNRAS Volume 474, Issue 1, Kraljic et al. (2017) Figure 8.

1.5 The Three Hundred Project

The Three Hundred project is a set of 324 hydrodynamical galaxy cluster simulations (Cui et al. 2018). The clusters selected for this suite are zoom re-simulations of the most massive clusters identified at $z = 0$ from the dark-matter-only MDPL2 MultiDark Simulation (Klypin et al. 2016). These re-simulations were conducted using the GADGET-X (Beck et al. 2015) code, a version of the GADGET3 smoothed particle hydrodynamics (SPH) code, which is based on the GADGET2 code (Springel 2005). GADGET-X applies black hole and active galactic nucleus feedback methods, metal-dependent UV cooling, star formation and stellar evolution, and stellar feedback with varying star particle masses (Cui et al. 2018). Each cluster has a total of 128 snapshots at pre-determined redshifts from $z = 0$ to 17. Clusters have masses ranging from $10^{14} M_\odot$ to $10^{15} M_\odot$, and vary from relaxed to unrelaxed.

SPH is an approach to hydrodynamical fluid modelling first proposed by Lucy (1977) and Gingold and Monaghan (1977) which treats continuous fluids as discrete particles flowing with the fluid. The formulation is fully Lagrangian, meaning that equations are solved in the particles' frame of reference. All desired properties are found by interpolating (summing up) over nearby particles. While the intricacies of SPH are beyond the scope of this thesis, the most fundamental quantity needed for this interpolation is worth discussing. Details beyond what is discussed below can be found in excellent reviews by Monaghan (1992) and Price (2012) coupled with the specifics of the SPH code used in The Three Hundred, GADGET-X, in Beck et al. (2015).

The fundamental quantity for interpolating relevant properties is the density estimator for an individual particle a, using the contributions of N neighbouring particles b of mass m_b each at a distance x_{ab} from a. This is defined as

$$\rho_a = \sum_{b=1}^{N} m_b W_{ab}\left(x_{ab}, h_a\right).$$ (1.1)

Here, h is the smoothing length, whose adaptivity is a key component of SPH, and is defined as

$$h_a = \eta \left(\frac{m_a}{\rho_a}\right)^{1/3}$$ (1.2)

where η is the ratio of the smoothing length to the mean distance between particles. Equations 1.1 and 1.2 are solved simultaneously by SPH codes. W is a weight function, known as the smoothing kernel. In GADGET-X, the smoothing kernel chosen is the Wendland C^4 (WC4) kernel (Dehnen and Aly 2012), with $N = 200$ neighbours. This was chosen to improve numerical convergence with a high number of neighbours (Beck

et al. 2015) and to avoid the pairing instability discussed in Price (2012). Using the notation $q = \frac{x_{ab}}{h_a}$, the WC4 kernel is defined as

$$W_{ab}(x_{ab}, h_a) = \frac{w(q)}{h_a^3} = \frac{495}{32\pi h_a^3}(1-q)^6\left(1 + 6q + \frac{35}{3}q^2\right). \tag{1.3}$$

With the density estimator in hand, properties of interest, A_a, can then be calculated as

$$A_a \approx \sum_{b=1}^{N} m_b \frac{A_b}{\rho_b} W_{ab}\left(x_{ab}, h_a\right). \tag{1.4}$$

Given the nature of SPH, the cluster re-simulations are run with dark matter, stellar, and gas particles, meaning they contain a wealth of knowledge including particle position, velocity, density, stellar age, metallicity, and gas temperature. Note that the halo finder and filament extractor used on the simulations for this thesis are discussed in Chapter 2, and I touch specifically on the limitations of the resolution in this simulation suite in Chapter 3.

1.6 Thesis Overview

As discussed above, the relationship between filaments and quenching has been explored for galaxies in the field environment. This thesis represents the first body of work to examine quenching in the context of filaments diving deep into galaxy clusters. Thanks to the large sample size of the Three Hundred simulation suite, we are able to examine trends in the cluster environment with a high level of statistical significance, with the tradeoff of lower resolution. This, in combination with a robust filament extractor and halo finder, provides us with the necessary tools to conduct our work.

In Chapter 2, we show that intra-cluster filaments are markedly delaying quenching for cluster galaxies. This presents a stark contrast to trends established for galaxies and filaments outside the cluster environment. We discuss the evidence we see for this delay, and establish the mechanisms by which intra-cluster filaments are achieving this effect. Then, in Chapter 3, we expand on our decision in the preceding chapter to not use direct calculations of star formation rates available through the simulation set. This Chapter sets out underlying issues with the simulation set that we used. In Chapter 4, we briefly discuss an additional measure aimed at classifying galaxies in the simulation as dry or wet by way of a binary cut on a dynamical measure. Finally, in Chapter 5, I summarize the conclusions of this thesis and point to further work that could confirm our results via simulations and observations.

Chapter 2

Cosmic Filaments: Delaying Quenching Inside Clusters

This chapter is a replica of an article that has been prepared for submission to the Monthly Notices of the Royal Astronomical Society, restyled to fit the formatting guidelines for this thesis. The various contributions to this Chapter have been outlined in the Declaration of Authorship.

2.1 Introduction

On the largest scales of the Universe, matter is distributed in a complex structured network visible in the galaxy field from spectroscopic surveys (e.g. 2dFGRS (Colless et al. 2001), SDSS (Stoughton et al. 2002)). This large-scale structure, often referred to as 'the cosmic web' (Bond et al. 1996), naturally arises from the gravitational collapse of initial perturbations in the density field of the early Universe (Peebles 1980). We observe large under-dense regions, or voids. These voids are segmented by sheet-like regions of higher density known as walls, which attract matter from voids. In turn, these walls are further collapsing into a network of dense filaments that delineate them. These filaments channel matter towards the highest density regions of the Universe, the cosmic nodes,

where they meet. It is at the nodes of this cosmic web that we find galaxy clusters, with filaments diving deep into their centres. Galaxy clusters are the densest and most massive gravitationally-bound structures in the Universe, hosting thousands of galaxies. They are therefore a hotspot for both galaxy interactions and complex non-linear dynamics. In particular, the intra-cluster medium is a place of increased galaxy quenching: the rapid shutting down of star formation in galaxies evolving in dense environments.

It is well-established that the star formation activity of galaxies in today's Universe distributes in a clear bimodal fashion, easily detected in observations through the corresponding colour bimodality of the light they emit (e.g. Strateva et al. (2001), Balogh et al. (2004), Baldry et al. (2004)). Bluer galaxies are home to younger, hotter stars and are hence more actively star forming, while their reddest peers no longer form stars, and are effectively 'dead'. Between these two populations, few galaxies are found to display intermediate star formation patterns, suggesting that galaxies undergo a rapid shutting down of their star formation at some point in their history. A perennial question of galaxy evolution is therefore exactly how galaxies turn off their star formation, or quench.

It is well understood that stars form when cold, dense gas collapses, and as such, star formation shuts off when cold gas supply in or around a galaxy becomes scarce (Gabor et al. 2010). This quenching occurs mostly in dense environments such as clusters and possibly involves a variety of processes. For instance, strangulation occurs when there is no more gas inflow to a galaxy (e.g. Larson et al. (1980), Balogh et al. (2000), Peng et al. (2015)). Stars continue to form using up the available gas until there is little to none left, at which point a galaxy is quenched. Harassment and mergers occur due to interactions between galaxies, whereby gas is heated and/or stripped, causing star formation to shut down in such galaxies (e.g. Moore et al. (1996), Smith et al. (2015)).

The radial trends resulting from the progressive quenching of galaxies falling into

clusters have been extensively described in both simulations and observations: it is now established that the fraction of star-forming galaxies decreases towards the centre of clusters (e.g. Balogh et al. (2000), Haines et al. (2015), Raichoor and Andreon (2012), Pintos-Castro et al. (2019)).

In recent years, increasingly robust computational models and capabilities have allowed more accurate and effective simulations of the complex environments of galaxy clusters and improved understanding of how galaxies evolve in these regions (e.g. C-EAGLE (Barnes et al. 2017), The Three Hundred (Cui et al. 2018), RomulusC (Tremmel et al. 2018)). Among other mechanisms, ram pressure stripping seems to play a major role deep into the cluster (e.g. Wetzel et al. (2013), Roberts et al. (2019), Maier et al. (2019)). We define ram pressure stripping as the interaction of galaxies with the hot gas they are moving through (Gunn and Gott 1972).

Interestingly, outside of clusters, some recent studies suggest cosmic filaments might also play a role in the early quenching of field galaxies. Indeed, in the field, cosmic filaments are denser than their surroundings, and as such may be associated with pre-processing (e.g. Kraljic et al. (2017), Laigle et al. (2017), Sarron et al. (2019)). Galaxies near filaments tend to display higher stellar masses (Welker et al. 2019). They also undergo more interactions, and thus may quench faster and become redder than their counterparts further away from the filaments (Kraljic et al. 2017).

On the other hand, it has long been theorized that, since gas shocks and cools into cosmic filaments, such filaments should be able to funnel streams of cold gas crucial to star formation (e.g. Katz and White (1993), Brooks et al. (2009), Kereš et al. (2009), Kleiner et al. (2016)), at least at $z > 1$, and that such cold streams might partially persist deep into clusters, past the virial shock. More recently, this filamentary gas was directly observed for the first time stretching between galaxies in the SSA22 protocluster at $z = 3.1$ with the Multi Unit Spectroscopic Explorer on the Very Large Telescope

(Umehata et al. 2019). As such, it is therefore reasonable to suspect that filaments plunging into clusters might modify the local dynamics of the intra-cluster medium and have an impact on the evolution of the galaxies around them too.

However, the impact of large inter-cluster cosmic filaments on quenching deep into clusters ('intra-cluster' filaments) remains seldom analysed. Therefore, their role on local star formation remains to be explored. This is in part because most cosmic web extractors identify cosmic structures as either a filament or a cluster, so do not allow for the analysis of intra-cluster filaments. To bridge this gap, we use DisPerSE, a topological extractor that identifies the spine of the cosmic web and therefore allows us to track filaments down to the core of clusters.

The focus of this study is thus to analyze the impact of intra-cluster cosmic filaments on quenching, that is, in regions where the background is now dense hot intra-cluster medium and where effects such as ram pressure stripping become one of the dominant quenching mechanisms. In this work we use a robust set of simulations along with data of filaments diving deep into the centre of clusters to analyse the effects the cosmic filaments on galaxy evolution inside the cluster environment, and in particular determine whether cold gas streams in filaments might be able to delay quenching in cluster galaxies.

The remainder of this paper is structured as follows. In Section 2.2 we discuss the data products and numerical quantities used for this work. In Section 2.3 we present the results of our analysis on the quenching of galaxies in relation to cosmic filaments in different environments through numerous measures, indicating a novel result. In Section 2.4 we look at the dynamics surrounding filaments themselves to support our result. Finally, in Section 2.5 we summarize our findings and discuss next steps.

2.2   Numerical Methods

In this section, we describe the galaxy cluster simulation set used for this research in Section 2.2.1, as well as the halo finder in Section 2.2.2, and the filament extractor in Section 2.2.3. We then discuss the tracers we use to investigate the evolution of star formation in Section 2.2.4, and the measures we use to investigate the dynamics of gas and galaxies in Section 2.2.5.

2.2.1   Simulation Sample: The Three Hundred

A large sample size of galaxy cluster simulations with sufficient resolution is required in order to have robust statistics on intra-cluster filaments and galaxy populations. For this study, we use The Three Hundred project (Cui et al. 2018), a set of 324 simulated galaxy clusters run with a smoothed-particle hydrodynamic (SPH) scheme.

The clusters in this set are hydrodynamic zoom re-simulations of the most massive halos in the dark matter-only MultiDark MDPL2 simulation (Klypin et al. 2016) at $z = 0$, run with GADGET-X, a version of the GADGET3 with the improved SPH scheme of Beck et al. (2015) (itself an updated version of the GADGET2 code (Springel 2005)).

The Three Hundred suite was run with cosmological parameters $\Omega_M = 0.307, \Omega_B = 0.048, \Omega_\Lambda = 0.693, h = 0.678$, a dark matter particle mass of $M_{DM}^0 = 1.27 \times 10^9 h^{-1} M_\odot$, and gas particle mass of $M_{gas}^0 = 2.36 \times 10^8 h^{-1} M_\odot$, corresponding to a typical spatial resolution of 8 kpc. The simulation suite includes advanced prescriptions for processes such as metal-dependent UV cooling, black hole growth and active galactic nucleus feedback, star formation and stellar evolution, and stellar feedback with varying star particle masses (Cui et al. 2018).

Clusters range from $4 \times 10^{14} M_\odot$ to $10^{15} M_\odot$, and vary from relaxed to unrelaxed.

We conduct the study at $z = 0$. In order to avoid boundary effects at the edge of the re-simulated regions, we limit our analysis of simulation data, halos, and filaments to a 10 Mpc h^{-1} spherical region from the centre of each cluster. In practice, since most of our analysis focuses on halos within 2 R_{vir} of the clusters, our results are not affected by this cut.

With varying star particle masses on the order of $M_* = 4 \times 10^7 h^{-1} M_\odot$, galaxies with more than 50 particles are resolved down to stellar masses of $10^{9.47} M_\odot$.

2.2.2 Halo identification with VELOCIraptor

Halos hosting galaxies were identified with the VELOCIraptor halo finder (Elahi et al. 2019). For this work, we use the mixed-component version of the finder, which operates on dark matter, gas, and star particles. The finder conducts a multi-step algorithm to identify structures. It begins by identifying halos with a 3D friend of friends (FOF) first pass search, followed by a 6D FOF search in phase space. The process allows us to identify kinematically coherent substructures and mergers. Basic properties such as virial radii, virial masses, and stellar masses are computed on the fly.

Note that this mixed-component finder is particularly efficient at identifying halos and sub-halos hosting galaxies but not galaxies on their own. As a consequence, a single, intermediate size halo containing an advanced galaxy merger with no remaining identifiable dark matter sub-halo will appear as a single structure rather than two, corresponding to the two galaxies in the process of merging.

The limited resolution of the simulation does not allow for a robust separation of distinct galaxies late in the process of merging across the stellar mass range analysed. Our study is therefore conducted at the halo/sub-halo level for halos hosting galaxy candidates.

It should then be noted that this study focuses on gas content and star formation within the halo virial radius. In practice, the stellar content is however mostly concentrated at the centre of halos, on galactic scales, and is therefore typically easily associated with the appropriate dark matter halo.

To ensure that a halo is sufficiently resolved and does contain a galaxy candidate, we exclude any halo with less than 100 dark matter particles or with a stellar mass less than $10^{9.5} M_\odot$.

We further exclude the brightest cluster galaxies (BCGs) - which we identify as the halo with the highest stellar mass within a quarter of the virial radius of each cluster. This work focuses on the fate of satellite galaxies falling into a cluster environment either along filaments or on deviated orbits. Such mechanisms do not directly govern the evolution of BCGs, which seem to be more sensitive to the connectivity of the cosmic web (Kraljic et al. 2020).

2.2.3   Filament extraction with DisPerSE

The DisPerSE persistent structure finder (Sousbie 2011) is used to identify filaments diving deep into our simulated galaxy clusters. DisPerSE has been successfully used on both simulations (e.g. Laigle et al. (2014), Codis et al. (2018), Kraljic et al. (2018)) and observational studies (e.g. Laigle et al. (2017), Bird et al. (2019), Welker et al. (2019)).

DisPerSE is based on on topology rather than geometry, as one of its main advantages. It characterizes topological features (minima, maxima, saddle points, and ridge lines) as the various components of the cosmic web, including walls, voids, and filaments. The software identifies ridge lines of a given density field to produce a network of filaments. Further trimming is based on persistence, the ratio of the value at the two critical points (pairs of maximum, minimum, or saddle points), and local robustness, the density contrast between these points and filaments with respect to local background. The

persistence threshold translates to a minimum signal-to-noise ratio in this context. These techniques make DisPerSE excellent for the context of large-scale structures, with noisy data, and inherent scale-invariant nature.

For this analysis, DisPerSE was applied to the gas density field of the simulations, first projected on a 30 Mpc wide 3D grid centred on each cluster, with pixels of 150 kpc on each side. It was then smoothed over 8 pixels with a Gaussian kernel. This method allows us to focus on the larger cosmic filaments by effectively getting rid of thinner filaments between large satellites, which can appear as contrasted peaks in the density field.

As an example, a visual representation of Cluster 50 is shown in Figure 2.1. The left panel depicts a 3D representation with filaments in green, galaxy halos defined by their virial radius in blue, and dark matter particles in pink. The cluster's virial radius appears as the large central halo. Two infalling groups are visible, and numerous galaxies clearly align along the spine of the cosmic web. The right panel of Figure 2.1 displays a zoom-in of the same cluster projected along the z axis. The color palette varies linearly with the log of the gas density. Projected filaments are in red and virial radii are indicated as white dashed circles. One can clearly see the gas filaments diving deep into the cluster, with gas-rich haloes along them. We demonstrate in A1 (Section 2.6) how the most massive halos reside along the spines of filaments

For each satellite halo within 10 Mpc of its host cluster, we further define D_{fil} as the distance of a halo to its nearest cosmic filament and D_{cent} as its distance to the cluster centre (in pink on the right panel of Fig. 2.1). The reader will notice that D_{fil} and D_{cent} are not by construction independent variables, as especially near the cluster centre the nearest filament is towards the cluster centre. We therefore systematically compute the ratio $D_{\mathrm{fil}}/D_{\mathrm{cent}}$, which is in essence the angle of the halo with respect to its nearest filament. Throughout this work we call this ratio the 'angular separation'. This quantity
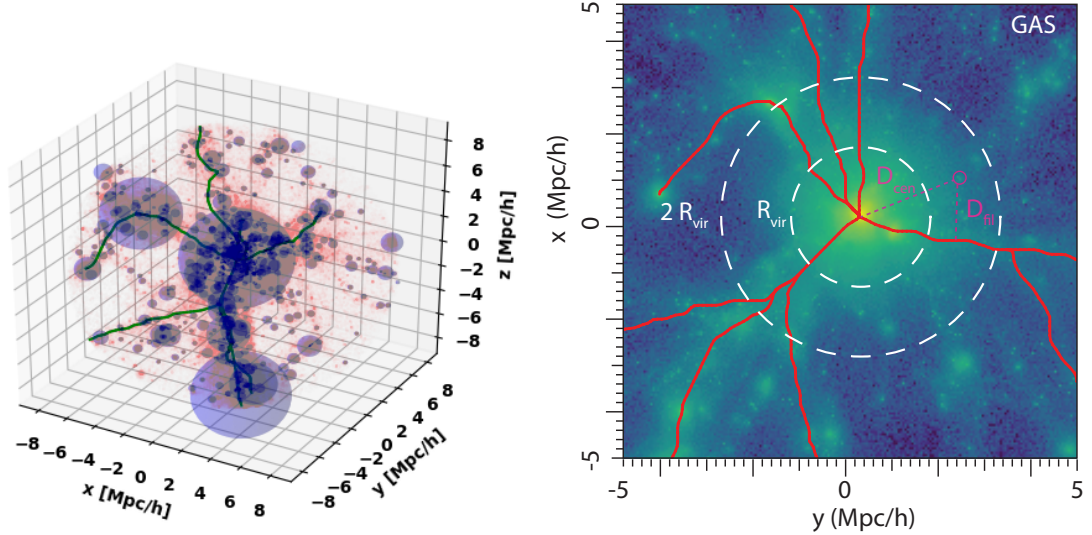
FIGURE 2.1: **Left panel**: 3D map of cluster 50, with filaments in green, dark matter in pink, and halo virial radii as blue circles. **Right panel**: 2D z-projected map of the gas density in cluster 50. Filaments are overplotted in red and the cluster's virial radius is indicated as white dashed circles. D_{fil} and D_{cen} for a given satellite appear in pink.

allows us to isolate the evolution of halo properties driven specifically by the proximity to a filament and not simply by the progressive infalling into a dense cluster.

2.2.4 Quenching Tracers

In the following section, we outline the various tracers and observables we designed to investigate quenching in this study.

Star Formation Rate

The most direct property to examine when it comes to quenching is the star formation rate (SFR), the number of stars a galaxy is forming per year, or the specific star formation rate (sSFR), which is the SFR divided by the stellar mass of the galaxy.

We use two avenues to compute SFR values in The Three Hundred. In the first method, we identify gas particles within a virial radius of the centre of the halo and

sum up SFR values assigned to gas particles by the GADGET-X subgrid star-formation recipe to obtain an instantaneous SFR in $M_\odot/yr$.

In the second method, we sum up the stellar masses of the star particles within a virial radius of the centre of the halo that have formed within the past 1 Gyr based on the stellar ages of star particles to obtain a more integrated SFR in $M_\odot/yr$. This method is expected to be less sensitive to short-lived interactions and to the limited resolution of star formation in the simulation (mainly because of the long time interval chosen).

However, owing to the limited resolution of the simulation itself, the subgrid star formation recipe of the simulation is also low resolution and suffers discrete numerical effects that affect both methods. Low mass galaxies can easily appear to not be star forming due to the lack of new star particles. On the contrary, massive galaxies do not stop star formation early or fast enough as a result of over-compensation in the tuning of the subgrid recipe and weak AGN feedback.

As a result, simulated SFRs trend strongly and linearly with stellar mass across the full mass range, including for galaxies with $M_{\mathrm{star}} > 10^{11.5} M_\odot$, suggesting that quenching evaluated from SFRs will be significantly underestimated.

Careful use of sSFR and analysis at fixed mass can still be used to obtain reliable qualitative results. To this end, we restrict the analysis to the fraction of star-forming galaxies in a given population of N galaxies, defined as:

$$f_{\mathrm{SFG}} = \frac{n(\mathrm{sSFR} > \mathrm{sSFR}_0)}{N} \tag{2.1}$$

with N the total number of galaxies in the population considered and $n(\mathrm{sSFR} > \mathrm{sSFR}_0)$ the number of galaxies with $\mathrm{sSFR} > \mathrm{sSFR}_0 = 10^{-11}$ yr^{-1}, a typical value used for such a cut (eg. Wetzel et al. (2013), Roberts et al. (2019)).

There is nevertheless a need for less direct but more robust tracers of quenching, which we detail in the following sections.

Galaxy Colours

Galaxy colours are directly tied to star formation and are more related to the specific stellar make-up of the galaxy than to its mass, and are integrated over its whole history, thus less sensitive to aforementioned resolution limits. They also allow for direct observational comparisons. As galaxies quench, their stellar content ages without being refreshed by new stars, hence galaxies become redder.

We therefore compute galaxy colours for all our populated halos using stellar population models. We follow the method detailed in Dubois et al. (2014), whereby we apply a Single-Burst Stellar Population model (SSP) from Bruzual and Charlot (2003) to the star particles in the simulation using the metallicity, age, and mass (obtained using the Salpeter initial mass function) of the particles to obtain the flux per frequency. The contributions from the stars are passed through the various SDSS filters. In this simple model, we do not take into account any extinction from dust. From this, we obtain stellar luminosities which we mass average to assign luminosities to the galaxies. We then use these luminosities to obtain the galaxy colours. In this work, results are presented for $g - r$ but consistent results are obtained for other standard colours. Based on the simulated colour bimodality, a typical red galaxy in our simulation is one with $g - r \geq 0.65$.

Gas Fraction

Gas content, particularly cold gas content, is the fuel for star formation and therefore reliably traces the ability of halos to form stars.

In The Three Hundred, all halos with $M_{\text{tot}} > 10^{10.5} M_\odot$ have a gas-to-total initial mass fraction resolved with at least 0.1% precision.

Note however that, at our resolution, pressure is resolved only down to a lower threshold P_{floor}, resulting in a typical lower limit of 10^4 K for temperatures in haloes. This is comparable to other flagship kpc scale cosmological simulations (e.g. Horizon-AGN (Dubois et al. 2012a), Eagle (Schaye et al. (2014) and Crain et al. (2015)), IllustrisTNG (Nelson et al. 2018)). In particular, we do not resolve the formation of molecular clouds.

We therefore identify as cold halo gas any gas particle with a temperature at or below 10^5 K within 1 R_{vir} of a satellite halo. Based on the cooling model used in The Three Hundred clusters and subsequent analysis of corresponding temperature-density diagrams, gas in this temperature range trapped within simulated halos corresponds to gas that would typically cool down into the ISM in real galaxies.

We define the cold gas fraction of the galaxy-hosting halos in our sample as:

$$f_{\text{gas}}^{\text{cold}} = \frac{M_{\text{gas}}(\text{T} \leq 10^5 \text{ K})}{M_{\text{gas}}(\text{T} \leq 10^5 \text{ K}) + M_{\text{star}}} \tag{2.2}$$

with $M_{\text{gas}}(\text{T})$ the total mass of the gas with temperature below T within 1 R_{vir} of the halo, and M_{star} its total stellar mass within 1 R_{vir}.

2.2.5 Dynamical Measures

To analyse the origin of satellite quenching in clusters, we also study the dynamics of these galaxies through the gaseous medium surrounding them. This section outlines the quantities we define to investigate these dynamics.

Filament Kinematics

In order to investigate how coherent flows of gas and galaxies are along cosmic filaments, we measure the angle between the velocity vector of halos and gas particles with respect to their nearest filaments. More specifically, for every halo and gas particle with cluster-centric velocity, $\vec{v}$, and its nearest filament segment, $\vec{f}_{near}$, we compute:

$$\cos\theta = \frac{\vec{f}_{\text{near}} \cdot \vec{v}}{|\vec{f}_{\text{near}}||\vec{v}|}. \tag{2.3}$$

By definition, filament segments are increasingly radial towards the cluster centre, which is a node of the cosmic web. Motions of galaxies and gas accreted into clusters are also expected to be radial on average, with various degrees of dispersion depending on proximity to the cluster centre.

Thus, even in the absence of any specific filamentary kinematic enhancement, the correlation between $\vec{v}$ and $\vec{f}_{near}$ is expected to increase with decreasing D_{fil} and $D_{\text{fil}}/D_{\text{cen}}$.

In order to separate a potential filament boost from this purely geometrical effect, we compute the null hypothesis (pure geometrical correlation only) by calculating $\cos\theta_{\text{H}_0}$ after rotating the filament network of each cluster by $45°$ in a random direction. Any filament-specific correlation with D_{fil} is destroyed in the flip, whereas purely geometric effects should be left unchanged on average by this procedure.

Accreting Fraction

The inability of a halo to accrete and/or retain cold gas, often referred to as strangulation, is key to its environmental quenching. We compute the inflow/outflow into/from a given halo. We first identify cold ($T < 10^5 K$) gas particles within a spherical shell with thickness $\Delta r = 0.1$ Mpc/h, at 0.5 R_{vir} of the halo. This ensures that the gas is indeed associated with the halo. The net outflow is then computed as:

$$\dot{M}_{\text{gas}}^{\text{cold}} = \frac{\sum_{\text{shell}} m_i \vec{v}_i \cdot \hat{r}}{\Delta r} \tag{2.4}$$

with m_i the mass and $\vec{v}_i \cdot \hat{r}$ the halo-centric outward radial velocity of gas particle i.

Note that a negative outflow is actually a net inflow, in which case the corresponding halo is accreting cold gas.

This allows us to define the accreting fraction of a given sample of N halos as:

$$f_{\text{acc}} = \frac{n(\dot{M}_{\text{gas}}^{\text{cold}} < 0)}{N} \tag{2.5}$$

Ram Pressure Stripping

Ram pressure stripping is expected to be the dominant quenching mechanism in the core of clusters (e.g. Wetzel et al. (2013), Roberts et al. (2019), Maier et al. (2019)). We estimate the ram pressure term on a given halo as:

$$P_{\text{ram}} = \rho_{\text{shell}} (\delta v)^2 \tag{2.6}$$

with δv the halo to intra-cluster medium relative velocity and ρ_{shell} the density of the hot intra-cluster gas that the halo is passing through. ρ_{shell} is estimated as a volume-weighted average of individual densities for all particles within a 0.5 Mpc/h thick spherical shell past the halo's virial radius, which we call the 'environment'. Only gas particles with T $> 10^5$K are considered since colder particles are expected to be escaping or bound to the halo.

δv is defined as $|\vec{v}_{\text{halo}} - \vec{v}_{\text{enviro}}|$, with $\vec{v}_{\text{enviro}}$ the mass-weighted average velocity of hot gas particles in the 'environment' shell and $\vec{v}_{\text{halo}}$ the mass-weighted average velocity of all particles (dark matter, star, gas) within 1 R_{vir} of the halo.

We note that we expect the stripping due to ram pressure to be excessive in this simulation, as in most numerical simulations with similar resolutions, as inner halos are not resolved with enough particles to properly account for their inner core density and tend to be more easily stripping. The relative differences in values, not the exact amounts, are the focus in this work.

Gas Unbinding Parameter

To better estimate the individual degree of gas stripping a galaxy-hosting halo undergoes, we construct for each halo an instantaneous gas unbinding parameter, B_g, which quantifies the degree of displacement between the gas particles and the stellar and dark matter particles in their phase-space distributions, within 1 R_{vir} of the halo. For a given halo, B_g is defined as:

$$B_g = \frac{\sqrt{(v_{x,\mathrm{g}} - v_{x,\mathrm{sdm}})^2 + (v_{y,\mathrm{g}} - v_{y,\mathrm{sdm}})^2 + (v_{z,\mathrm{g}} - v_{z,\mathrm{sdm}})^2}}{\sqrt{\sigma_{v_x,\mathrm{s}}^2 + \sigma_{v_y,\mathrm{s}}^2 + \sigma_{v_z,\mathrm{s}}^2}} \tag{2.7}$$

where $\vec{v}_{\mathrm{g}}$, $\vec{v}_{\mathrm{s}}$ and $\vec{v}_{\mathrm{sdm}}$ are the mean velocities of the gaseous, stellar, and stellar+dark matter components of the halo respectively, computed within 1 R_{vir} as averages over corresponding particles. Star and dark matter particles averages are mass-weighted while gas particles averages are density-weighted to avoid biases due to high-velocity, fly-through gas particles from the hot but less dense ICM. $\sigma_{v,s}$ is the stellar velocity dispersion within 1 R_{vir}.

Figure 2.2 is a 1-D phase space diagram which shows how B_g is constructed on an example of a dry galaxy (one with limited to no associated gas content), illustrated on one component direction of B_g only. The panel indicates the stellar mass and B_g value of the halo, with the x component of the Euclidean distance to the centre of the cluster on the horizontal axis and x velocities on the vertical axis (in the frame of the galaxy on
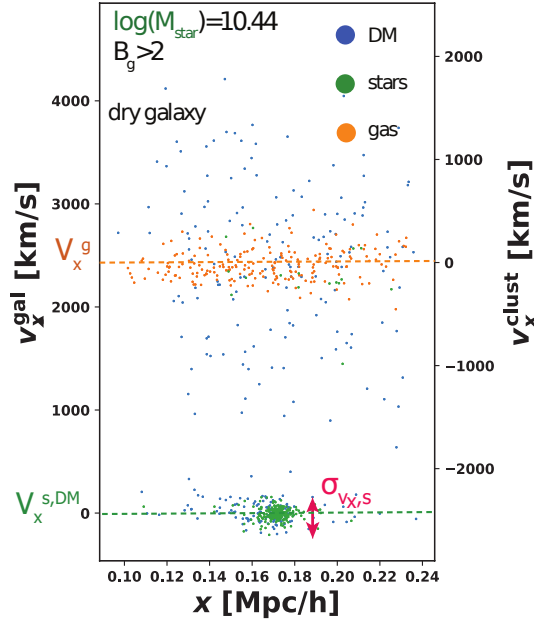
FIGURE 2.2: A pictoral representation of the construction of B_g. B_g quantifies the velocity offset of gas from the stellar and dark matter content of a halo, in terms of the stellar velocity dispersion. The stellar velocity dispersion is chosen as the stars represent the heart of the halo (where the galaxy is).

the left and the frame of the cluster on the right). Gas particles are plotted in orange, stellar particles in green, and dark matter particles in blue. The gas content is offset from the from the stellar content and the bulk of the dark matter content. As the dark matter content is more diffuse, it is more accurate to compare the offset to where the stellar content is, at the heart of the halo (the actual galaxy). B_g thus quantifies the displacement of the gas content from the galaxy and can therefore be used as a more local and adaptive measure of the effect of stripping and strangulation on a given halo.

Figure 2.3 displays 1-D phase-space diagrams of selected halos to illustrate the evolution of B_g on a few examples. Note that these diagrams use the cluster-centric distance r and radial velocities as the direction of analysis, to visually emphasize stripping.

The leftmost panel shows a typical gas-rich galaxy. Here, the dark matter, gas,
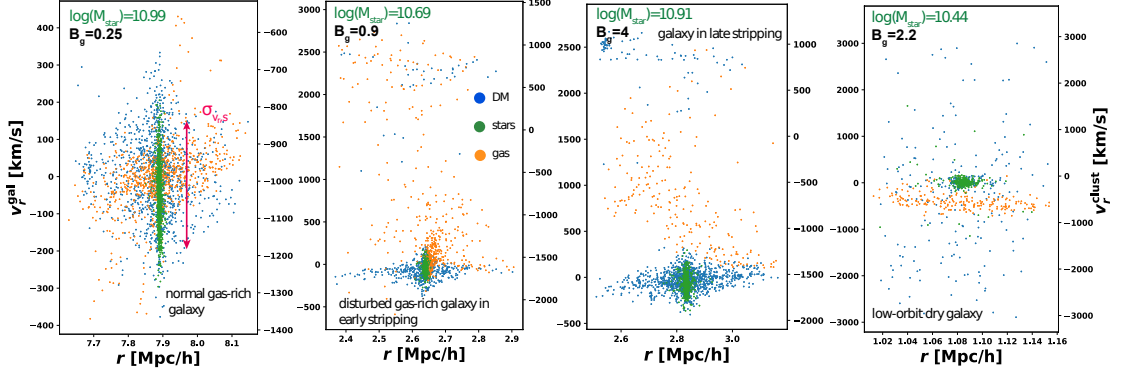
FIGURE 2.3: Varying scenarios of gas binding for halos depicted on the phase space plane. Dark matter particles are in blue, stellar particles are in green, and gas particles in orange. Cluster-centric position denoted on the horizontal axis, with velocity in two reference frames on the vertical axes (galaxy frame on the left and cluster frame on the right). Note that negative v_r^{clust} values indicate the halo is moving towards its host cluster centre. B_g is clearly lower for bound, gas-rich situations (**two left panels**) and higher for unbound, gas-poor situations (**two right panels**).

and stellar content are all centred together in phase space, and the stellar content is distinctly tightly positioned in the cluster with high velocity dispersion. The centre-left panel shows a gas-rich galaxy early in the process of undergoing stripping. Here, gas content visibly varies in velocity, with a significant fraction reaching or exceeding the escape velocity, compared to the bulk of the gas, stars, and dark matter. Depicted in the centre-right panel is a galaxy late in the process of stripping. There is little gas content associated with the same phase-space location as the dark matter and stellar content, with the majority moving at different velocities. One can see that the gas closest to the centre of the cluster is escaping while the gas further away is at the velocity of the galaxy. The rightmost panel shows the same galaxy as Figure 2.2 whose gas content is fully disassociated kinematically from the stellar content, meaning the gas displayed here is purely the ICM, and the galaxy is dry and unable to form stars. This galaxy displays almost no relative radial velocity to the cluster, and is on a nearly pure tangential motion.

2.3 Quenching of galaxies near and far from intra-cluster filaments

In this section, we use the galaxy properties outlined in Section 2.2.4 - specific star formation rates (Section 2.3.1), galaxy colours (Section 2.3.2), and cold gas fraction (Section 2.3.3) - to quantify the specific effects of intra-cluster filaments on the quenching of cluster galaxies. We highlight the specific influence of intra-cluster filaments as opposed to stellar mass effects in Section 2.3.4 and explain this influence in Section 2.3.5.

2.3.1 Survival of star forming galaxies near filaments

In this section, we analyse how filaments locally influence the fraction of star forming galaxies. Recall that we define a star-forming galaxy as a galaxy with $sSFR > 10^{-11}$ yr^{-1}, a cut chosen in accordance with observational papers (eg. Wetzel et al. (2013), Roberts et al. (2019)).

In Figure 2.4, galaxies within one virial radius of their host cluster are split into different bins based on their filamentary distance, D_{fil}, and the fraction of star forming galaxies per stellar mass bin is presented versus the stellar mass. Shaded contours display 1-σ bootstrap errors, with each stellar mass bin containing at least 750 halos. We do not investigate beyond 3 Mpc/h as there are very few galaxies this far from a filament in cluster environments.

Irrespective of distance to filament, the fraction of star forming galaxies steadily increases with stellar mass across the whole range investigated. The majority of galaxies in this simulation above stellar mass $10^{11} M_{\odot}$ are forming stars. This trend aligns with established work in that the specific star formation rate of galaxies increases steadily with stellar mass at low masses. However, as galaxies grow and quench, this relationship is expected to reverse, which in this simulation is limited to a flattening at high mass as we discussed in Section 2.2.4. Additionally, the kink observed at $10^{10.5} M_{\odot}$ is numerical
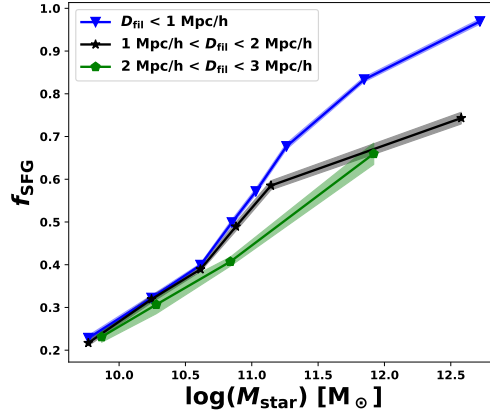
FIGURE 2.4: Evolution of the fraction of star forming galaxies, f_{SFG}, with stellar mass, split by filamentary distance D_{fil}, for all halos within 1 R_{vir} of their cluster. At fixed mass, the closer to a filament, the higher the fraction of star forming galaxies. Shaded contours are 1-σ bootstrap errors.

in origin and corresponds to the mass at which AGN feedback becomes active in the simulation.

More interestingly, at fixed stellar mass, galaxies are more star forming closer to filaments. Below $10^{10.5} M_{\odot}$ this trend is visible for galaxies less than 2 Mpc/h from a filament (green to black). It becomes increasingly significant for galaxies within 1 Mpc/h (green/black to blue) at stellar masses above $10^{11} M_{\odot}$. This result suggests that filament proximity increases the ability of cluster galaxies to form stars, irrespective of stellar mass.

We investigate this trend in the next section using SDSS galaxy colours, which do not suffer the same limitations as sSFR.

2.3.2   Galaxy colours around intra-cluster filaments

In the following, we show that the trend of filaments being a region of increased star formation is recovered with higher significance for standard SDSS galaxy colours.
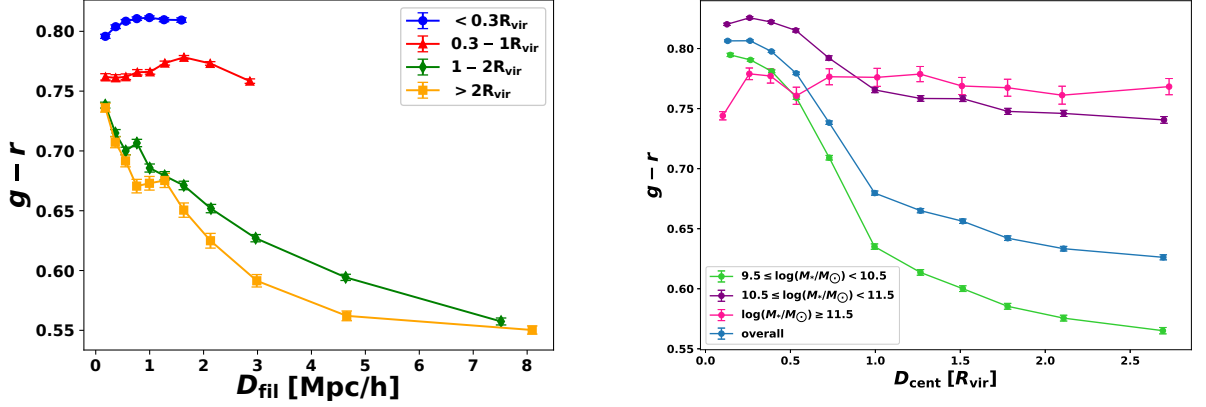
FIGURE 2.5: **Left Panel:** Mean galaxy colour $g - r$ versus distance to nearest filament D_{fil}, split by cluster-centric distance. Galaxies outside the virial radius progressively redden approaching field filaments due to pre-processing. In contrast, galaxies inside the virial radius exhibit a decrease in redness close to intra-cluster filaments. **Right Panel:** Mean $g - r$ versus distance to centre of cluster D_{cent}, for four different stellar mass bins. The majority of galaxies progressively redden towards the cluster centre. The most massive galaxies maintain their red colour across cluster-centric distances, indicating they are centrals of their own groups. All error bars are standard error on the mean. $g - r$ values above 0.65 are considered red, based on the simulated colour bimodality.

In the left panel of Figure 2.5 galaxies are split by cluster-centric distance and their mean $g - r$ colours plotted against the distance to the nearest filament. Error bars are standard error on the mean.

At fixed distance to filament, D_{fil}, galaxies are redder at smaller cluster-centric distances. Galaxies residing at 1-2 and >2 R_{vir} are similar with respect to $g - r$ colours at fixed filamentary distance, and are noticeably bluer than the $g - r$ colours of galaxies residing at <0.3 and 0.3-1 R_{vir}. This difference clearly demarcates the expected environmental differences inside and outside the cluster, where galaxies inside a cluster's virial radius are significantly redder due to quenching.

Galaxies further than 0.3 R_{vir} from cluster centre are progressively redder closer to filaments up until 2 Mpc/h away, an increase of approximately 0.12 in colour in all cases.

Galaxies at 1-2 and >2 R_{vir} continue to redden even closer to filaments. This trend beyond the cluster virial radius is consistent with what is observed for filaments in the field, which host on average more massive galaxies than their surroundings (A1, Section 2.6) and are increasingly considered a region of pre-processing, due to increased turbulence and interactions (e.g. Kraljic et al. (2017), Laigle et al. (2017), Sarron et al. (2019)). On the contrary, those galaxies in the inner two cluster-centric bins display a smooth decrease in redness of approximately 0.02 coming within 2 Mpc/h from a filament, despite the fact that they are still on average more massive than their counterparts further away (A1, Section 2.6). This novel trend inside the cluster indicates that intra-cluster filaments tend to alleviate the reddening of galaxies in their vicinity.

While this the effect may seem small compared to a seemingly large increase of $g - r$ towards filaments outside of their immediate vicinity, it is important to remember that distance to filament and distance to the centre of the cluster are correlated and therefore the specific filamentary effect must be disentangled from effects due to proximity to the cluster's core.

On the right panel of Figure 2.5, mean $g - r$ galaxy colour is plotted against cluster-centric distance, separated into stellar mass bins.

The trend for all galaxies up to $10^{11.5} M_{\odot}$ indicates that galaxies redden ($g - r$ increases) as they approach the cluster centre. This increase is most marked inside the cluster virial radius, consistent with established expectations for galaxies, which quench as they fall into clusters (e.g. Balogh et al. (2000), Haines et al. (2015), Raichoor and Andreon (2012), Pintos-Castro et al. (2019)).

By construction, galaxies closer to the cluster centre have smaller distances to filament on average. Most of the $g - r$ initial increase with D_{fil} within the cluster observed on the left panel can actually be traced back to this effect and the fact that galaxies closest to

filaments tend to be more massive and therefore redder, and is not a genuine correlation with the filament.

Beyond the virial radius ($D_{\text{cent}} \geq 1R_{\text{vir}}$), the most massive galaxies are the reddest, and the least massive galaxies are bluest, with a $g - r$ separation of at least 0.15. This trend is consistent with observations of galaxies in the field (e.g. Strateva et al. (2001), Baldry et al. (2004)).

However, note that galaxies in all mass bins display a difference in $g - r$ colour of less than 0.08 between 1 and 2 R_{vir}. This indicates that the proximity to the cluster has little effect on galaxy colour beyond the cluster virial radius, consistent with more limited quenching for galaxies residing at 1-2 and >2 R_{vir} shown in the left panel.

The rarest, most massive ($M_{\text{star}} > 10^{11.5} M_{\odot}$) galaxies are largely unchanged in $g - r$ colour irrespective of their cluster-centric distance. This is due to the fact that most of these galaxies are likely centrals of their own massive groups/small satellite clusters, and are therefore less impacted by the main cluster than by their local environment.

To summarize, evolution of $g - r$ with D_{cent} indicates that the galaxies closest to the cluster centre are reddest, and that the more massive galaxies, excluding those that are centrals of their own groups, are also reddest. Given the mass distribution of halos near the spines of filaments (A1, Section 2.6), the population of cluster galaxies within a 2 Mpc/h distance to filament are dominated by these reddest of galaxies, and thus while the decrease in redness of cluster galaxies close to filaments exhibited may seem small, it is actually significant. We stress again that this decrease in redness cannot be attributed to a mass or cluster-specific effect, but is in fact an effect of the filament environment.

The fact that the colour becomes bluer, and thus the star formation exhibits a local upturn, due to intra-cluster filaments suggests that there must be an uptick in the
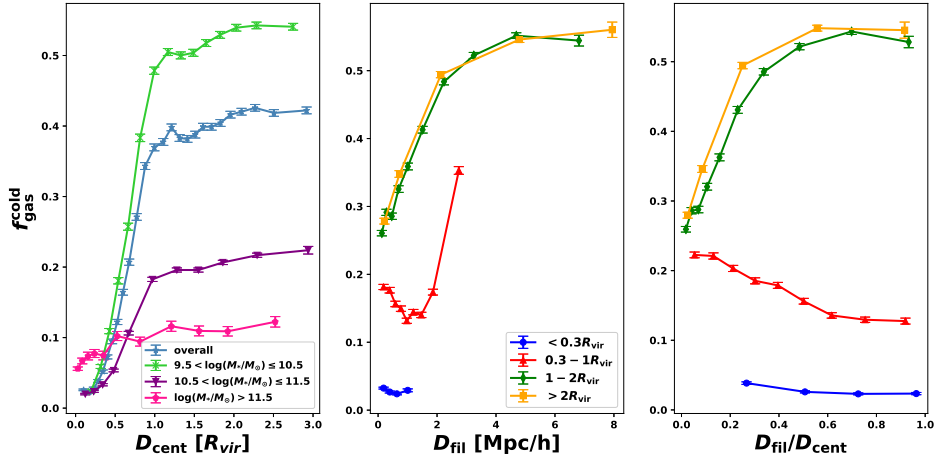
FIGURE 2.6: **Left Panel:** Mean cold gas fraction versus distance to centre of cluster, for four different stellar mass bins. Halos lose cold gas as they approach the cluster centre. **Centre Panel:** Mean cold gas fraction versus distance to nearest filament, split by cluster-centric distance. Halos outside the virial radius progressively lose their cold gas stores closer to filaments due to pre-processing. Comparatively, halos inside the virial radius exhibit an uptick in available cold gas approaching intra-cluster filaments. **Right Panel:** Mean cold gas fraction versus a halo's nearest filament distance over its cluster-centric distance, in essence an angular separation. The trends from the centre panel are replicated, with a more progressive increase for halos within the virial radius. All error bars are standard error on the mean.

amount of cold gas available to galaxies in the vicinity of filaments, which we explore in the following section.

2.3.3   Cold Gas Fraction

When galaxies are unable to refresh or retain their cold gas reserves, they quench. In the following we analyse how intra-cluster filaments affect the cold gas stores of cluster galaxies in their vicinity, by way of the cold gas fraction (as defined by Equation 2.2) of halos.

The left panel of Figure 2.6 shows the evolution of the mean cold gas fraction of halos with their cluster-centric distance, split by stellar mass. Error bars indicate standard

errors on the mean, with 5000 halos per bin, except for the curve with the most massive halos with 300 halos per bin.

Overall (light blue), the cold gas fraction of halos decreases approaching the cluster centre, with a sharp decrease inside of 1 R_{vir}. This is consistent with the result obtained for galaxy colours in the previous section and simply indicative of expected environmental quenching.

The cold gas fraction of halos decreases by at most 0.05 from 3 to 1 virial radii in any given mass bin. The least massive galaxies (light green) exhibit the largest drop in cold gas fraction, from approximately 0.5 to approximately 0.03, while more massive galaxies (purple) drop from approximately 0.2 to approximately 0.03. This aligns with the expectation that galaxies are stripped of their cold gas stores by ram pressure as they fall through the intra-cluster medium (e.g. Wetzel et al. (2013), Roberts et al. (2019), Maier et al. (2019)), with the smaller galaxies having a weaker gravitational potential to hold onto their cold gas. This figure again demonstrates that galaxy quenching is strong and progressive within the simulated clusters.

The most massive galaxies (pink) consistently maintain a cold gas fraction of approximately 0.1, dropping to approximately 0.06 only in the heart of clusters. This is again in line with the fact that these are most likely the centrals of massive groups or small clusters, affected by their local environment rather than the main cluster environment.

We examine the impact of cosmic filaments in the centre panel of Figure 2.6, which shows the mean cold gas fraction of halos in relation to their distance to closest filament, again split by cluster-centric distance. Error bars indicate standard errors on the mean, with 5000 halos per bin.

Halos residing 1-2 R_{vir} and >2 R_{vir} away from the cluster centre have similar average cold gas fractions at fixed distance to filament D_{fil}, but this gas fraction decreases sharply

with decreasing D_{fil}. This is consistent with the fact that filament galaxies are on average more massive hence redder and more gas-poor than their counterparts further away (Kraljic et al. (2017), Welker et al. (2019)).

Moreover, field filaments are the site of markedly increased galaxy numbers compared to their surroundings where galaxies are more isolated and evolve in a lower density, less violent environment. This increase in galaxy count near filaments translates into an increase in galaxy interactions and mergers. Recent studies suggest that this increase in interactions and turbulence drives some early quenching or pre-processing in filament galaxies (e.g. Kraljic et al. (2017), Laigle et al. (2017), Sarron et al. (2019)). This likely also explains the steep decrease of $f_{\mathrm{gas}}^{\mathrm{cold}}$ towards filaments for galaxies outside R_{vir}, as is investigated in the next subsection.

A different trend is observed for halos between 0.3-1 R_{vir}. The cold gas fraction increases by approximately 50% for halos closer than 1 Mpc/h to an intra-cluster filament. This upturn is in line with our previous section on galaxy colour, again indicating that intra-cluster filaments are effectively delaying quenching.

Note however that the cold gas fraction for halos beyond R_{vir} is always at least 0.1 higher at fixed filamentary distance than halos in the 0.3-1 R_{vir} bin. This is expected as halos transition from the field environment to the harsh cluster environment where cold gas is stripped, as per the left panel.

To accommodate for the bias whereby halos residing closer to the cluster centre are by definition be closer to a filament, we introduce the measure $D_{\mathrm{fil}}/D_{\mathrm{cent}}$, the angular separation of a halo/galaxy to its nearest filament, in the right panel of Figure 2.6. Error bars again indicate standard error on the mean, with 5000 halos per bin.

We see that the halos outside the cluster virial radius still exhibit a strong decrease in cold gas fraction at small filament separations, consistent with the centre panel.
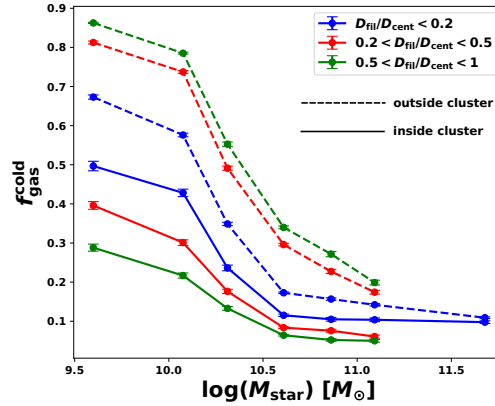
FIGURE 2.7: Average cold gas fraction versus halo stellar mass, binned by angular separation to filament and residency inside or outside a cluster. Cold gas fraction decreases with increasing stellar mass as galaxies use up cold gas for star formation. Outside a cluster, cold gas fraction decreases as angular separation to filament decreases. Inside a cluster, cold gas fraction conversely increases as angular separation to filament decreases.

But this new measure reveals a strong, progressive increase of the average cold gas fraction as the angular separation to an intra-cluster filament decreases (red). This occurs despite the increase in stellar mass associated with filament proximity and clearly points towards the ability of cluster galaxies residing near filaments to retain or accrete cold gas. In the next section, we proceed to specifically investigate any possible mass effect that might be behind the trends described in this and the previous section.

2.3.4   Mass-driven effects

We have established that halos close to intra-cluster filaments appear bluer and contain more cold gas than their counterparts further away, while halos outside clusters display the opposite trend. It is important to ensure that these effects are due to filaments and not merely due to a halo's stellar mass as there is a strong increase in stellar mass near the spine of filaments (A1, Section 2.6). We therefore analyse the direct relationship of the cold gas fraction with stellar mass in this section.

Figure 2.7 shows the average cold gas fraction for halos against their stellar mass, distinguished by both angular separation ($D_{\mathrm{fil}}/D_{\mathrm{cent}}$) and residency inside or outside the cluster virial radius. All errors are standard error on the mean. The smallest bin contains at least 350 halos.

Across all angular separations and distances to the cluster centre, the average cold gas fraction markedly decreases with increasing stellar mass. This is expected as galaxies use up their cold gas stores to form stars and become more massive. It also confirms that it is not possible for the increase in cold gas fraction exhibited by halos near intra-cluster filaments in Figure 2.6 to be caused by the increase in stellar mass associated with filament proximity.

The most massive halos, those with stellar masses greater than approximately $10^{11} M_{\odot}$, are usually found along the spine of cosmic filaments (often being secondary nodes of the cosmic web), hence reside at the smallest angular separations (blue). Noticeably, there is less than 0.05 difference in cold gas fraction between these massive halos that reside outside (dashed) versus inside (solid) the cluster environment, the smallest difference across any fixed mass. This re-iterates that these halos are centrals of massive groups which do not feel the effects of the transition to, and journey through, the cluster environment.

At fixed stellar mass outside the cluster environment (dashed lines), cold gas fraction decreases as angular separation to filament ($D_{\mathrm{fil}}/D_{\mathrm{cent}}$) decreases. This effect is present irrespective of stellar mass and largest for the lowest mass halos. This is in line with our previous results but now indicates clear pre-processing of field galaxies in filaments outside clusters at all stellar masses.

Opposing this, at fixed stellar mass inside the cluster environment (solid lines), cold gas fraction increases as angular separation to filament decreases, again most effectively

for the lowest mass halos, although apparent across the stellar mass range. This indicates that the halting of quenching we established in these regions is caused by the presence of the intra-cluster filaments, rather than an effect of the mass distribution. We discuss this novel contrast in the following section.

2.3.5   Contrasting intra-cluster filaments with their field counterparts

The fact that the impact of intra-cluster filaments on local galaxies run contrary to those of field filaments may seem surprising. It should however be stressed that in the field, filaments are a region of increased interaction and disruption compared to the lower density background governed by less turbulent cosmic flows (Aragon Calvo et al. 2019). However, in clusters, interactions and stripping by the dense, hot, turbulent intra-cluster medium are ubiquitous and dominant effects. Thus, while field filaments represent a more dynamic environment relative to their surroundings, intra-cluster filaments may on the contrary be quiet in comparison to the rest of the cluster. Indeed, the ability of filaments to channel colder, more laminar gas streams along their spine deep into the cluster may help galaxies resist quenching from ram pressure stripping or strangulation, either by allowing more gas accretion onto galaxies or by lowering the local ram pressure onto halos.

Figure 2.8 summarizes these expectations and illustrates this scenario, which we investigate in Section 2.4 by carefully analyzing the dynamics of both the intra-cluster medium and galaxies around filaments.

2.4   Halting quenching: dynamics of gas and galaxies around filaments

Having established that cluster galaxies in proximity to cosmic filaments exhibit telltale signs of delayed quenching, we investigate the dynamics of halos and gas flows around
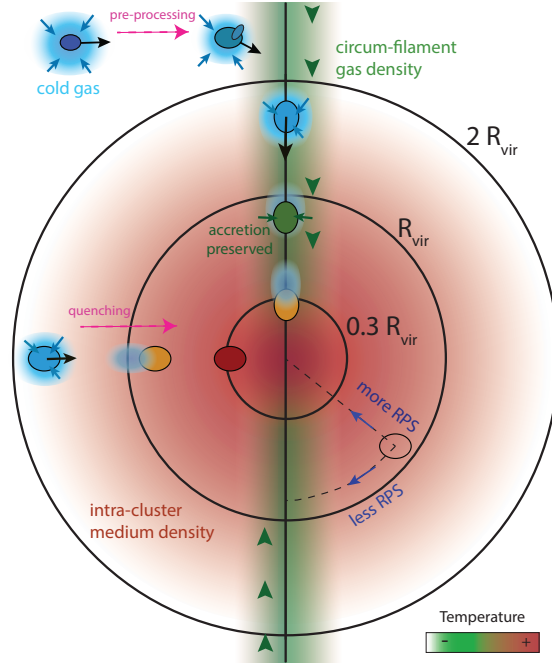
FIGURE 2.8: A schematic representation of our physical hypothesis. Galaxies closer to intra-cluster filaments experience delayed quenching due to protection from strangulation (since accretion is preserved) and ram pressure stripping (RPS).

filaments in the cluster environment to understand the origin of this effect. We begin by analyzing the density and temperature of the gas around filaments in Section 2.4.1. We then analyze the flows of galaxies and diffuse gas in their vicinity in Section 2.4.2. In turn, we look at how halos become starved or continue accreting cold gas near filaments in Section 2.4.3. We specifically estimate ram pressure around halos in Section 2.4.4. Finally, we further our analysis by estimating dynamically, at the halo scale, the degree of gas disturbance of individual halos in Section 2.4.5.

2.4.1 Density and temperature of intra-cluster filaments

As gas, specifically cold gas, is crucial to star formation, we examine the gas around filaments to understand the intra-filament medium and how it delays the quenching of cluster galaxies.
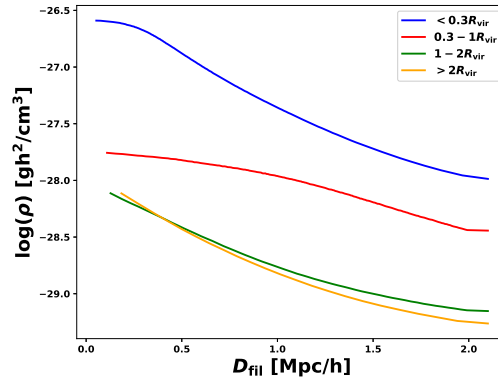
FIGURE 2.9: Density profile of gas around filaments. Gas within one virial radius of halos is excluded to focus on the intra-filament medium. Values are volume-weighted averages of gas particle densities. Density increases approaching the spine of filaments.

Figure 2.9 shows the cylindrical density profile of diffuse gas around filaments in our simulation. Gas is binned by its cluster-centric distance, and we exclude all gas within the virial radius of satellite halos in order to focus on the background gas profile of the intra-cluster medium rather than the gas already within halos. We verified that including gas in halos did not qualitatively modify the results. We present volume-weighted average values.

Irrespective of distance to the centre of the cluster, all curves progressively see an increase in diffuse gas density approaching the spine of filaments. This is to be expected, as by definition density peaks at the spine of cosmic filaments. However, the overall increase in density of diffuse gas from 2 Mpc/h from a filament to its spine is approximately a factor of 10 for the 1-2 and >2 R_{vir} bins, compared to a factor of 3 in the 0.3-1 R_{vir} bin. This decrease in density contrast for diffuse gas near filaments within R_{vir} was found to be in part an effect of the correlation between D_{fil} and D_{cent} and the contrast is limited to less than a factor of 2 when correcting for this effect. Filaments are therefore not very contrasted in terms of density within the cluster.

In comparison, at fixed distance to filament (D_{fil}), gas is markedly denser closer to cluster centre. Moving from outside the cluster (1-2 and >2 R_{vir}) to the 0.3-1 R_{vir} region, an increase in density by at minimum a factor of 3 is present (≈ 6 on average), and similarly moving from that bin to the deepest cluster-centric bin (<0.3 R_{vir}). This shows that clusters are increasingly dense environments toward their centres and that this density increase is dominant over the filamentary increase within R_{vir}.

Therefore, while density-induced quenching mechanisms are relevant for field filaments, we cannot expect that same impact from intra-cluster filaments. This is re-visited in Section 2.4.4 when we examine ram pressure stripping in detail.

Gas closest to cluster centre exhibits the largest increase in density approaching filament spines. However, once again, for gas within 0.3 R_{vir} moving towards the closest filament is largely the same as moving towards the cluster centre where the central node of filaments resides. As such, this is more a representation of increasing cluster density rather than a trait of filaments at this depth within clusters.

While the density contrast of intra-cluster gaseous filaments is limited, this may not be the case for their temperature contrast.

Indeed, in the field, as it collapses into filaments, gas shocks and cools, so the spine of filaments may funnel cooler gas towards the nodes of the cosmic web (e.g. Katz and White (1993), Brooks et al. (2009), Kereš et al. (2009), Kleiner et al. (2016)).

However, whether cold flows persist deep into the cluster environment has been subject to debate as intense enough streaming instabilities, active galactic nuclei, and supernova feedback might shred them apart (e.g. Powell et al. (2011), Dubois et al. (2012b), Zinger et al. (2016), Zinger et al. (2018)).

Figure 2.10 shows the temperature profile of gas around filaments, cylindrically in
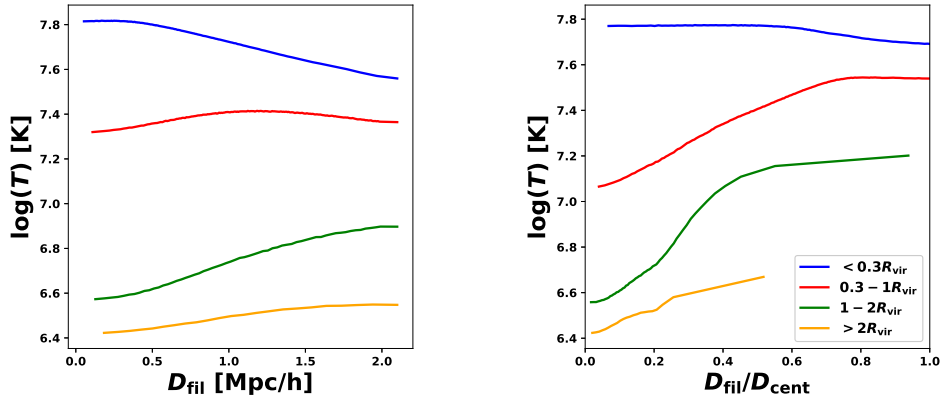
FIGURE 2.10: Temperature profile of gas around filaments, radially (**Left Panel**) and by angular separation (**Right Panel**). Values are volume-weighted averages of gas particle temperatures. Filaments persist as cooler gas streams down to 0.3 R_{vir}.

the left panel and with angular separation (D_{fil}/D_{cent}) to filament in the right panel. Gas is again separated by cluster-centric distance, and gas within the virial radius of halos is excluded. Values shown are volume-weighted averages.

Gas residing further than 0.3 R_{vir} from cluster centre does exhibit progressive cooling approaching filaments radially (left panel), an effect that is even sharper at decreasing angular separation (right panel). This demonstrates that filaments persist as cooler flows down to this depth in the cluster environment. Notably, gas in the 0.3-1 R_{vir} bin in the left panel exhibits cooling passing within a 1 Mpc/h radius to a filament, in line with the radius of influence exhibited for colour (Figure 2.5) and cold gas fraction (Figure 2.6).

Note that in both panels, gas deeper within a cluster (orange to blue) is consistently hotter across all distances to filament and angular separations. This is expected as temperature is demonstrated to increase deep within clusters due to the fact that density also increases. However, cluster gas within $0.3 - 1R_{vir}$ at small filament angular separations ($D_{fil}/D_{cent} < 0.2$) is actually colder than outskirt gas (within $1 - 2R_{vir}$) at large separations ($D_{fil}/D_{cent} > 0.4$), a region where galaxies typically undergo little to no

quenching.

Temperature strictly increases for the deepest gas bin. As discussed for the density profile, at this depth moving towards the filament highly correlated to moving towards the cluster centre. Thus, this rise in temperature is due to the fact that density increases towards the cluster centre.

Since both halos (Section 2.3.3) and filaments (this Section) exhibit a stark increase in cold gas out to 1 Mpc/h, and progressively with decreasing angular separation, this suggests that interactions between halos and the intra-filament medium might be the origin of the resistance of local halos to quenching. In the following section, we examine how both the diffuse gas and halos flow along intra-cluster filaments.

2.4.2 Flows near filaments

To understand how the cooler gas streams of intra-cluster filaments interact with halos, we first examine their respective flows along filaments.

In the left panel of Figure 2.11, we plot the median evolution of the cosine of θ, the angle between the velocity vector of a halo and its nearest filament direction, as computed in Equation 2.3 (oriented inwards). The angular separation version of this plot can be found in A2 (Section 2.7). Halos are split into bins by their cluster-centric distance. The dashed lines represents the null hypothesis (no specific impact of filaments) whereby the filament network of each cluster is rotated by 45° in a random direction before the measurements as explained in Section 2.2.5. A median value of $\cos(\theta) = 1$ would mean all halos are flowing inwards parallel to their nearest filament, and in case of random flows we expect a median $\cos(\theta) = 0$. In theory, values close to 0 can also be obtained if all halos flow perpendicular to the filament but in such a case we would also have a median $|\cos(\theta)| \approx 0$ and we verified that $|\cos(\theta)| > 0.5$ in all bins up to 4 Mpc/h
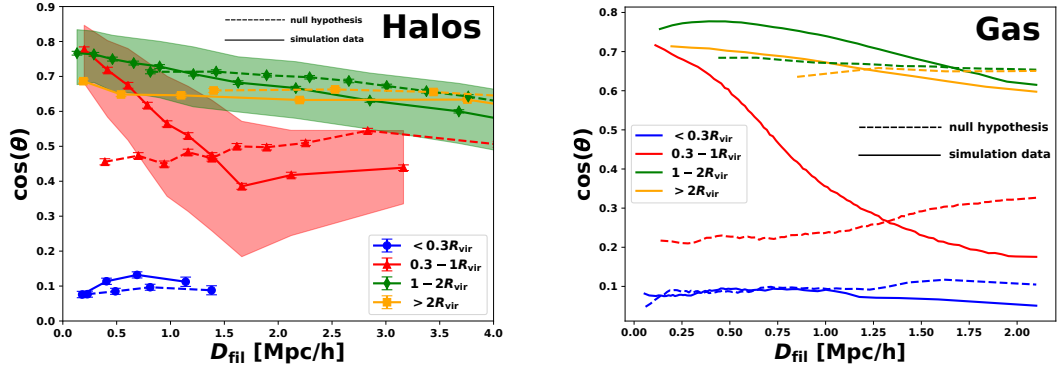
FIGURE 2.11: **Left Panel:** The median evolution of the cosine of the angle between the velocity vector of a halo and its nearest filament versus distance to filament. Error bars are standard error on the mean and coloured contours indicated the 40-60 percentile spread. Dashed lines represent the null hypothesis whereby the full filament network of each cluster is rotated 45° in a random direction to separate any geometric effect (any geometric effects are left untouched by this flip). Halo flows between 0.3 and 1 virial radius become sharply aligned with their nearest filament closer than 2 Mpc/h away. **Right Panel:** The median evolution of the cosine of the angle between the velocity vector of a gas particle and its nearest filament versus distance to filament. Dashed lines again indicate the null hypothesis. As with halos, gas flows within the cluster becomes strongly aligned with their nearest filament.

away from filaments, suggesting at least relative alignment due to radial flows into the cluster.

Error bars indicate standard error on the mean, while coloured contours indicate the spread from the 40th to the 60th percentile. There are 5000 halos per bin.

At distances to filament (D_{fil}) greater than 2 Mpc/h, halos residing beyond 1 virial radius (1-2 and >2 R_{vir}) have $\cos(\theta)$ values above 0.6 and are higher than those residing inside 1 virial radius (<0.3 and 0.3-1 R_{vir}). This indicates that halos outside the cluster environment tend to flow more parallel to their filaments and more consistently inwards than halos inside the cluster environment, which evolved in a highly mixed, multi-streaming region and can also experience backsplash.

In contrast, halos 0.3 to 1 R_{vir} away from the cluster centre display a strong increase in median $\cos(\theta)$ within 2 Mpc/h from the filaments, from 0.4 to 0.8. This indicates that galaxy flows go from less to more aligned with intra-cluster filaments as they approach them. It is important to notice that this sharp increase in $\cos(\theta)$ values is not replicated in the null hypothesis for these haloes, indicating that it is not simply a geometric effect due to radial flows.

Moving to the cluster's core, halos closest to the centre ($< 0.3R_{\text{vir}}$) have $\cos(\theta)$ values close to 0 across the filamentary distance range they are found. This indicates high mixing and little to no correlation between the flow of these halos and their nearest filament. In line with our discussion in the previous section, we do not expect filaments to stand out as cold gas flows in this regime.

We next look at how the diffuse gas is flowing around and away from filaments using the same measure. The right panel of Figure 2.11 displays the evolution of median $\cos(\theta)$, computed from the gas particles' velocities, against D_{fil}. (The angular separation version of this plot can be found in A2 (Section 2.7).) Similar to halos, gas beyond the cluster virial radius (orange and green curves) tends to have higher $\cos(\theta)$ values than gas inside of the cluster virial radius (blue and red curves). This indicates that flows of gas outside of the cluster environment are strongly radial to the cluster and coherent along filaments even 2 Mpc/h away from filaments. The specific enhancement of alignment with filaments (compared to the null hypothesis in dashed lines) is clear within 1.5 Mpc/h from the nearest filament.

Gas in the 0.3-1 R_{vir} bin sees a strong, progressive increase in $\cos(\theta)$ values at distances lower than 1.3 Mpc/h from intra-cluster filaments, going from 0.2 to 0.7. The null hypothesis in this bin clearly does not exhibit this same increase, indicating that gas streams are markedly more coherent along intra-cluster filaments than further away and that this is not simply a geometric correlation with radial cluster flows.

Once again, gas closest to the cluster centre (blue curve) exhibits the lowest $\cos(\theta)$ values with fluctuation of less than 0.05 across the filamentary distance range. As with the halos in this regime, we are seeing mostly random flows, strengthening the conclusion that gas filaments do not persist at this cluster depth.

In summary, both gas and halos hosting galaxies are flowing together in coherent streams along filaments inside the cluster in the region down to 0.3 $R_{\rm vir}$. This supports the idea that cluster galaxies close to filaments may retain the ability to accrete gas efficiently, and/or undergo reduced ram pressure stripping. This is further investigated in the next sections.

2.4.3   Fraction of accreting halos

Given that halos and cooled gas flow together along intra-cluster filaments, we now analyse the ability of cluster halos to keep accreting cold gas near and far from filaments. We quantify how galaxies are accreting cold gas using Equations 2.4 and 2.5.

Figure 2.12 shows the fraction of halos accreting cold (T$<10^5$ K) gas against their angular separation ($D_{\rm fil}/D_{\rm cent}$) to their nearest filament. As usual, halos are binned based on their cluster-centric distance. Coloured contours indicate 1-σ bootstrap errors. There are 2500 halos per bin.

As expected, halos residing beyond one virial radius (1-2 and $>$2 $R_{\rm vir}$) have consistently higher accreting fractions than those residing inside one virial radius ($<$0.3 and 0.3-1 $R_{\rm vir}$), across the entire angular separation range. Given that the field environment is colder and less turbulent than the cluster environment, it follows that it is generally more likely for a galaxy to be accreting cold gas in the field than inside the cluster.

These halos mostly experience a progressive decrease in accreting fraction at smaller angular separations. The secondary increase of accreting fraction at the spine of filaments
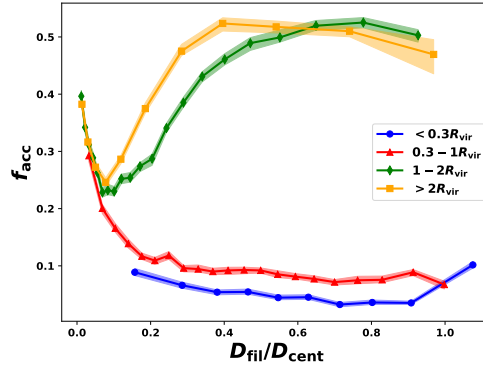
FIGURE 2.12: The fraction of halos which are accreting cold (T<10^5 K) gas versus angular separation to filament. Halos are binned based on cluster centric distance, and 1-σ bootstrap errors are indicated by the coloured contours. Halos between 0.3 to 1 virial radius experience a resurgence in accretion closer than an angular separation of 0.2 from their nearest filament.

($D_{\mathrm{fil}}/D_{\mathrm{cent}} < 0.1$) is a bias, once again due to the presence of massive groups (hosting massive centrals) at the spine of filaments (A3, Section 2.8). For these halos outside the cluster, their accretion essentially decreases near filaments, as they undergo more interactions and experience pre-processing.

In contrast, halos between 0.3 and 1 virial radius exhibit a progressive increase in accreting fraction from below 10% to 30% when approaching the spine of a filament, from an angular separation of 0.3 to 0.1. In A3 (Section 2.8), Figure 2.17, we show that this increase in accreting fraction at low angular separations is observed at all stellar masses and not simply related to the underlying mass distribution near filaments.

At angular separations $D_{\mathrm{fil}}/D_{\mathrm{cent}} > 0.3$, only around 10% of halos in this cluster-centric distance range are accreting. This indicates that the coherent flows of gas and halos along filaments result in effective accretion of cold gas into filament halos inside the cluster environment.

No more than 10% of halos within 0.3 R_{vir} are accreting at any given angular separation. As we have established before, this regime does not contain filaments as cool gas flows, and the centre of the cluster environment contains the warmest gas as established in Figure 2.10.

Within the cluster environment, these are clear indicators that the cold gas flows that galaxies are streaming along with near filaments are refreshing their fuel supply in an otherwise extremely hot, violent environment. This supports the idea that intra-cluster filaments provide relief from quenching by reducing local strangulation.

2.4.4   Ram pressure stripping

We quantify the ram pressure stripping that our halos experience near and far from filaments to assess whether filaments can in fact reduce it, given that it is a dominant effect deep within clusters. We estimate ram pressure, $P_{\mathrm{ram}} = \rho_{\mathrm{shell}}(\delta v)^2$, as described in Section 2.2.5.

Outside clusters, simulations suggest that ram pressure values are typically lower than 10^{-13} Pa·h^2, while deep inside clusters, they can increase to around 10^{-11} Pa·h^2 (e.g. Tonnesen and Bryan (2009), Tecce et al. (2010), Marshall et al. (2017)).

Figure 2.13 displays the variation of ram pressure around halos with angular separation ($D_{\mathrm{fil}}/D_{\mathrm{cent}}$) to their nearest filament, separated by cluster-centric distance. Halos residing at 0.3-1 R_{vir} are further separated by the mass of the cluster in which they reside.

Halos residing at 1-2 and >2 R_{vir} experience much lower ram pressure than those halos at <0.3 and 0.3-1 R_{vir}. This is to be expected as halos enter the hot, dense, intra-cluster medium within a cluster's virial radius. We explore the evolution of ram pressure with a halo's cluster-centric distance in A4 (Section 2.9), Figure 2.19.
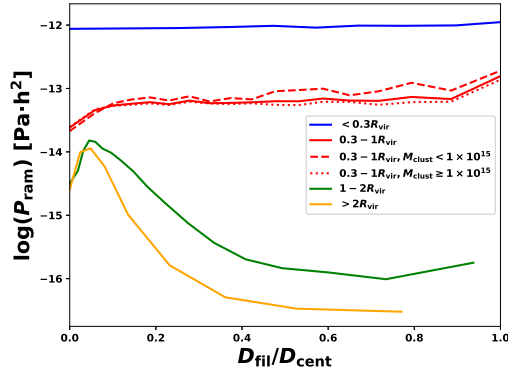
FIGURE 2.13: The ram pressure, $\rho_{\text{shell}}(\delta v)^2$, of halos against their angular separation to nearest filament. Halos are binned by cluster-centric distance, and for those 0.3-1 R_{vir} further separated by host cluster mass. Regardless of host cluster mass, ram pressure for galaxies within the cluster environment does not increase approaching filaments and in fact decreases at small angular separation. The coherent flows of halos and galaxies around intra-cluster filaments and the small density contrast to the intra-cluster medium leads to this result.

For halos living at 1-2 and >2 R_{vir}, ram pressure significantly increases from less than $10^{-16.5}$ to $10^{-14.5}$ Pa·h^2 at decreasing angular separation to nearest filament. The decrease noted at less than 0.1 angular separation from approximately 10^{-14} to $10^{-14.5}$ Pa·h^2 is of little significance for quenching considering the median ram pressure values within cluster virial radii, where ram pressure is important for quenching, are greater than 10^{-14} Pa·h^2 for halos in the simulation, as seen in Figure 2.19 in A4 (Section 2.9). The large increase in ram pressure approaching filaments in the field can largely be explained by the increase in density approaching field filaments in comparison to the background field.

Starkly different, halos living at <0.3 and 0.3-1 R_{vir} away from the cluster centre see no increase in ram pressure stripping with decreased angular separation to filaments. Of particular interest, halos in the 0.3-1 R_{vir} bin experience a slight decrease in median ram pressure from around $10^{-13.3}$ to around $10^{-13.6}$ Pa·h^2 coming within an angular separation of 0.1 from their nearest filament, regardless of host cluster mass. This is the

equivalent of median decrease in ram pressure a halo would experience being at 0.7 R_{vir} from the cluster centre rather than 0.6 R_{vir}, as seen in Figure 2.19, a very significant difference in the context of quenching.

Ram pressure stripping not only relies upon the ram pressure a galaxy experiences, but the gravitational potential of the galaxy. Given that halos are increasingly massive approaching the spine of filaments (A1, Section 2.6), it follows that these halos have larger gravitational potentials. This, in combination with the fact that ram pressure experiences a significant decrease approaching intra-cluster filaments, indicates that ram pressure stripping is actually decreased for cluster galaxies near filaments.

This is evidence that the coherent streams of cold gas along intra-cluster filaments and the filaments' limited contrast in density to the intra-cluster medium mean that filaments are delaying quenching for cluster galaxies by reducing the stripping of gas from cluster galaxies. We further analyse the dynamical extent of this stripping on the halo scale in the next section.

2.4.5   Quantifying the gas stripping in halos: the gas unbinding parameter

Where ram pressure stripping is dominant, galaxies have long tails of gas trailing behind them (e.g. Ebeling et al. (2014), Poggianti et al. (2017)). Once effectively stripped, nearly all cold, star-forming gas is completely disassociated with the star and dark matter content of a halo. That is, the gas is unbound. The unbinding parameter, B_g, defined in Section 2.2.5 quantifies how stripped/disturbed the gas content in a given halo is. The lower the B_g of a halo, the more associated its gas content is with the stellar and dark matter components, and thus the less stripped (and more bound) it is. For B_g greater than about 2, the gas is mostly unbound and increasing values relate to increasing differential velocity between the halo and the ICM.
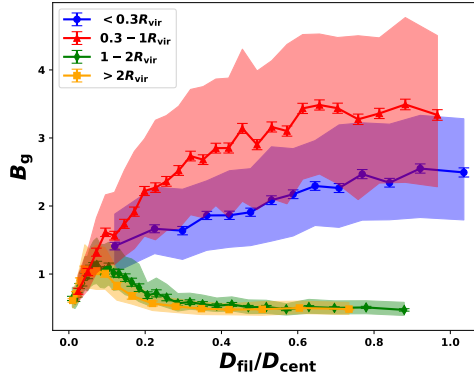
FIGURE 2.14: The median gas unbinding parameter, B_g, of halos against their angular separation, from their nearest filament. Halos are split by cluster-centric distance. Coloured contours indicate the 40th to 60th percentile spread, error bars indicate the standard error on the mean. Lower B_g values indicate more bound gas. Cluster halos exhibit a smooth decrease in B_g towards filaments, while outskirt halos mostly exhibit an increase of B_g.

Figure 2.14 shows the median evolution of B_g with respect to a halo's angular separation ($D_{\text{fil}}/D_{\text{cent}}$) to its nearest filament. Halos are binned by their cluster-centric distance and coloured contours indicated the 40th to 60th percentile spread, while error bars indicate the standard error on the mean. There are 1500 halos per bin.

Halos that reside at 1-2 and >2 R_{vir} have significantly lower B_g values than those that reside at <0.3 and 0.3-1 R_{vir} when further than 0.2 angular separation from their nearest filament. As seen with other measures in this work, this is expected as galaxies in the field are in a quiet environment and thus retain their gas, while those in clusters are at various stages of being stripped.

Halos residing at 1-2 and >2 R_{vir} see an increase in their B_g value at smaller filament angular separations, particularly within $D_{\text{fil}}/D_{\text{cent}} < 0.2$. This indicates that galaxies closer to field filaments see an increased disassociation from their gas content, with tails of gas streaming behind them. This is consistent with the increased density and ram pressure stripping established in outskirt filaments. Note that the sudden decrease of

B_g at the spine is once again a mass effect related to the local over-representation of massive group centrals (A1, Section 2.6).

In clear contrast with this result, halos residing 0.3 to 1 R_{vir} from the cluster centre display a strong, progressive decrease in their B_g values at decreasing angular separation to their nearest filament, progressing from a median B_g of over 3 at $D_{\mathrm{fil}}/D_{\mathrm{cent}} > 0.5$ to below 1 at $D_{\mathrm{fil}}/D_{\mathrm{cent}} < 0.1$. Cluster galaxies far from filaments are expected to be heavily stripped as they pass through the intra-cluster medium, resulting in high B_g values reflecting gas mostly completely disassociated from the stellar and dark matter components of the halo. The decreased B_g values of halos closer to intra-cluster filaments indicates that the gas in such halos is significantly less disturbed than that of halos further away from filaments. Hence such filaments are indeed providing galaxies relief from gas stripping, resulting in more bound gas in these galaxies.

We further verify in A3 (Section 2.8, Figure 2.18) that these results hold at all stellar masses. These trends in gas binding are therefore distinctly correlated with the presence filaments.

Note that virtually all halos less than 0.3 R_{vir} from their cluster centre have B_g values greater than 1 but usually less than 3. Galaxies in this region are significantly stripped of their gas, yet their differential velocity with the ICM is much reduced as they lie in the cluster centre.

Overall, we have demonstrated that the combination of increasingly coherent, colder gas flows allowing for effective accretion and decreased ram pressure stripping in filaments makes them an environment where cluster galaxies are protected from environmental quenching, and can see increased star formation rates.

2.5   Discussion and Conclusion

In this study, we used 324 simulated clusters to analyse how the properties of cluster galaxies vary with respect to their proximity to cosmic filaments. We find that galaxies exhibit delayed quenching closer to intra-cluster filaments, in contrast to established trends for galaxies near field or outskirt filaments. We find that decreased strangulation and ram pressure in the vicinity of intra-cluster filaments provide a mechanism to explain these trends.

In detail, the trends we find for galaxies are that:

- The fraction of star forming cluster galaxies increases closer to filaments, irrespective of stellar mass. This indicates that intra-cluster filaments play an important role in modulating star formation that extends beyond hosting more massive galaxies than their surroundings.

- Outside clusters, galaxies are redder closer to filaments. Inside clusters, they level off in colour and are bluer closer to filaments.

- Outside clusters cold gas fraction decreases for galaxies closer to filaments. Inside clusters, galaxies near filaments display significantly increased cold gas fractions compared to their counterparts further from filaments.

These results show that, while filaments are associated with pre-processing in low or average density environments, deep cluster filaments delay the quenching of galaxies in the hot, dense cluster environment. Further investigating the origin of this quenching delay we find that:

- Filaments diving deep into clusters, down to $0.3R_{\mathrm{vir}}$, are regions of coherent gas flows markedly colder than the ICM.

- The density contrast of intra-cluster filaments with the intra-cluster medium is less than for field or outskirt filaments with their background environments.

- Galaxies and cold gas flow together more coherently along filaments closer to their spines.

- The fraction of galaxies accreting cold gas within the general cluster environment dramatically increases approaching filaments, indicating a decrease in strangulation.

- Ram pressure slightly decreases closer to intra-cluster filaments. In addition, galaxy mass and thus gravitational binding tends to increase. As a consequence, ram pressure stripping is decreased for cluster galaxies closer to filaments.

- The gas in galaxies closer to intra-cluster filaments is more bound and less disturbed than for galaxies in the rest of the ICM.

Intra-cluster filaments are therefore clearly a region of reduced quenching where cluster galaxies can keep forming stars as they fall deeper into the cluster, a striking difference from their field and outskirt counterparts.

Further work will focus on investigating the time evolution of halos in the simulation, tracking halos as they evolve with the filaments to identify how quickly and strongly the delay in quenching appears. Higher resolution cluster simulations such as RomulusC (Tremmel et al. 2018) which better resolve the cluster regime, where hydrodynamic streaming instabilities and feedback processes may affect the structure of intra-cluster filaments, could also be used to confirm our analysis. DisPerSE has been used on data from large surveys such as GAMA (Kraljic et al. (2018) and Welker et al. (2019)) and COSMOS (Laigle et al. 2017) to build the cosmic web. This can in principle be used to detect filaments plunging into clusters in 2D. This could be combined with detailed

information on galaxy colour and gas content to confirm and extend our results in observations.

2.6   A1: Evolution of stellar mass with filament proximity

Figure 2.15 shows the median halo stellar mass versus distance to nearest filament ($D_{\rm fil}$ - **left panel**) and angular separation to nearest filament ($D_{\rm fil}/D_{\rm cent}$ - **right panel**). Halos are separated by cluster-centric distance, and coloured contours indicate the 40th-60th percentile spread. Overall, as expected, stellar mass is increasing at lower distance to filament and angular separation but the increase is actually very peaked at the spine of filaments. Indeed, no change in median stellar mass is observed across cluster-centric bins further away than 1Mpc/h from filaments (or at angular separation larger than 0.2). An increase in halo stellar mass is detectable at $D_{\rm fil} < 1$ Mpc/h, but the most significant increase in stellar mass is confined within very low filament distances/angular separations ($\approx 80\%$ increase towards the spine across the inner 0.5 Mpc/h or $D_{\rm fil}/D_{\rm cent} < 0.05$).
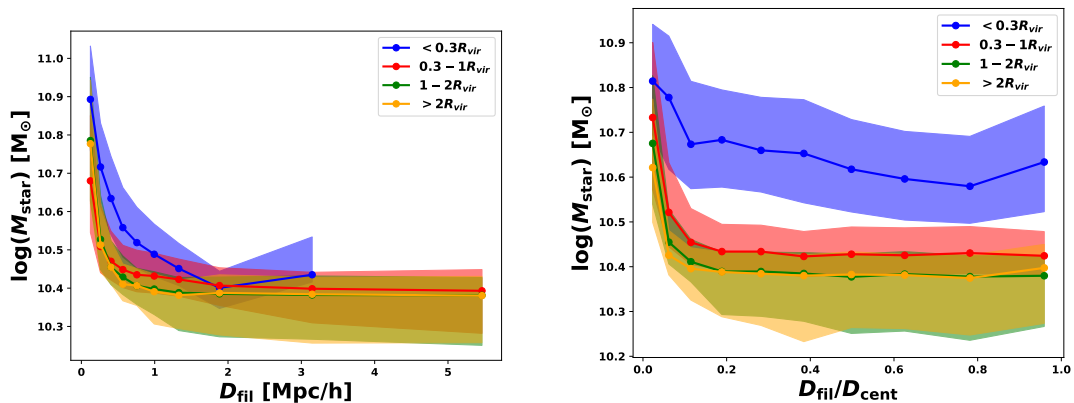
FIGURE 2.15: Median halo stellar mass versus distance **(left panel)** and angular separation **(right panel)** to nearest filament. Coloured contours indicated 40-60 percentile spread. Stellar mass of halos increases approaching the spine of filaments.

It is notably clear that halo mass is also increasing towards cluster centres, as inner halos (orange to green to red to blue) have higher stellar masses at fixed distance or

angular separation to filament.

2.7   A2: Cosmic flow alignments versus angular separation

Figure 2.16 shows the median evolution of the cosine of the angle between the velocity vector of halos (**left panel**) and gas particles (**right panel**) and their nearest filament versus angular separation ($D_{\mathrm{fil}}/D_{\mathrm{cent}}$). For the left panel, error bars indicate standard error on the mean, and coloured contours indicate the 40th-60th percentile spread. On both plots, dashed lines stand for the null hypothesis (isotropic cluster flows) discussed in Section 2.2.5, which quantifies purely geometric correlations due to the enhanced radial component of flows into clusters. For both halos and gas particles between 0.3 and 1 R_{vir}, there is a clear increase in cosine with smaller angular separation, beyond the mere geometric correlation between filaments and radial flows. This indicates that gas and halos flow effectively together along intra-cluster filaments.

Notably, separate analysis of $|\cos(\theta)|$ found that for halos outside their cluster virial radius (1-2 and >2 R_{vir}), further than angular separations of 0.7, $|\cos(\theta)| < 0.5$. For all other angular separations for halos at any cluster-centric distance, $|\cos(\theta)| \geq 0.5$. This is in line with a picture where for field galaxies and filaments, matter is attracted perpendicularly at first towards filaments and then flows bend towards alignment with the filament in their vicinity.

2.8   A3: Evolution of fraction of accreting halos and gas unbinding parameter with stellar mass inside and outside the cluster

Figure 2.17 shows the fraction of halos accreting cold gas versus stellar mass, binned by their angular separation (colours) and residency inside (solid lines) or outside (dashed
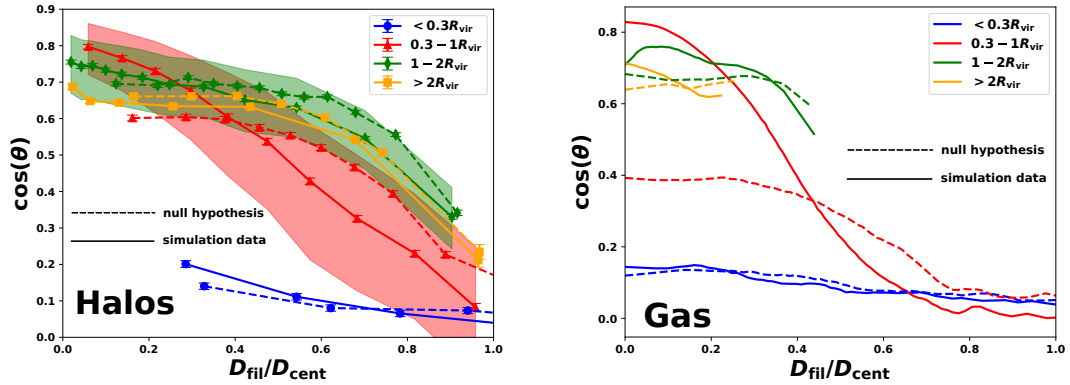
FIGURE 2.16: **Left Panel:** The median evolution of the cosine of the angle between the velocity vector of a halo and its nearest filament versus angular separation to filament. Error bars are standard error on the mean and coloured contours indicated the 40-60 percentile spread. Dashed lines represent the null hypothesis whereby any geometric effects are left untouched. Halo flows between 0.3 and 1 virial radius become sharply aligned with their nearest filament. **Right Panel:** The median evolution of the cosine of the angle between the velocity vector of a gas particle and its nearest filament versus distance to filament. Dashed lines again indicate the null hypothesis. As with halos, gas flows within the cluster become more aligned with their nearest filament.

lines) the virial radius of clusters. Coloured contours indicate 1-σ bootstrap errors. As expected, the fraction of accreting halos is higher outside clusters than inside clusters at all angular separations.

Outside clusters, at fixed stellar mass, the accreting fraction decreases at smaller angular separation (green to red to blue), consistent with pre-processing in field/outskirt filaments.

Inside clusters, this trend reverses, and the accreting fraction increases at smaller angular separation, irrespective of stellar mass. This indicates that intra-cluster filaments are regions where halos are more readily able to accrete than in the rest of the cluster environment.

Note also that most massive halos (hosting massive centrals $> 10^{11.5} M_{\odot}$) lie in
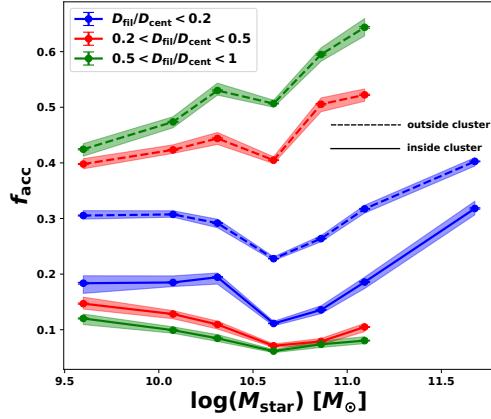
FIGURE 2.17: Fraction of accreting halos versus halo stellar mass, binned by angular separation to filament and residency within a cluster. Coloured contours represent 1-σ bootstrap errors. Outside a cluster, accreting fraction decreases as angular separation to filament decreases. Inside a cluster, accreting fraction conversely increases as angular separation to filament decreases.

the smallest angular separation range (blue), and these tend to have higher accreting fractions. This f_{acc} trend with stellar mass in the high mass range is responsible for the apparent secondary increase of accreting fraction at the spine of filaments ($D_{\mathrm{fil}}/D_{\mathrm{cent}} < 0.07$) seen in Figure 2.12.

Figure 2.18 shows the median gas unbinding parameter (B_g) versus stellar mass, binned by their angular separation and residency inside (solid) or outside (dashed) the virial radius of clusters. Coloured contours indicate the 40th-60th percentile spread. Halo gas is markedly less bound/more disturbed inside clusters than outside clusters at all angular separations, as demonstrated by smaller B_g values outside clusters compared to inside.

Outside clusters, the median B_g value remains below 1 across the full range of stellar masses and angular separations. It is however clear that, at fixed stellar mass, B_g increases at smaller angular separation (green to red to blue), again consistent with pre-processing in field filaments causing more gas disturbance.

Inside the cluster environment however, this trend reverses, and B_g decreases at smaller angular separations. This indicates that intra-cluster filaments are regions where halo gas is less disturbed and binds better to halos than in the rest of the cluster environment.

Notably at fixed angular separation either inside or outside the cluster, B_g exhibits little mass dependence. This indicates that across all masses, halos feel the gas disturbances from their environment in similar ways, but the key for the star formation context is that larger halos at the centres of groups with substantial gas stores will take longer to be depleted by stripping, whereas smaller halos will be rapidly stripped.
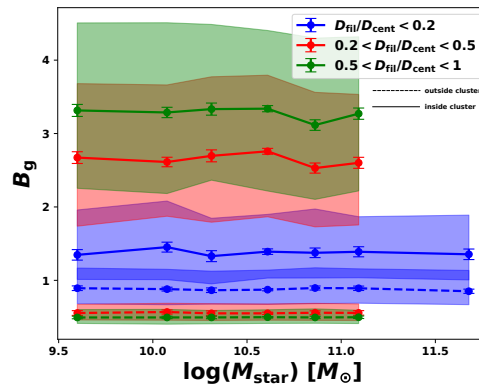
FIGURE 2.18: Median gas unbinding parameter, B_g, versus halo stellar mass, binned by angular separation to filament and residency within a cluster. Coloured contours represent 40-60 percentile spread. A lower B_g value indicates that gas is less perturbed in a halo. Outside a cluster, B_g increases as angular separation to filament decreases. Inside a cluster, B_g conversely decreases as angular separation to filament decreases. Notably at fixed angular separation, B_g does not appear to depend on mass.

2.9 A4: Evolution of ram pressure with distance to the centre of the cluster.

Figure 2.19 shows the median ram pressure experienced by halos against their cluster-centric distance. Results are presented for the full sample (in blue) and for different

stellar mass bins (green to pink). Error bars indicate standard error on the mean. For all stellar masses, ram pressure increases dramatically from approximately 10^{-14} Pa·h^2 beyond 1 R_{vir} up to approximately 10^{-12} Pa·h^2 at the cluster centre. Only most massive halos lying in the innermost core of the cluster ($D_{\mathrm{cent}} < 0.2R_{\mathrm{vir}}$) deviate from this trend as they have virtually no differential velocity with the host cluster. Most are cluster central candidates or the second brightest cluster galaxy.
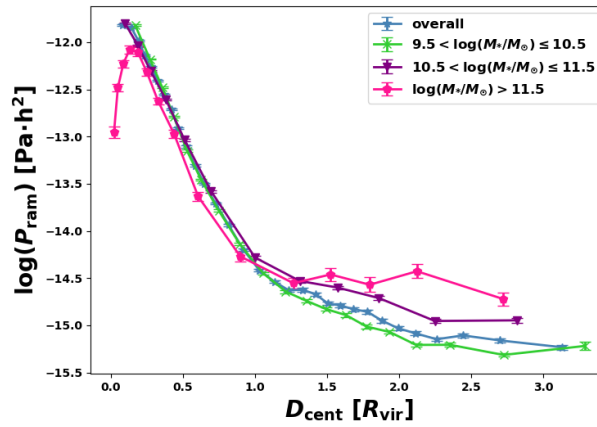
FIGURE 2.19: Median ram pressure exerted on a halo against its cluster-centric distance. Halos are binned by their stellar mass. Error bars indicated standard error on the mean. Ram pressure steadily increases overall for halos deeper within clusters.

Chapter 3

Measuring Star Formation

When initiating the research outlined in this thesis, we first attempted to use star formation rate (SFR) values derived directly from simulation data, and verified if these values were reasonable and in line with expectations of observers. In this Chapter I discuss in greater detail the process and decision behind choosing to examine star formation using galaxy colour (which tells us if star formation was active recently) and cold gas fraction (which tells us about the fuel available for star formation) in the preceding Chapter, rather than using these direct SFR values calculated thromeugh the data from the simulation suite.

3.1 Star Formation in the Simulation Suite

In this thesis, we examine the evolution of galaxies in the cluster environment, more specifically with respect to the cosmic web. The most relevant direct property we are able to examine in simulations is the star formation rate (SFR), the number of stars a galaxy is birthing per year, or the specific star formation rate (sSFR), which is the SFR divided by the stellar mass of the galaxy, which is useful as a measure which is less influenced by galaxy mass. We used sSFR in Chapter 2 to create a measure which quantifies the fraction of star-forming galaxies (f_{SFG}).

As discussed in Section 2.2.1, The Three Hundred suite was run with a dark matter particle mass of $M_{DM}^0 = 1.27 \times 10^9 h^{-1} M_\odot$, gas particle mass of $M_{gas}^0 = 2.36 \times 10^8 h^{-1} M_\odot$, and varying star particle masses on the order of $M_* = 4 \times 10^7 h^{-1} M_\odot$. This results in a typical spatial resolution of 8 kpc, with galaxies containing at least 50 star particles being resolved down to stellar masses of $10^{9.5} M_\odot$. The GADGET-X code used for the simulations includes processes such as metal-dependent UV cooling, black hole growth and AGN feedback, star formation and stellar evolution, and stellar feedback (Cui et al. 2018).

From observations, we understand the relationship between gas and star formation. The Kennicutt-Schmidt Law is an empirical relation which quantifies the relationship between the amount of gas required to maintain a given star formation rate. More specifically, it correlates the star formation rate density (Σ_{SFR} $[M_\odot/(yr \cdot kpc^2)]$) with gas surface density (Σ_{gas} $[M_\odot/pc^2]$). The relation takes the form

$$\Sigma_{\text{SFR}} \propto \Sigma_{\text{gas}}^n \tag{3.1}$$

where Kennicutt finds n to be 1.4 and the constant of proportionality to be 2.5×10^{-4} (Schmidt (1959) and Kennicutt (1998)).

In GADGET-X, star formation is a stochastic process derived instead from a Schmidt-type law (Schmidt 1959), which involves volume densities, obtainable from particles in the simulation, rather than surface densities (Tornatore et al. 2007). Specifically, gas particles in the simulation are transformed into star particles based on their (in principle self-regulated) star formation rate, defined as

$$\dot{m}_* = xm/t_*. \tag{3.2}$$

Here x is the fraction of gas in cold clouds, and is dependent on cooling function, density, and temperature. t_* is the density-dependent star formation timescale, defined itself as

$$t_*(\rho) = t_0^* \left(\rho/\rho_{\text{th}}\right)^{-1/2}. \tag{3.3}$$

Here, ρ_{th} is a threshold density, which for this simulation suite is set at 0.1 cm^{-3}, and t_0^* is set to be 1.5 Gyr in order to reproduce a Kennicutt-Schmidt-style law with $n = 1.5$.

In the stochastic model of star formation, based on Equation 3.2, a star particle is created when a random number from [0,1] is drawn and falls below the probability

$$p = N_* \left[1 - \exp\left(-\frac{x\Delta t}{t_*}\right)\right] \tag{3.4}$$

where N_* is the number of star particles each gas particle is allowed (Tornatore et al. 2007). This stochastic model converges towards the continuous star formation history when the number of star formation events becomes large.

Notably, in this simulation suite, star particles may assign some of their mass to surrounding gas particles. This means that star particles can vary in mass due to their own mass loss or due to the differences in mass of their parent gas particles.

I describe established observational expectations for SFR in the next section, before proceeding in the final two sections of this chapter to explain how we calculate SFR directly from the simulation suite and why what we see using these direct SFR calculation methods is at odds with observational expectations, and thus led us to use star formation proxies.
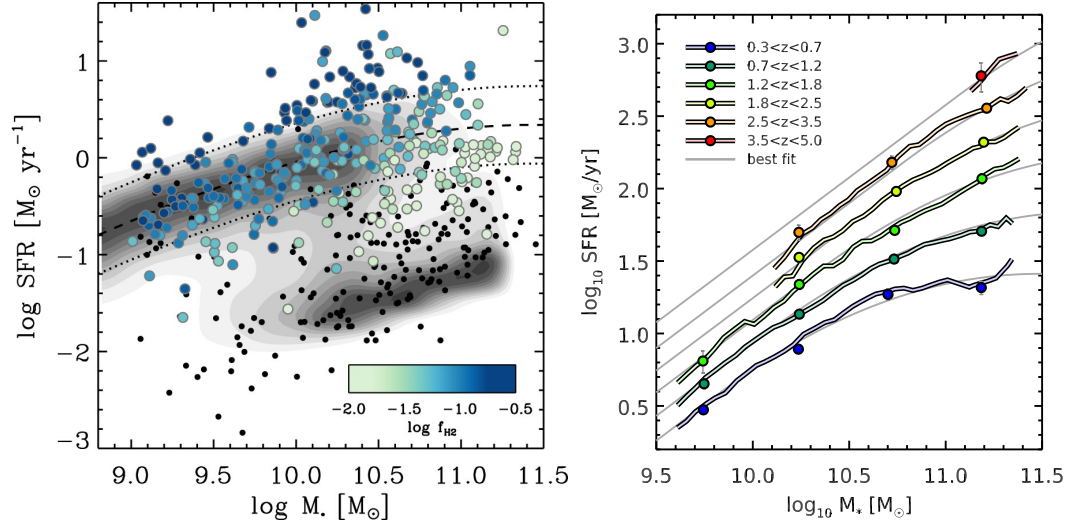
FIGURE 3.1: **Left panel:** Galaxies from the xCOLD GASS survey are shown colour-coded by their molecular gas fraction, with black dots indicating galaxies with no detected molecular gas. An SDSS parent sample is shown in contours. Reproduced with permission from Saintonge et al. (2017). **Right panel:** SFR-M_{star} curves at various redshifts from Herschel data. The relationship flattens at high mass for low redshift. Reproduced with permission © ESO, Schreiber+, A&A, 575, A74, 2015.

3.2 Observational Expectations for Star Formation

A key relationship that has been explored extensively in literature is that of the SFR and the stellar mass (M_{star}) of galaxies (eg. Brinchmann et al. (2004), Noeske et al. (2007), Whitaker et al. (2012)).

We see in the left panel of Figure 3.1 a figure reproduced from Saintonge et al. (2017) that shows over 500 galaxies from the xCOLD GASS survey colour-coded by their fraction of molecular gas (black dots represent galaxies undetected in the CO (1-0) line used to trace H_2) overlaid on a contour plot of SDSS galaxies on the SFR-M_{star} plane. It is clear that initially at lower mass, SFR increases with stellar mass. In this regime, cold gas supply is not an issue, this is clear as these galaxies have high molecular gas fractions. Thus, the more massive a galaxy, the more gas it contains and the higher the star formation rate. This trend continues towards higher masses, and is called the 'main

sequence'. However, at higher masses ($M \geq 10^{10.5} M_\odot$) we see that a large secondary population of galaxies have a much lower SFR than the standard trend. This is the population of 'red and dead' galaxies which have been deprived of their cold gas (see the increase in number of black dots) and have therefore seen a marked decrease in the ability to form stars. That is, they have quenched.

The xCOLD GASS survey focused on galaxies in the redshift range $0.01 < z < 0.05$, but similar work has been done out to larger redshifts. The right panel of Figure 3.1 shows the SFR-M_{star} relation for multiple redshifts reproduced from Schreiber et al. (2015) with data from Herschel. It is evident that the SFR-M_{star} relation flattens, or can even decrease, at high stellar mass. This is an effect only seen at low redshift, where most of the remaining gas in the Universe is contained in denser environments.

As is discussed in Chapters 1 and 2, there are also certain established expectations for star formation and how it should evolve in the framework of galaxy clusters. We discussed that a basic expectation is that as galaxies gravitationally traverse towards the cluster centre through the dense, hot intra-cluster medium, and pass through a harsh environment filled with galaxy-galaxy interactions, they should be progressively stripped and starved of their star-forming gas. That is, they increasingly shut down star formation and quench with smaller cluster-centric distance. This trend although polluted by 'backsplash' galaxies, those galaxies which have traversed to the cluster centre already and are moving back out of the cluster, remains strong. For context, on average, over half of the galaxies between 1 and 2 virial radii of clusters in the Three Hundred are backsplash galaxies (Haggar et al. 2020).

If the values for SFR computed as outlined in the previous section were reliable, we would thus expect to see them decrease approaching cluster centres, and for them to follow the established SFR-M_{star} relation at low redshift, as we are exclusively investigating simulation snapshots at $z = 0$ in this work.

3.3   Methods of Direct Calculation

There are two avenues to directly compute SFR values from the Three Hundred simulation data. The first method of halo SFR computation (SFR_{gas}) relies on SFR values assigned to gas particles by the GADGET-X code, as described in the previous section. We identify, at $z = 0$, gas particles within one virial radius of halos, as identified by VELOCIraptor. We then sum up the SFR values prescribed to these particles by GADGET-X, to obtain an SFR for the halo in $M_{\odot}/yr$. As these values are obtained from a single snapshot, they are the average over the timescale since the previous snapshot, which for these snapshots in the simulation is approximately 30 Myr. Given the stochastic nature of the star formation recipe in the simulation (see Section 3.1), low mass halos identified with very few gas particles have poorly constrained star formation rates. In particular, this means that the lower end of star formation rates from this method suffer from statistical noise. In order to reduce this noise, one solution is to increase the time interval over which star formation is averaged.

In the second method (SFR_{star}), we rely on the star particles in the simulation. Star particles have a smaller mass in the simulation than gas particles. Star particles by definition have a stellar age, a continuous quantity prescribed by GADGET-X. After identifying the star particles within a virial radius of the centre of the halo, we identify how many of the star particles formed within the past 1 Gyr. We sum up the masses of these particles and then divide by 1×10^9 to obtain a value in $M_{\odot}/yr$. Based on an average stellar particle mass of $4 \times 10^7 \ h^{-1} M_{\odot}$ and a time interval of 1 Gyr, the minimum resolvable star formation rate using this method is approximately 0.06 $M_{\odot}/yr$.

Both of these computations of SFR are meant to be representative at $z = 0$, but their average timescales are vastly different. Specifically, SFR_{gas} represent the gas conditions over 30 Myr, while SFR_{star} is averaged over a 1 Gyr timescale, in order to minimize
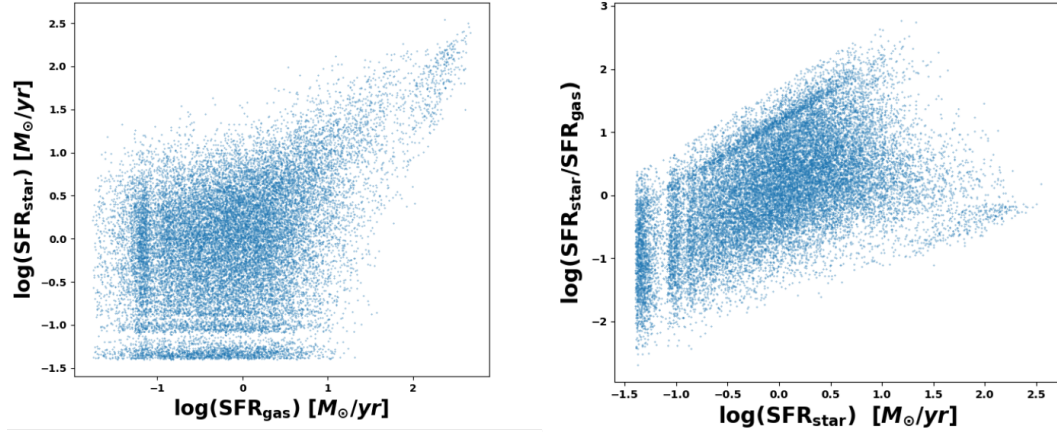
FIGURE 3.2: Two comparisons of SFR$_{gas}$ (calculated using the SFRs of gas particles) and SFR$_{star}$ (calculated using the stellar ages of star particles). The **left panel** directly compares the two values, showing no correlation below 10 $M_\odot/yr$ and a weak positive correlation for higher SFRs. The **right panel** shows the ratio against SFR$_{star}$, highlighting where each computation of SFR has higher values than the other.

noise. In both methods, there are issues for low star formation halos, due to the stochastic nature of the star formation recipe in combination with the mass resolution of the simulation.

Figure 3.2 compares these two computations of SFR for all of the halos in the simulation suite. In the left panel, we see that there is a correlation between the two methods across the entire range. The large dispersion at low SFR is expected given the differing timescales between the measures and stochasticity at low mass. Banding is visible for SFR$_{star}$ due to numerical effects from increases in star particle counts. The right panel demonstrates that SFR$_{gas}$ tends to be higher than SFR$_{star}$ at low SFR$_{star}$, where the creation of a star drastically depletes the gas content available. This relationship flips at higher SFR$_{star}$ where there is more gas content available. The ratio of the two computations converges towards 1 at the highest star formation rates due to convergence of the stochastic star formation recipe.

3.4   Illuminating Underlying Technical Issues

After computing the SFR values as outlined in Section 3.3, we proceeded to verify whether they followed the trends discussed in Section 3.2.

Out of the over 150000 halos identified in the simulation suite, SFR_{gas} returns only around 30000 halos with nonzero SFR, while SFR_{star} returns just over 80000 halos with nonzero SFR. While there are certainly halos with absolutely no active star formation, these zero fractions generally reflect again the limitations of our ability to resolve low SFRs.

The left panels of Figures 3.3 and 3.4 show the SFR-M_{star} scatter relations for SFR_{gas} and SFR_{star} respectively. It is clear from the left panels of both figures that while there are high mass halos with low star formation rates, there is no distinct peak of red and dead galaxies. The main sequence is also dominant at the highest masses where in actuality the red population should dominate. Additionally, there is a great deal of spread in both SFR values at lower stellar mass. As discussed previously, this spread exemplifies the lower resolution of the simulation, whereby low mass galaxies can see their SFR heavily influenced by a difference of just a few stellar particles. We also see a clear vertical feature near $10^{10.5} M_{\odot}$ in stellar mass, which as we mention in Chapter 2 corresponds to the stellar mass at which AGN feedback in the simulation becomes active. Horizontal features again indicate discrete effects caused by the acquisition of single star particles for increases in SFR near the resolution limit.

The right panels of the figures show the median SFR-M_{star} relation, with error bars indicating standard error on the mean and coloured contours representing the 40th-60th percentile spread. In neither computation of SFR do we witness the expected flattening or decrease of SFR at high stellar mass for low redshift. Instead, we see SFR consistently increasing with M_{star}, as is the expectation for $z > 1$. This indicates that the star
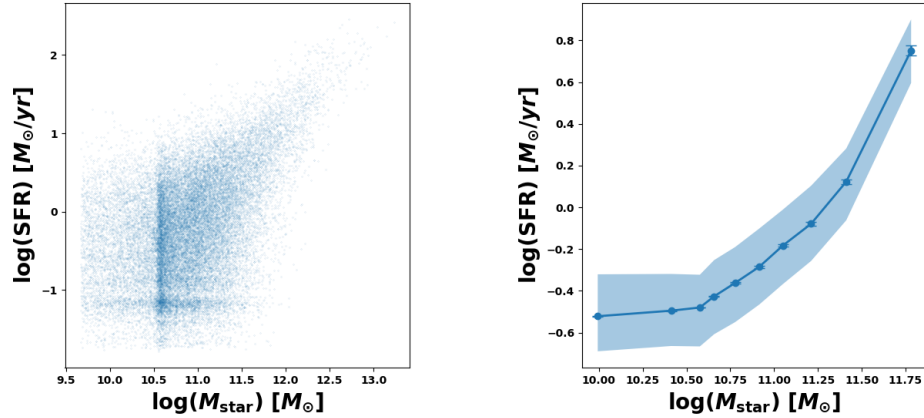
FIGURE 3.3: The SFR$_{\text{gas}}$-M_{star} relation. The **left panel** shows the scatter relation while the **right panel** shows the median curve with 3000 halos per bin. Error bars are standard errors on the mean and coloured contours are the 40th-60th percentile spread.

formation recipe for the simulations was tuned to be too permissive in an attempt to mitigate the consequences of the lower resolution. That is, the star formation threshold is too low for gas density and too high for temperature, such that massive galaxies do not desist star formation rapidly enough to reflect reality.

To further investigate the reliability of these SFR values, we proceeded to construct a measure to investigate how the calculated SFR values trend with cluster-centric distance. We define $f+$ to be the fraction of halos in a given bin that are above the median SFR-M_{star} relation. We show how this evolves with cluster-centric distance in Figure 3.5, where the left panel is for SFR$_{\text{gas}}$ and the right panel is for SFR$_{\text{star}}$. This evolution is depicted for all halos, as well as split for those above and below stellar masses of $10^{11} M_{\odot}$.

In both panels, the overall trend is that $f+$ remains nearly constant at cluster-centric distances larger than 1 virial radius, and then sharply increases inside the virial radius towards the cluster centres. This trend would indicate that closer to the cluster centre, more galaxies are forming stars above the median SFR for their mass. This is definitively counter to observations for the SFR trend towards the cluster centre whereby
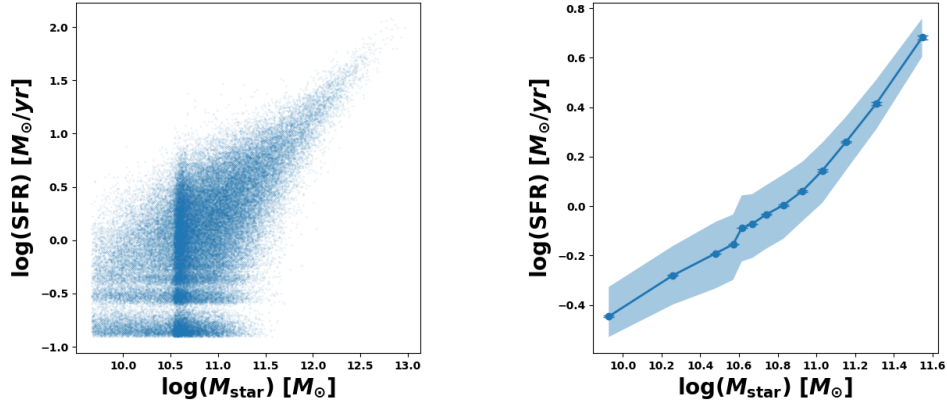
FIGURE 3.4: The SFR$_{\text{star}}$-M_{star} relation. The **left panel** shows the scatter relation while the **right panel** shows the median curve with 6000 halos per bin. Error bars are standard errors on the mean and coloured contours are the 40th-60th percentile spread.

more galaxies have lower SFR, and thus we expect smaller $f+$ values towards the centre. The trend is largely dominated by halos in the lower mass bin, which is to be expected given the large population in this bin compared with the higher mass bin. This trend for smaller halos in the simulation is in line with the star formation recipe being too permissive, even near the cluster centre. The higher mass bin has consistently higher $f+$ values than the lower mass bin, in line with Figures 3.3 and 3.4.

Figure 3.6 shows the evolution of stellar mass with cluster-centric distance, with error bars indicating standard error on the mean and coloured contours showing the 40th-60th percentile spread. This demonstrates that there is a sharp increase in halo meidan stellar mass approaching cluster centres, in line with a picture where smaller galaxies are shredded on their journey deeper into the cluster. This, in combination with the SFR-M_{star} relations, indicates that the SFR values calculated directly from the simulation suite are strongly correlated with stellar mass alone. The most massive halos are found at the cluster centres, and these are the halos with the highest SFR values. This would cause the directly computed SFR to be increasing towards the cluster centre in the simulation, counter to observational expectations.
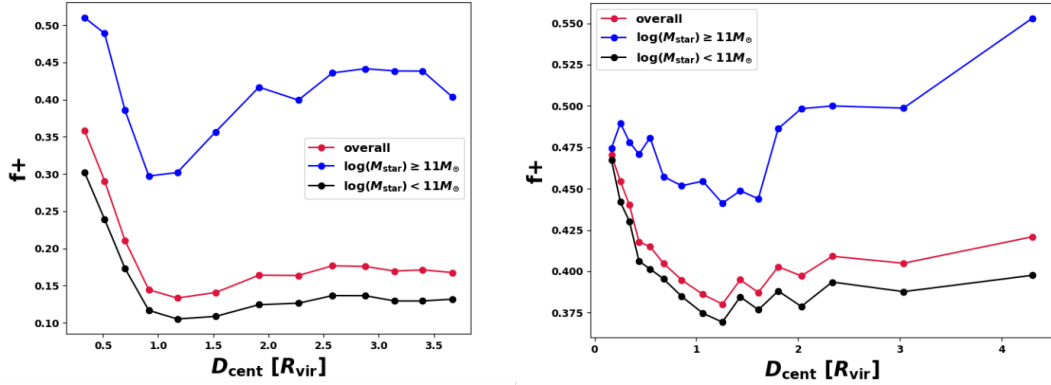
FIGURE 3.5: The fraction of galaxies with SFR above the median of the SFR versus M_{star} relation ($f+$) versus cluster-centric distance. The **left panel** is for SFR_{gas} and the **right panel** is for SFR_{star}. These trends indicate that according to SFR_{gas} and SFR_{star}, star formation increases towards the cluster centre.

We utilized SFR in Chapter 2 in a very specific way to control for this strong mass effect. We first converted SFR values to sSFR as a first measure to reduce reliance on mass. We then constructed the measure f_{SFG} (the fraction of star-forming galaxies) based on a threshold value of the sSFR. We then analysed its variation with distance to filament at fixed stellar masses. The trends observed at fixed stellar masses, at least above $10^{11} M_{\odot}$ (where $f+$ doesn't trend with D_{cent}) are then reliably due to the effects of filaments, and not stellar mass. We see this clearly in Figure 2.4.

While this technique suggested that filaments are having a discernible impact on quenching, it was desirable to use measures that were less affected by the lower resolution of the simulation, and that followed expectations of observers. Galaxy colour and cold gas fraction are tracers of quenching that do not rely upon the star formation model of the simulation, and instead only upon the gas particles, which are better resolved than stars. These measures are integrated quantities over time and do not depend on numerical counts between snapshots based on subgrid recipes. We demonstrated in Figures 2.5 and 2.6 that both of these measures evolve as observers expect for quenching in relation
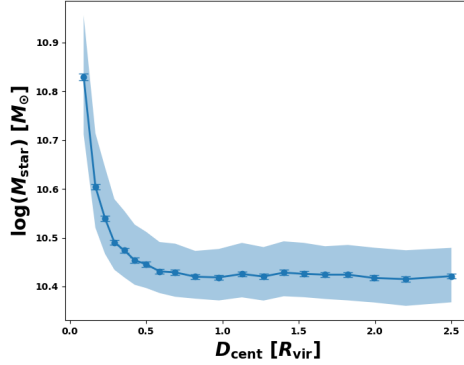
FIGURE 3.6: The median evolution of stellar mass versus cluster-centric distance. Error bars are standard error on the mean and coloured contours represent the 40th-60th percentile spread. Stellar mass increases markedly within $0.5R_{\mathrm{vir}}$ closer to cluster centres.

to the cluster-centric distance. As such, these are reliable proxies for examining star formation.

Given that we have established that galaxy colours are a reliable tracer for quenching in this work, it is valuable to examine how the less reliable SFR values correlate with them. In Figure 3.7, we show the distribution of $g - r$ galaxy colours for those galaxies with a computed $\mathrm{SFR}_{\mathrm{gas}}$ value of zero. We clearly see the expected bimodal distribution of galaxy colour, and this shows why we used a cut of 0.65 to differentiate between blue and red galaxies. Those galaxies with $g - r < 0.65$ are considered blue, and should thus be actively forming stars. It is clearly unphysical for these galaxies to have SFR values of exactly zero, further evidence of our limited resolution impacting our ability to calculate low SFRs and that quenching in this work should instead be traced with proxies.
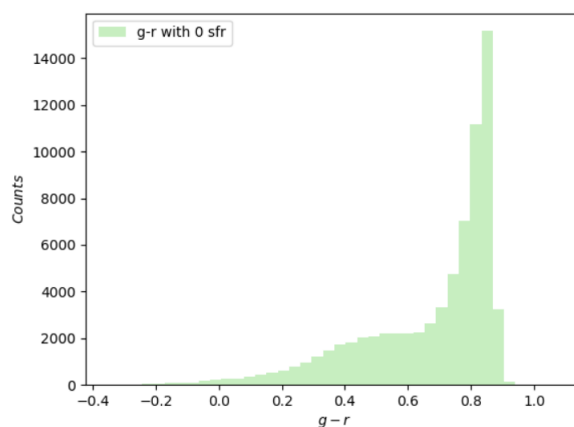
FIGURE 3.7: Colour distribution of galaxies with 0 SFR_{gas}, where blue galaxies in this work are those with $g-r < 0.65$. It is unphysical for blue galaxies to have no star formation, but we understand that this stems from issues with our resolution-limited ability to measure low SFRs.

Chapter 4

Classifying Galaxies as Wet or Dry

In Chapter 2, we not only found signs of delayed quenching for cluster galaxies caused by intra-cluster filaments of the cosmic web, but we also investigated the dynamics of cluster gas and galaxies to determine the origins of this effect. Given the fact that ram pressure stripping is a key mechanism for quenching for cluster galaxies, we were particularly interested in creating a measure to examine how stripped of gas halos in the simulation are. We thus attempted to extend this measure for use as a binary classifier as to whether a galaxy was wet (rich with gas as fuel for star formation) or dry (stripped almost entirely of gas), and present this work here.

4.1   Revisiting the Gas Unbinding Parameter, B_g

We discussed and defined the gas unbinding parameter, B_g, in Section 2.2.5 as a measure of how stripped the halos in the simulations suite are of gas. The phase space plane is an effective way to examine gas stripping, as it is immediately, visually, clear when there are tails of gas streaming from halos or when gas has suddenly been violently removed,

as seen in Figure 2.3. As gas is stripped out in either situation, its velocity and position varies from that of the stellar and dark matter components of halos.

The measure was specifically constructed as a ratio of the offset between gas and stars and dark matter in velocity space with the velocity dispersion of the stellar component of halos. Here, the velocity dispersion of the stellar component acts as a proxy for the potential well of the halo. The larger the B_g value, the larger the offset of the gas from the stars and dark matter should be in relation to the dispersion of the stellar velocities. That is, large values of B_g signify very perturbed gas whereas lower values of B_g indicate galaxies with largely unperturbed gas, and hence more potential for star formation.

Different choices of weighting for the gaseous component were possible when creating this measure, depending on the end goal. Choosing to mass-weight gas particles would mean that B_g would increase rapidly to reflect any plumes of disassociated gas. On the other hand, a density-weighting would down-weight the unbound cluster gas and focus more specifically on the disassociation of gas from the core of the galaxy.

The measure B_g presented in Chapter 2 was defined as

$$B_g = \frac{\sqrt{(v_{x,\mathrm{g}} - v_{x,\mathrm{sdm}})^2 + (v_{y,\mathrm{g}} - v_{y,\mathrm{sdm}})^2 + (v_{z,\mathrm{g}} - v_{z,\mathrm{sdm}})^2}}{\sqrt{\sigma_{v_x,\mathrm{s}}^2 + \sigma_{v_y,\mathrm{s}}^2 + \sigma_{v_z,\mathrm{s}}^2}} \tag{4.1}$$

and used density-weighted average gas particle velocities, as our focus was on removal of gas crucial for star formation.

We present a few examples of the phase space plane of halos with various degrees of gas stripping in Figures 4.1 and 4.2, labelled with the B_g values computed with density-weighted ($B_{g,\rho}$) and mass-weighted ($B_{g,m}$) gas particle velocities.

Figure 4.1 highlights cases where both measures return similar values. The left panel is a case of the situation where it is clear that gas is heavily associated with the stellar
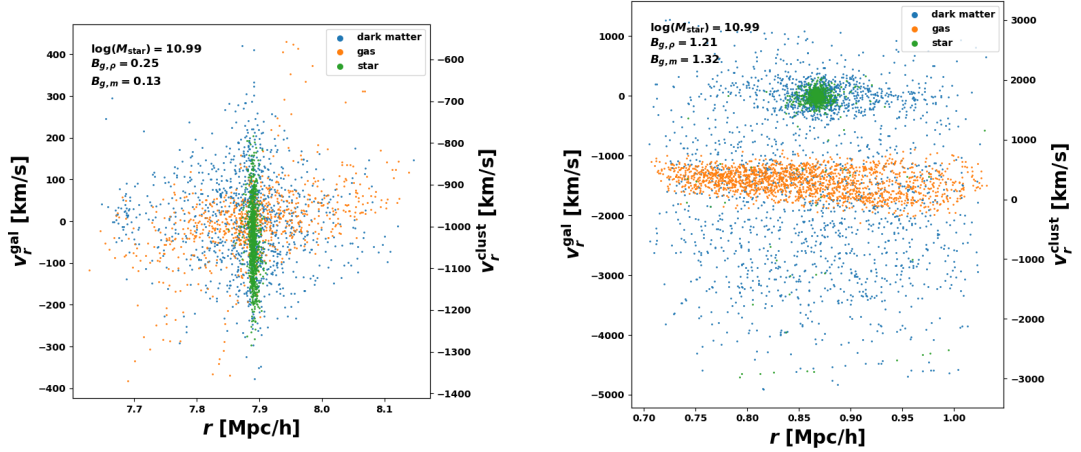
FIGURE 4.1: Phase space planes for two halos where $B_{g,\rho}$ and $B_{g,m}$ are similar. The **left panel** shows a definitively wet galaxy and the **right panel** shows a definitively dry galaxy.

and dark matter component of the galaxy, and hence is very bound. Here, $B_{g,\rho} = 0.25$ and $B_{g,m} = 0.13$. In the right panel, we see a case of the situation where a galaxy is completed stripped of its gaseous content. In this case, $B_{g,\rho} = 1.21$ and $B_{g,m} = 1.32$. Both of these are scenarios where the gas content is tight across the velocity space, and is (or was) thus clearly associated with the galaxy itself rather than the less dense intra-cluster medium.
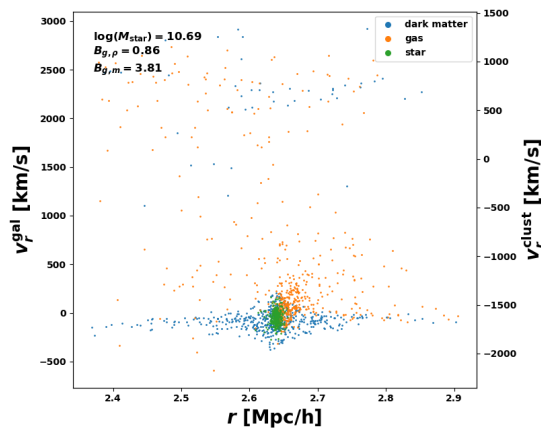
FIGURE 4.2: Phase space plane of a halo where $B_{g,\rho}$ and $B_{g,m}$ differ. This is a galaxy undergoing stripping but with a large amount of gas still bound.

Figure 4.2 serves to showcase the situation where the two measures return very different values. It is visually clear that this is a galaxy that is undergoing stripping, but the majority of the gas is still bound. Here, $B_{g,\rho} = 0.86$ and $B_{g,m} = 3.81$. The less dense gas content spread across velocity space is clearly associated with the intra-cluster medium, rather than bound gas crucial to star formation in the galaxy. Cluster gas is unbound, so a measure which includes this gas ends up favouring an unbound result. Specifically, since all the gas particles in this simulation are of similar mass, the weighting of $B_{g,m}$ is skewed towards any high velocity ICM gas. Instead, the weighting of $B_{g,\rho}$ better focuses on the state of binding of the key gas to the galaxy over the cluster gas. That is, $B_{g,\rho}$ controls for the less dense gas of lesser importance, keeping galaxies with mostly bound gas at $B_g \leq 1$, whereas $B_{g,m}$ blows up rapidly. We thus made the decision to use density-weighted averages on gas particles for computation of B_g in Chapter 2.

4.2   The Dry Fraction

The right panel of Figure 4.1 clearly depicts a dry galaxy, whereas the left panel is definitively wet (having additionally confirmed that cold gas is present). This classification is useful in the context of star formation, so we strived to use B_g as a binary cut as part of an attempt to separate dry and wet galaxies. We designated $B_g = 2$ as the distinction point. Those halos with gas separated from the stars and dark matter by more than twice the velocity dispersion of the stars would be considered significantly stripped of the fuel required of star formation ($B_g > 2$) and labelled as dry.

Dry halos are not only those with gas content heavily disassociated from the core of the galaxy, but also those halos with no gas content at all (analogous to non-detections in observations). B_g being a measure of gas disassociation requires the presence of gas particles in order to be computed. Thus to accurately capture all halos which are dry, we must also consider those halos with $M_{\text{gas}} = 0$ where B_g cannot be computed. Failure

to include $M_{\text{gas}} = 0$ halos would particularly lead to bias whereby disregarding lower mass halos in the cluster environment which become fully stripped more quickly (achieve $M_{\text{gas}} = 0$) would incorrectly decrease the count of realistically dry galaxies.

Using these qualifiers for dry galaxies, we then investigated the evolution of the dry fraction, f_{dry}, of halos in relation to proximity to filaments. The dry fraction for N halos in a given bin is

$$f_{\text{dry}} = \frac{n(B_g > 2) + n(M_{\text{gas}} = 0)}{N} \tag{4.2}$$

Figure 4.3 shows how f_{dry} evolves with angular separation to nearest filament ($D_{\text{fil}}/D_{\text{cent}}$). Error bars indicate standard error on the mean and coloured contours indicate the 1-σ bootstrap error.
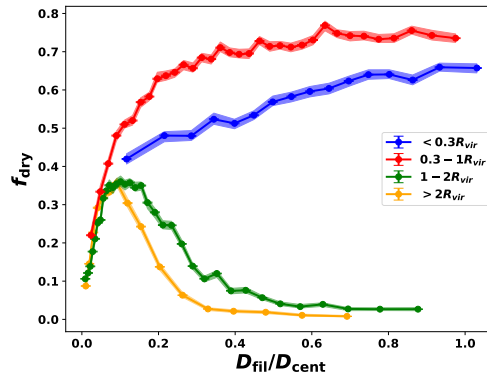
FIGURE 4.3: The fraction of dry halos versus angular separation to filament. Halos are binned based on cluster centric distance, error bars indicate standard error on the mean, and 1-σ bootstrap errors are indicated by the coloured contours. The fraction of dry galaxies in the cluster environment smoothly decreases with filament proximity.

Halos residing beyond one virial radius (1-2R_{vir} and >2R_{vir}) are consistently less dry than those inside the virial radius (<0.3R_{vir} and 0.3-1R_{vir}). This is to be expected given the stripping processes underway in the cluster environment. Halos outside the virial radius increasingly dry nearer to filaments up to 0.1 away, before seeing a significant drop in the dry fraction closer than this filamentary distance. We saw similar sudden

reversal of trends for field halos with other measures in Chapter 2 (f_{acc} and and B_g) which were simply due to the mass distribution close to filament spines. For halos within the virial radius ($<0.3R_{\mathrm{vir}}$ and 0.3-$1R_{\mathrm{vir}}$) the dry fraction shows a progressive steady decrease with decreasing angular separation. These trends would seem to indicate that filaments are a region in the cluster where galaxies more easily remain wet.

We proceed to examine how dry fraction is related to stellar mass, just as we did for $f_{\mathrm{gas}}^{\mathrm{cold}}$ (Figure 2.7), f_{acc} (Figure 2.17), and B_g (Figure 2.18). Figure 4.4 shows this control plot, with halos split by whether they are inside (solid) or outside (dashed) the virial radius of their host cluster, and by their angular separation to nearest filament (colours). Error bars indicate standard error on the mean and coloured contours indicated 1-σ bootstrap errors.
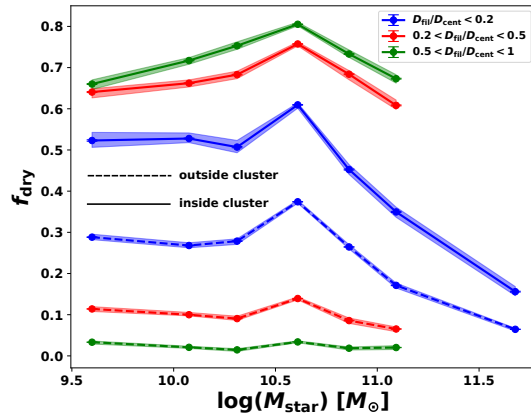
FIGURE 4.4: Fraction of dry halos versus halo stellar mass, binned by angular separation to filament and residency within a cluster. Coloured contours represent 1-σ bootstrap errors. Outside clusters, dry fraction increases as angular separation to filament decreases. Inside clusters, dry fraction decreases as angular separation to filament decreases.

For those halos residing outside the cluster environment (dashed), at fixed stellar mass, the dry fraction increases with smaller angular separation (green to red to blue). This is in line with the removal or consumption of gas caused by the pre-processing expected for galaxies near field filaments.

The trend for halos inside the cluster environment (solid) is reversed, whereby the dry fraction decreases with decreasing angular separation at fixed stellar mass. This reflects the same reversal in trend found for all other measures in this thesis, and is another indicator that intra-cluster filaments are a region where galaxies experience delayed quenching, partially due to the fact that they are able to remain wet.

Note that the most massive halos ($M > 10^{11} M_\odot$) reside in the smallest angular separation bin, and both inside and outside clusters experience large decreases in dry fraction. This bias is responsible for the sudden decrease in dry fraction for field halos. We demonstrate this in Figure 4.5, which is the same as Figure 4.3 except with the most massive halos with stellar masses above $10^{10.5} M_\odot$ removed. We see that the sharp dip in dry fraction closer than 0.1 angular separation from filaments for halos in living from 0.3 to beyond 2 $R_{\rm vir}$ is greatly decreased from Figure 4.3. However, the crucial progressive decrease in dry fraction is clearly still present between angular separations of 0.2 to 0.1 for those halos living between 0.3-1 $R_{\rm vir}$.
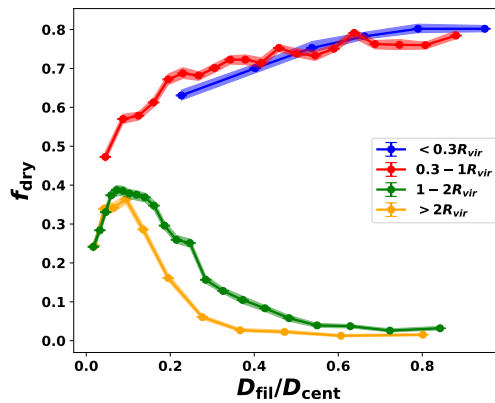
FIGURE 4.5: This is the same as Figure 4.3 except with halos with stellar masses above $10^{10.5} M_\odot$ removed. Halos are binned based on cluster centric distance, error bars indicate standard error on the mean, and 1-σ bootstrap errors are indicated by the coloured contours. The fraction of dry galaxies in the cluster environment (red curve) still smoothly decreases with filament proximity (from 0.2 to 0.1 angular separation).

Chapter 5

Conclusions

5.1 Summary of Findings

In this thesis, we presented the first study to examine the impact of filaments of the cosmic web on the quenching of cluster galaxies. Using a suite of over 300 galaxy cluster simulations, along with a robust filament extractor and halo finder, we found evidence that intra-cluster filaments are delaying the quenching of galaxies in their vicinity in comparison to those cluster galaxies residing further from filaments. This is in opposition to the impact of filaments in the field on galaxies, whereby pre-processing hastens the removal or consumption of key gas for star formation and thereby leads to increased quenching.

We first established that intra-cluster filaments play an important role in star formation beyond simply hosting the most massive halos. This was accomplished by finding that the fraction of star forming galaxies at fixed stellar mass increased with increased proximity to filaments in the cluster environment. Due to the lower resolution of the simulations and the underlying star formation recipe, we found issues with relying on the star formation information directly from the simulations. We thus proceeded to examine star formation via other measures that are readily realized in observations. We

investigated trends in galaxy colours and found that, as has been established, galaxies redden as they approach filaments outside the cluster environment. However, within the cluster virial radius we found that instead galaxies level off in colour and become slightly bluer when in closer proximity to filaments. Probing the fuel for star formation directly, we found that the fraction of cold gas in galaxies residing closer to filaments in the cluster environment was increased compared to those residing further from filaments, again in contrast to what we found for field galaxies. We also showed that this effect is not merely an effect of increased stellar mass closer to filaments.

We worked to demonstrate that decreases in strangulation and in ram pressure stripping are plausible mechanisms behind these trends. We found that even down to $0.3R_{\mathrm{vir}}$, filaments of the cosmic web maintain coherent dense flows of cooler gas. Notably different for filaments inside clusters compared to those outside is the lesser contrast in density to the background. This hints that cluster filaments do not boost density-related quenching compared to the ICM, whereas field filaments provide such a boost compared to voids in the field. We analysed the flows of cold gas and galaxies in proximity to intra-cluster filaments, and found that they flow together more effectively closer to the spines of filaments, signalling that galaxies in this region may be able to more effectively accrete cold gas. We specifically found that the fraction of accreting galaxies does indeed increase in closer proximity to intra-cluster filaments, beyond a simple correlation with the mass distribution near the spine of filaments. We showed that ram pressure slightly decreases for galaxies with increased filament proximity, which in combination with the larger stellar masses and thus gravitational forces of these galaxies implies a decrease in ram pressure stripping. With regards to stripping, we created a measure to quantify the extent of the disturbance of gas in halos. We constructed this measure to ensure that it was not biased by gas in the intra-cluster medium, and instead focused on gas crucial to star formation in the galactic context. We were able to extend this measure as a binary discriminator as part of a classification between wet and dry galaxies.

5.2   Limitations and Future Work

Astrophysical simulations are applied models of our understanding of physics; crucial for theorizing and understanding that which we cannot observe on human timescales. However, due to limitations on resolution and complexity, all simulations come with inherent assumptions, biases, and tradeoffs. The Three Hundred Project set of simulations is no exception. This suite was an effective choice for this work due in large part to its size, meaning we could get excellent statistical significance. However, the low resolution of the simulation leads to poor hydrodynamical modelling, of which one consequence is overstripping. I discussed in Chapter 3 how the low resolution coupled with the subgrid star formation model caused issues with directly obtaining star formation rates. Specifically, we found that the star formation model was too permissive, leading to massive galaxies not quenching effectively enough. Additionally, the poor hydrodynamics in combination with the cooling model can lead to overcooling and thus excessive star formation. Further, the star formation model is based on stars forming stochastically when gas is beyond a density threshold of 0.1 cm^{-3}, meaning there is no direct comparison to molecular clouds or dense ISM. We also touched on the numerical stellar mass pileup at $10^{10.5} M_\odot$ throughout this work. This feature coincides with the mass at which the AGN feedback kicks in. Weak AGN feedback is also another potential contributing factor to the excessive star formation at high mass in the simulation. The limited resolution also means we cannot explore morphology in any detail, a particularly interesting avenue of investigation in the context of stripping. The simulation suite also had no prescription for magnetic fields, which in reality may affect how cold flows fragment or impact the effectiveness of ram pressure stripping. These tradeoffs in the simulation mean that while we have large number statistics, our work not only focused on indirect measures of star formation, but relied on quantitative differences of values rather than exact quantities.

One excellent avenue of further investigation is thus to utilize other galaxy cluster simulations that do not have these specific issues in order to validate the trends and mechanisms presented in this work. In particular, RomulusC, the highest resolution galaxy cluster simulation run to date with observationally sound ICM and star formation histories presents an excellent testing ground for this kind of analysis (Tremmel et al. 2018). Given the higher resolution, it could be possible to directly rely on star formation rates in this simulation down to subtle boosts, rather than rely on examination of galaxy colour and cold gas fraction. The resolution of the simulation would allow us to explore the morphology of cluster galaxies, specifically having resolved the tails of jellyfish galaxies undergoing intense ram pressure stripping. The simulation could potentially be used to more exactly quantify ram pressure in the cluster and the regimes where it boosts star formation versus causes stripping. With improvement in resolution, further refinement is also possible in the choice of finder. We utilized a halo finder in this work, and as such conducted analysis on the halo scale. Choosing a galaxy finder would instead focus more pointedly on the galactic scale for more in-depth analysis than would be possible in this work. In particular, we would be able to differentiate and track galaxy mergers and see if and how they are effected by intra-cluster filaments. We will also be able to separate lower mass galaxies deep in groups, as well as resolve dwarf galaxies, extending our analysis robustly to a lower mass range below $10^9 M_\odot$.

As this thesis focused only on $z = 0$, there is still a great deal to be examined throughout cosmic time. Given merger trees and halo finder outputs at all redshifts, studies can be done to track halos as they approach intra-cluster filaments to determine how quickly, and to what extent, they experience delays in quenching. For the Three Hundred, separating cluster filament and ICM halos and tracing their evolution through redshift would further confirm the trends we find in this work by showing specifically that ICM galaxies quench on shorter timescales. While the resolution of simulation suite again means trends would be of interest in the relative sense, it could be possible to determine

what affects how strong the delay in quenching caused by intra-cluster filaments is: halo mass, state of star formation upon cluster entry, backsplash versus infalling, cluster-centric radius. By utilizing time evolution, it could also be possible to find out if filaments are not only delaying quenching, but rejuvenating star formation. Higher resolution simulations could once again illuminate exact star formation values over cosmic time, pinning down the exact impact of intra-cluster filaments. These simulations could also be used in conjunction with redshift evolution to further examine the spatial extent of filament influence within the cluster.

Having established that large-scale filaments of the cosmic web impact star formation of satellite in dense environments, there are other scenarios to test whether these effects hold. In particular, work could focus on the impact of galaxy-scale filaments on dwarf satellites of Milky Way-type galaxies using simulations such as New Horizon (Dubois et al. in prep). New Horizon is a zoom re-simulation from the Horizon-AGN (Dubois et al. 2014) with a 10 Mpc radius spherical region, with approximately 50 pc spatial resolution ($10^5 M_\odot$ for dark matter particles) and advanced physics prescriptions such as turbulent star formation, dust production, and improved AGN and supernovae feedback. It contains a few thousand galaxies, mostly dwarfs and 10-20 Milky Way-like systems. This set-up is similar in nature to the cluster context in that it is an examination of filaments impacting satellites (rather than centrals as in the cold flows context), but on a smaller scale than with clusters. Yet another interesting examination would be to see if these effects are replicated in a large galaxy group environment, rather than in a cluster. The high resolution large galaxy group presented in Joshi et al. (2018) could serve as a testing ground, with data out to 3 R_{vir} being sufficient to run DisPerSE to construct the cosmic web.

In Chapter 4, I discussed an attempt at using the gas unbinding parameter that we constructed as a quantifier of whether a galaxy was wet or dry. This approach could

be modified and taken further to be used in future research as a classification system for galaxies in simulations. Specifically, further work could be done to more accurately develop the B_g cutoff for dry galaxies based on stellar mass, especially within the cluster context. The Three Hundred or another large cluster simulation set could be used to refine the measure based on 1D phase space diagrams and human or computational visual classification as wet or dry. With a standardized measure, simulations at low and high resolution could systematically classify galaxies as wet or dry based solely on particle phase space information, and gain quick insights into the degree of stripping of halos.

Of course, work should be done to confirm and extend our findings using observations. We use quantities that are obtainable from observations such as galaxy colour and cold gas content in this work. Existing large-scale surveys such as GAMA have been coupled with the DisPerSE filament extractor (Kraljic et al. (2017) and Welker et al. (2019)), and this work could be extended to building the network of cosmic filaments plunging into clusters in 2D. Note that work in 2D is necessary for these observational surveys to mitigate for redshift space distortions along the line of sight. Work from Kuchner et al. (2020) indicates that this 2D approach shows promise at accurately identifying filament galaxies. The SAMI Galaxy Cluster Survey could be a viable target with eight low redshift clusters selected that overlap the SDSS and 2dFGRS (Owers et al. 2017). Using the filament network and SAMI kinematics for gas and stars, combined with detailed information on galaxy colours and star formation from SDSS and 2dFGRS, it is in principle possible to probe to how real galaxies are interacting with filaments of the cosmic web deep within clusters.

The new VERTICO survey which aims to map molecular hydrogen gas for 51 galaxies in the Virgo cluster will also be a rich source of information. It would be interesting to examine angular separation trends for galaxies in the Virgo cluster.

Given the difficulties in directly observing the gaseous cosmic web, any advancements in this context would be excellent. The Square Kilometre Array (SKA) is a radio telescope which hopes to be able to identify diffuse filaments directly through a variety of methods including imaging synchrotron emission and mapping the distribution of low column density neutral hydrogen (Wilcots 2004).

Bibliography

Abadi, M. G., Moore, B., and Bower, R. G. (Oct. 1999). Ram pressure stripping of spiral galaxies in clusters. *Monthly Notices of the Royal Astronomical Society* 308(4), 947–954. ISSN: 1365-2966.

Ade, P. A. R., Aghanim, N., Alves, M. I. R., Armitage-Caplan, C., Arnaud, M., Ashdown, M., Atrio-Barandela, F., Aumont, J., Aussel, H., and al., et (Oct. 2014). Planck2013 results. I. Overview of products and scientific results. *Astronomy Astrophysics* 571, A1. ISSN: 1432-0746.

Ade, P. A. R., Aghanim, N., Arnaud, M., Ashdown, M., Aumont, J., Baccigalupi, C., Banday, A. J., Barreiro, R. B., Barrena, R., and al., et (Sept. 2016). Planck2015 results. *Astronomy Astrophysics* 594, A27. ISSN: 1432-0746.

Aragon Calvo, M. A., Neyrinck, M. C., and Silk, J. (July 2019). Galaxy Quenching from Cosmic Web Detachment. *The Open Journal of Astrophysics* 2(1).

Baldry, I. K., Glazebrook, K., Brinkmann, J., Ivezić, Ž., Lupton, R. H., Nichol, R. C., and Szalay, A. S. (Jan. 2004). Quantifying the Bimodal Color-Magnitude Distribution of Galaxies. *The Astrophysical Journal* 600(2), 681–694. ISSN: 1538-4357.

Balogh, M. L., Baldry, I. K., Nichol, R., Miller, C., Bower, R., and Glazebrook, K. (Nov. 2004). The Bimodal Galaxy Color Distribution: Dependence on Luminosity and Environment. 615(2), L101–L104.

Balogh, M. L., Navarro, J. F., and Morris, S. L. (Sept. 2000). The Origin of Star Formation Gradients in Rich Galaxy Clusters. *ApJ* 540(1), 113–121.

Bamford, S. P., Nichol, R. C., Baldry, I. K., Land, K., Lintott, C. J., Schawinski, K., Slosar, A., Szalay, A. S., Thomas, D., Torki, M., and al., et (Mar. 2009). Galaxy Zoo: the dependence of morphology and colour on environment. *Monthly Notices of the Royal Astronomical Society* 393(4), 1324–1352. ISSN: 1365-2966.

Barnes, D. J., Kay, S. T., Bahé, Y. M., Dalla Vecchia, C., McCarthy, I. G., Schaye, J., Bower, R. G., Jenkins, A., Thomas, P. A., Schaller, M., and al., et (June 2017). The Cluster-EAGLE project: global properties of simulated clusters with resolved galaxies. *Monthly Notices of the Royal Astronomical Society* 471(1), 1088–1106. ISSN: 1365-2966.

Beck, A. M., Murante, G., Arth, A., Remus, R.-S., Teklu, A. F., Donnert, J. M. F., Planelles, S., Beck, M. C., Förster, P., Imgrund, M., Dolag, K., and Borgani, S. (Nov. 2015). An improved SPH scheme for cosmological simulations. *MNRAS* 455(2), 2110–2130. ISSN: 0035-8711.

Bennett, C. L., Hill, R. S., Hinshaw, G., Nolta, M. R., Odegard, N., Page, L., Spergel, D. N., Weiland, J. L., Wright, E. L., Halpern, M., Jarosik, N., Kogut, A., Limon, M., Meyer, S. S., Tucker, G. S., and Wollack, E. (Sept. 2003). First-Year Wilkinson Microwave Anisotropy Probe (WMAP) Observations: Foreground Emission. 148(1), 97–117.

Bird, J. B., Davis, J., Luber, N., Gorkom, J. H. van, Wilcots, E., Pisano, D. J., Gim, H. B., Momjian, E., Fernandez, X., Hess, K. M., Lucero, D., Dodson, R., Vinsen, K., Popping, A., Chung, A., Kreckel, K., Hulst, J. M. van der, and Yun, M. (2019). CHILES VI: HI and H Observations for z < 0.1 Galaxies; Probing HI Spin Alignment with Filaments in the Cosmic Web. *MNRAS*.

Birnboim, Y. and Dekel, A. (Oct. 2003). Virial shocks in galactic haloes? *Monthly Notices of the Royal Astronomical Society* 345(1), 349–364. ISSN: 1365-2966.

Bond, J. R. and Myers, S. T. (Mar. 1996). The Peak-Patch Picture of Cosmic Catalogs. I. Algorithms. 103, 1.

Bond, J. R., Kofman, L., and Pogosyan, D. (Apr. 1996). How filaments of galaxies are woven into the cosmic web. 380(6575), 603–606.

Brinchmann, J., Charlot, S., White, S. D. M., Tremonti, C., Kauffmann, G., Heckman, T., and Brinkmann, J. (July 2004). The physical properties of star-forming galaxies in the low-redshift Universe. *Monthly Notices of the Royal Astronomical Society* 351(4), 1151–1179. ISSN: 1365-2966.

Brooks, A., Governato, F., Quinn, T., Brook, C., and Wadsley, J. (2009). The role of cold flows in the assembly of galaxy disks. *The Astrophysical Journal* 694(1), 396.

Bruzual, G. and Charlot, S. (Oct. 2003). Stellar population synthesis at the resolution of 2003. 344(4), 1000–1028.

Carroll, B. W. and Ostlie, D. A. (2007). *An Introduction to Modern Astrophysics.* Ed. by S. F. P. Addison-Wesley. 2nd (International).

Codis, S., Jindal, A., Chisari, N. E., Vibert, D., Dubois, Y., Pichon, C., and Devriendt, J. (Sept. 2018). Galaxy orientation with the cosmic web across cosmic time. *MNRAS* 481(4), 4753–4774. ISSN: 1365-2966.

Colless, M., Dalton, G., Maddox, S., Sutherland, W., Norberg, P., Cole, S., Bland-Hawthorn, J., Bridges, T., Cannon, R., Collins, C., and al., et (Dec. 2001). The 2dF Galaxy Redshift Survey: spectra and redshifts. *MNRAS* 328(4), 1039–1063. ISSN: 1365-2966.

Cornuault, N., Lehnert, M. D., Boulanger, F., and Guillard, P. (Feb. 2018). Are cosmological gas accretion streams multiphase and turbulent? *Astronomy Astrophysics* 610, A75. ISSN: 1432-0746.

Crain, R. A., Schaye, J., Bower, R. G., Furlong, M., Schaller, M., Theuns, T., Dalla Vecchia, C., Frenk, C. S., McCarthy, I. G., Helly, J. C., and al., et (Apr. 2015). The EAGLE simulations of galaxy formation: calibration of subgrid physics and model variations. *Monthly Notices of the Royal Astronomical Society* 450(2), 1937–1961. ISSN: 0035-8711.

Cui, W., Knebe, A., Yepes, G., Pearce, F., Power, C., Dave, R., Arth, A., Borgani, S., Dolag, K., Elahi, P., and al., et (Mar. 2018). The Three Hundred project: a large catalogue of theoretically modelled galaxy clusters for cosmological and astrophysical applications. *MNRAS* 480(3), 2898–2915.

Dehnen, W. and Aly, H. (Sept. 2012). Improving convergence in smoothed particle hydrodynamics simulations without pairing instability. 425(2), 1068–1082.

Dekel, A., Birnboim, Y., Engel, G., Freundlich, J., Goerdt, T., Mumcuoglu, M., Neistein, E., Pichon, C., Teyssier, R., and Zinger, E. (Jan. 2009). Cold streams in early massive hot haloes as the main mode of galaxy formation. *Nature* 457(7228), 451–454. ISSN: 1476-4687.

Dressler, A. (Mar. 1980). Galaxy morphology in rich clusters: implications for the formation and evolution of galaxies. 236, 351–365.

Dubois, Y., Pichon, C., Welker, C., Borgne, D. L., Devriendt, J., Laigle, C., Codis, S., Pogosyan, D., Arnouts, S., Benabed, K., and al., et (2014). Dancing in the dark: galactic properties trace spin swings along the cosmic web. *MNRAS* 444(2), 1453–1468.

Dubois, Y., Devriendt, J., Slyz, A., and Teyssier, R. (Jan. 2012a). Self-regulated growth of supermassive black holes by a dual jet-heating active galactic nucleus feedback mechanism: methods, tests and implications for cosmological simulations. *Monthly Notices of the Royal Astronomical Society* 420(3), 2662–2683. ISSN: 0035-8711.

Dubois, Y., Pichon, C., Devriendt, J., Silk, J., Haehnelt, M., Kimm, T., and Slyz, A. (Nov. 2012b). Blowing cold flows away: the impact of early AGN activity on the formation of a brightest cluster galaxy progenitor. *Monthly Notices of the Royal Astronomical Society* 428(4), 2885–2900. ISSN: 1365-2966.

Ebeling, H., Stephenson, L. N., and Edge, A. C. (Jan. 2014). JELLYFISH: EVIDENCE OF EXTREME RAM-PRESSURE STRIPPING IN MASSIVE GALAXY CLUSTERS. *The Astrophysical Journal* 781(2), L40. ISSN: 2041-8213.

Elahi, P. J., Cañas, R., Poulton, R. J. J., Tobar, R. J., Willis, J. S., Lagos, C. D. P., Power, C., and Robotham, A. S. G. (2019). Hunting for galaxies and halos in simulations with VELOCIraptor. *Publications of the Astronomical Society of Australia* 36.

Fall, S. M. and Efstathiou, G. (Oct. 1980). Formation and rotation of disc galaxies with haloes. 193, 189–206.

Gabor, J. M., Davé, R., Finlator, K., and Oppenheimer, B. D. (2010). How is star formation quenched in massive galaxies? *MNRAS* 407(2), 749–771.

Gingold, R. A. and Monaghan, J. J. (Nov. 1977). Smoothed particle hydrodynamics: theory and application to non-spherical stars. 181, 375–389.

Gott J. R., I. and Rees, M. J. (Dec. 1975). A theory of galaxy formation and clustering. 45, 365–376.

Gunn, J. E. and Gott J. Richard, I. (Aug. 1972). On the Infall of Matter Into Clusters of Galaxies and Some Effects on Their Evolution. 176, 1.

Gursky, H., Solinger, A., Kellogg, E. M., Murray, S., Tananbaum, H., Giacconi, R., and Cavaliere, A. (May 1972). X-Ray Emission from Rich Clusters of Galaxies. 173, L99.

Guth, A. H. (Jan. 1981). Inflationary universe: A possible solution to the horizon and flatness problems. 23(2), 347–356.

Haggar, R., Gray, M. E., Pearce, F. R., Knebe, A., Cui, W., Mostoghiu, R., and Yepes, G. (Feb. 2020). TheThreeHundred project: backsplash galaxies in simulations of clusters. *Monthly Notices of the Royal Astronomical Society* 492(4), 6074–6085. ISSN: 1365-2966.

Haines, C. P., Pereira, M. J., Smith, G. P., Egami, E., Babul, A., Finoguenov, A., Ziparo, F., Mcgee, S. L., Rawle, T. D., Okabe, N., and al., et (Oct. 2015). LoCuSS: THE SLOW QUENCHING OF STAR FORMATION IN CLUSTER GALAXIES AND THE NEED FOR PRE-PROCESSING. *ApJ* 806(1), 101.

Hasselfield, M., Hilton, M., Marriage, T. A., Addison, G. E., Barrientos, L. F., Battaglia, N., Battistelli, E. S., Bond, J. R., Crichton, D., Das, S., and al., et (July 2013). The

Atacama Cosmology Telescope: Sunyaev-Zel'dovich selected galaxy clusters at 148 GHz from three seasons of data. *Journal of Cosmology and Astroparticle Physics* 2013(07), 008–008. ISSN: 1475-7516.

Hubble, E. P. (Dec. 1926). Extragalactic nebulae. 64, 321–369.

Joshi, G. D., Parker, L. C., Wadsley, J., and Keller, B. W. (Nov. 2018). The trajectories of galaxies in groups: mass-loss and preprocessing. *Monthly Notices of the Royal Astronomical Society* 483(1), 235–248. ISSN: 1365-2966.

Katz, N. and White, S. D. M. (Aug. 1993). Hierarchical Galaxy Formation: Overmerging and the Formation of an X-Ray Cluster. 412, 455.

Kawata, D. and Mulchaey, J. S. (Dec. 2007). Strangulation in Galaxy Groups. *The Astrophysical Journal* 672(2), L103–L106. ISSN: 1538-4357.

Kennicutt Jr., R. C. (May 1998). The Global Schmidt Law in Star-forming Galaxies. *The Astrophysical Journal* 498(2), 541–552. ISSN: 1538-4357.

Keres, D., Katz, N., Weinberg, D. H., and Dave, R. (Oct. 2005). How do galaxies get their gas? *Monthly Notices of the Royal Astronomical Society* 363(1), 2–28. ISSN: 1365-2966.

Kereš, D., Katz, N., Fardal, M., Davé, R., and Weinberg, D. H. (May 2009). Galaxies in a simulated CDM Universe - I. Cold mode and hot cores. *Monthly Notices of the Royal Astronomical Society* 395(1), 160–179. ISSN: 1365-2966.

Kleiner, D., Pimbblet, K. A., Heath Jones, D., Koribalski, B. S., and Serra, P. (Dec. 2016). Evidence for Hi replenishment in massive galaxies through gas accretion from the cosmic web. *MNRAS*, stw3328. ISSN: 1365-2966.

Klypin, A., Yepes, G., Gottlöber, S., Prada, F., and Heß, S. (Feb. 2016). MultiDark simulations: the story of dark matter halo concentrations and density profiles. *MNRAS* 457(4), 4340–4359. ISSN: 0035-8711.

Kraljic, K., Arnouts, S., Pichon, C., Laigle, C., Torre, S. D. L., Vibert, D., Cadiou, C., Dubois, Y., Treyer, M., Schimd, C., and al., et (Oct. 2017). Galaxy evolution in the metric of the cosmic web. *MNRAS* 474(1), 547–571.

Kraljic, K., Pichon, C., Dubois, Y., Codis, S., Cadiou, C., Devriendt, J., Musso, M., Welker, C., Arnouts, S., Hwang, H. S., and al., et (Nov. 2018). Galaxies flowing in the oriented saddle frame of the cosmic web. *Monthly Notices of the Royal Astronomical Society* 483(3), 3227–3254. ISSN: 1365-2966.

Kraljic, K., Pichon, C., Codis, S., Laigle, C., Davé, R., Dubois, Y., Hwang, H. S., Pogosyan, D., Arnouts, S., Devriendt, J., Musso, M., Peirani, S., Slyz, A., and Treyer, M. (Jan. 2020). The impact of the connectivity of the cosmic web on the physical properties of galaxies at its nodes. 491(3), 4294–4309.

Kuchner, U., Aragón-Salamanca, A., Pearce, F. R., Gray, M. E., Rost, A., Mu, C., Welker, C., Cui, W., Haggar, R., Laigle, C., and al., et (Apr. 2020). Mapping and characterization of cosmic filaments in galaxy cluster outskirts: strategies and forecasts for observations from simulations. *Monthly Notices of the Royal Astronomical Society* 494(4), 5473–5491. ISSN: 1365-2966.

Laigle, C., Pichon, C., Codis, S., Dubois, Y., Le Borgne, D., Pogosyan, D., Devriendt, J., Peirani, S., Prunet, S., Rouberol, S., and al., et (Nov. 2014). Swirling around filaments: are large-scale structure vortices spinning up dark haloes? *Monthly Notices of the Royal Astronomical Society* 446(3), 2744–2759. ISSN: 0035-8711.

Laigle, C., Pichon, C., Arnouts, S., McCracken, H. J., Dubois, Y., Devriendt, J., Slyz, A., Le Borgne, D., Benoit-Lévy, A., Hwang, H. S., and al., et (Nov. 2017). COSMOS2015 photometric redshifts probe the impact of filaments on galaxy properties. *Monthly Notices of the Royal Astronomical Society* 474(4), 5437–5458. ISSN: 1365-2966.

Larson, R. B., Tinsley, B. M., and Caldwell, C. N. (May 1980). The evolution of disk galaxies and the origin of S0 galaxies. 237, 692–707.

Lucy, L. B. (Dec. 1977). A numerical approach to the testing of the fission hypothesis. 82, 1013–1024.

Maier, C., Ziegler, B., Haines, C., and Smith, G. (2019). Slow-then-rapid quenching as traced by tentative evidence for enhanced metallicities of cluster galaxies at z 0.2 in the slow quenching phase. *Astronomy & Astrophysics* 621, A131.

Marshall, M. A., Shabala, S. S., Krause, M. G. H., Pimbblet, K. A., Croton, D. J., and Owers, M. S. (Nov. 2017). Triggering active galactic nuclei in galaxy clusters. *Monthly Notices of the Royal Astronomical Society* 474(3), 3615–3628. ISSN: 1365-2966.

Masters, K. L., Mosleh, M., Romer, A. K., Nichol, R. C., Bamford, S. P., Schawinski, K., Lintott, C. J., Andreescu, D., Campbell, H. C., Crowcroft, B., and al., et (Mar. 2010). Galaxy Zoo: passive red spirals. *Monthly Notices of the Royal Astronomical Society.* ISSN: 1365-2966.

Meekins, J. F., Fritz, G., Chubb, T. A., and Friedman, H. (May 1971). Physical Sciences: X-rays from the Coma Cluster of Galaxies. 231(5298), 107–108.

Merritt, D. (Jan. 1984). Relaxation and tidal stripping in rich clusters of galaxies. II. Evolution of the luminosity distribution. 276, 26–37.

Mohr, J. J., Mathiesen, B., and Evrard, A. E. (June 1999). Properties of the Intracluster Medium in an Ensemble of Nearby Galaxy Clusters. *The Astrophysical Journal* 517(2), 627–649. ISSN: 1538-4357.

Monaghan, J. J. (Jan. 1992). Smoothed particle hydrodynamics. 30, 543–574.

Moore, B., Katz, N., Lake, G., Dressler, A., and Oemler, A. (Feb. 1996). Galaxy harassment and the evolution of clusters of galaxies. 379(6566), 613–616.

Moore, B., Lake, G., and Katz, N. (Mar. 1998). Morphological Transformation from Galaxy Harassment. 495(1), 139–151.

Nelson, D., Springel, V., Pillepich, A., Rodriguez-Gomez, V., Torrey, P., Genel, S., Vogelsberger, M., Pakmor, R., Marinacci, F., Weinberger, R., Kelley, L., Lovell, M.,

Diemer, B., and Hernquist, L. (2018). *The IllustrisTNG Simulations: Public Data Release.*

Noeske, K. G., Weiner, B. J., Faber, S. M., Papovich, C., Koo, D. C., Somerville, R. S., Bundy, K., Conselice, C. J., Newman, J. A., Schiminovich, D., and al., et (Apr. 2007). Star Formation in AEGIS Field Galaxies since z =1.1: The Dominance of Gradually Declining Star Formation, and the Main Sequence of Star-forming Galaxies. *The Astrophysical Journal* 660(1), L43–L46. ISSN: 1538-4357.

Owers, M. S., Allen, J. T., Baldry, I., Bryant, J. J., Cecil, G. N., Cortese, L., Croom, S. M., Driver, S. P., Fogarty, L. M. R., Green, A. W., and al., et (Mar. 2017). The SAMI Galaxy Survey: the cluster redshift survey, target selection and cluster properties. *Monthly Notices of the Royal Astronomical Society* 468(2), 1824–1849. ISSN: 1365-2966.

Peebles, P. J. E. (1980). *The large-scale structure of the universe.*

Peng, Y., Maiolino, R., and Cochrane, R. (May 2015). Strangulation as the primary mechanism for shutting down star formation in galaxies. *Nature* 521(7551), 192–195. ISSN: 1476-4687.

Pintos-Castro, I., Yee, H. K. C., Muzzin, A., Old, L., and Wilson, G. (May 2019). The Evolution of the Quenching of Star Formation in Cluster Galaxies since z 1. *The Astrophysical Journal* 876(1), 40. ISSN: 1538-4357.

Poggianti, B. M., Moretti, A., Gullieuszik, M., Fritz, J., Jaffé, Y., Bettoni, D., Fasano, G., Bellhouse, C., Hau, G., Vulcani, B., and al., et (July 2017). GASP. I. Gas Stripping Phenomena in Galaxies with MUSE. *The Astrophysical Journal* 844(1), 48. ISSN: 1538-4357.

Postman, M. and Geller, M. J. (June 1984). The morphology-density relation - The group connection. 281, 95–99.

Powell, L. C., Slyz, A., and Devriendt, J. (May 2011). The impact of supernova-driven winds on stream-fed protogalaxies. *Monthly Notices of the Royal Astronomical Society* 414(4), 3671–3689. ISSN: 0035-8711.

Press, W. H. and Schechter, P. (Feb. 1974). Formation of Galaxies and Clusters of Galaxies by Self-Similar Gravitational Condensation. 187, 425–438.

Price, D. J. (Feb. 2012). Smoothed particle hydrodynamics and magnetohydrodynamics. *Journal of Computational Physics* 231(3), 759–794. ISSN: 0021-9991.

Raichoor, A. and Andreon, S. (June 2012). Galaxy mass, cluster-centric distance and secular evolution: their role in the evolution of galaxies in clusters in the last 10 Gyr. *Astronomy Astrophysics* 543, A19. ISSN: 1432-0746.

Rees, M. J. and Ostriker, J. P. (June 1977). Cooling, dynamics and fragmentation of massive gas clouds: clues to the masses and radii of galaxies and clusters. 179, 541–559.

Reichardt, C. L., Stalder, B., Bleem, L. E., Montroy, T. E., Aird, K. A., Andersson, K., Armstrong, R., Ashby, M. L. N., Bautz, M., Bayliss, M., and al., et (Jan. 2013). GALAXY CLUSTERS DISCOVERED VIA THE SUNYAEV-ZEL'DOVICH EFFECT IN THE FIRST 720 SQUARE DEGREES OF THE SOUTH POLE TELESCOPE SURVEY. *The Astrophysical Journal* 763(2), 127. ISSN: 1538-4357.

Roberts, I. D., Parker, L. C., Brown, T., Joshi, G. D., Hlavacek-Larrondo, J., and Wadsley, J. (Apr. 2019). Quenching Low-mass Satellite Galaxies: Evidence for a Threshold ICM Density. *ApJ* 873(1), 42.

Roberts, I. D. and Parker, L. C. (May 2020). Ram pressure stripping candidates in the coma cluster: evidence for enhanced star formation. *Monthly Notices of the Royal Astronomical Society* 495(1), 554–569. ISSN: 1365-2966.

Roediger, E. and Hensler, G. (Apr. 2005). Ram pressure stripping of disk galaxies. From high to low density environments. 433(3), 875–895.

Rosati, P., Tozzi, P., Ettori, S., Mainieri, V., Demarco, R., Stanford, S. A., Lidman, C., Nonino, M., Borgani, S., Della Ceca, R., and al., et (Jan. 2004). ChandraandXMM-NewtonObservations of RDCS 1252.9-2927, A Massive Cluster atz=1.24. *The Astronomical Journal* 127(1), 230–238. ISSN: 1538-3881.

Rudnick, L. (2019). *The Stormy Life of Galaxy Clusters: astro version.*

Saintonge, A., Catinella, B., Tacconi, L. J., Kauffmann, G., Genzel, R., Cortese, L., Davé, R., Fletcher, T. J., Graciá-Carpio, J., Kramer, C., and al., et (Dec. 2017). xCOLD GASS: The Complete IRAM 30 m Legacy Survey of Molecular Gas for Galaxy Evolution Studies. *The Astrophysical Journal Supplement Series* 233(2), 22. ISSN: 1538-4365.

Saintonge, A., Kauffmann, G., Kramer, C., Tacconi, L. J., Buchbender, C., Catinella, B., Fabello, S., Graciá-Carpio, J., Wang, J., Cortese, L., and al., et (June 2011). COLD GASS, an IRAM legacy survey of molecular gas in massive galaxies - I. Relations between H2, Hi, stellar content and structural properties. *Monthly Notices of the Royal Astronomical Society* 415(1), 32–60. ISSN: 0035-8711.

Sarron, F., Adami, C., Durret, F., and Laigle, C. (Nov. 2019). Pre-processing of galaxies in cosmic filaments around AMASCFI clusters in the CFHTLS. *Astronomy Astrophysics* 632, A49. ISSN: 1432-0746.

Schawinski, K., Lintott, C., Thomas, D., Sarzi, M., Andreescu, D., Bamford, S. P., Kaviraj, S., Khochfar, S., Land, K., Murray, P., and al., et (June 2009). Galaxy Zoo: a sample of blue early-type galaxies at low redshift. *Monthly Notices of the Royal Astronomical Society* 396(2), 818–829. ISSN: 1365-2966.

Schawinski, K., Urry, C. M., Simmons, B. D., Fortson, L., Kaviraj, S., Keel, W. C., Lintott, C. J., Masters, K. L., Nichol, R. C., Sarzi, M., and al., et (Mar. 2014). The green valley is a red herring: Galaxy Zoo reveals two evolutionary pathways towards quenching of star formation in early- and late-type galaxies. *Monthly Notices of the Royal Astronomical Society* 440(1), 889–907. ISSN: 0035-8711.

Schaye, J., Crain, R. A., Bower, R. G., Furlong, M., Schaller, M., Theuns, T., Dalla Vecchia, C., Frenk, C. S., McCarthy, I. G., Helly, J. C., and al., et (Nov. 2014). The EAGLE project: simulating the evolution and assembly of galaxies and their environments. *Monthly Notices of the Royal Astronomical Society* 446(1), 521–554. ISSN: 0035-8711.

Schmidt, M. (Mar. 1959). The Rate of Star Formation. 129, 243.

Schreiber, C., Pannella, M., Elbaz, D., Béthermin, M., Inami, H., Dickinson, M., Magnelli, B., Wang, T., Aussel, H., Daddi, E., and al., et (Feb. 2015). TheHerschelview of the dominant mode of galaxy growth fromz= 4 to the present day. *Astronomy Astrophysics* 575, A74. ISSN: 1432-0746.

Silk, J. (Feb. 1977). On the fragmentation of cosmic gas clouds. I. The formation of galaxies and the first generation of stars. 211, 638–648.

Smith, R., Sánchez-Janssen, R., Beasley, M. A., Candlish, G. N., Gibson, B. K., Puzia, T. H., Janz, J., Knebe, A., Aguerri, J. A. L., Lisker, T., Hensler, G., Fellhauer, M., Ferrarese, L., and Yi, S. K. (Oct. 2015). The sensitivity of harassment to orbit: mass loss from early-type dwarfs in galaxy clusters. *MNRAS* 454(3), 2502–2516. ISSN: 0035-8711.

Smoot, G. F., Bennett, C. L., Kogut, A., Wright, E. L., Aymon, J., Boggess, N. W., Cheng, E. S., de Amici, G., Gulkis, S., Hauser, M. G., Hinshaw, G., Jackson, P. D., Janssen, M., Kaita, E., Kelsall, T., Keegstra, P., Lineweaver, C., Loewenstein, K., Lubin, P., Mather, J., Meyer, S. S., Moseley, S. H., Murdock, T., Rokke, L., Silverberg, R. F., Tenorio, L., Weiss, R., and Wilkinson, D. T. (Sept. 1992). Structure in the COBE Differential Microwave Radiometer First-Year Maps. 396, L1.

Sousbie, T. (Apr. 2011). The persistent cosmic web and its filamentary structure - I. Theory and implementation. *MNRAS* 414(1), 350–383. ISSN: 0035-8711.

Springel, V. (Dec. 2005). The cosmological simulation code gadget-2. *MNRAS* 364(4), 1105–1134. ISSN: 0035-8711.

Springel, V., White, S. D. M., Jenkins, A., Frenk, C. S., Yoshida, N., Gao, L., Navarro, J., Thacker, R., Croton, D., Helly, J., and al., et (June 2005). Simulations of the formation, evolution and clustering of galaxies and quasars. *Nature* 435(7042), 629–636. ISSN: 1476-4687.

Stanford, S. A., Holden, B., Rosati, P., Tozzi, P., Borgani, S., Eisenhardt, P. R., and Spinrad, H. (May 2001). The Intracluster Medium inz>1 Galaxy Clusters. *The Astrophysical Journal* 552(2), 504–507. ISSN: 1538-4357.

Stoughton, C. et al. (Jan. 2002). Sloan Digital Sky Survey: Early Data Release. 123(1), 485–548.

Strateva, I., Ivezić, Ž., Knapp, G. R., Narayanan, V. K., Strauss, M. A., Gunn, J. E., Lupton, R. H., Schlegel, D., Bahcall, N. A., Brinkmann, J., and al., et (Oct. 2001). Color Separation of Galaxy Types in the Sloan Digital Sky Survey Imaging Data. *The Astronomical Journal* 122(4), 1861–1874. ISSN: 0004-6256.

Sunyaev, R. A. and Zeldovich, I. B. (Jan. 1980). Microwave background radiation as a probe of the contemporary structure and history of the universe. 18, 537–560.

Sunyaev, R. A. and Zeldovich, Y. B. (Apr. 1970). Small-Scale Fluctuations of Relic Radiation. 7(1), 3–19.

Sunyaev, R. A. and Zeldovich, Y. B. (Nov. 1972). The Observations of Relic Radiation as a Test of the Nature of X-Ray Radiation from the Clusters of Galaxies. *Comments on Astrophysics and Space Physics* 4, 173.

Tecce, T. E., Cora, S. A., Tissera, P. B., Abadi, M. G., and Lagos, C. d. P. (Sept. 2010). Ram pressure stripping in a galaxy formation model - I. A novel numerical approach. *Monthly Notices of the Royal Astronomical Society* 408(4), 2008–2021. ISSN: 0035-8711.

Tonnesen, S. and Bryan, G. L. (Mar. 2009). GAS STRIPPING IN SIMULATED GALAXIES WITH A MULTIPHASE INTERSTELLAR MEDIUM. *The Astrophysical Journal* 694(2), 789–804. ISSN: 1538-4357.

Tornatore, L., Borgani, S., Dolag, K., and Matteucci, F. (Nov. 2007). Chemical enrichment of galaxy clusters from hydrodynamical simulations. *Monthly Notices of the Royal Astronomical Society* 382(3), 1050–1072. ISSN: 0035-8711.

Tremmel, M., Quinn, T. R., Ricarte, A., Babul, A., Chadayammuri, U., Natarajan, P., Nagai, D., Pontzen, A., and Volonteri, M. (Dec. 2018). Introducing RomulusC: a cosmological simulation of a galaxy cluster with an unprecedented resolution. *MNRAS* 483(3), 3336–3362. ISSN: 1365-2966.

Umehata, H., Fumagalli, M., Smail, I., Matsuda, Y., Swinbank, A. M., Cantalupo, S., Sykes, C., Ivison, R. J., Steidel, C. C., Shapley, A. E., and al., et (Oct. 2019). Gas filaments of the cosmic web located around active galaxies in a protocluster. *Science* 366(6461), 97–100. ISSN: 1095-9203.

Welker, C., Bland-Hawthorn, J., Sande, J. V. D., Lagos, C., Elahi, P., Obreschkow, D., Bryant, J., Pichon, C., Cortese, L., Richards, S. N., and al., et (Dec. 2019). The SAMI Galaxy Survey: First detection of a transition in spin orientation with respect to cosmic filaments in the stellar kinematics of galaxies. *MNRAS* 491, 2864–2884.

Wetzel, A. R., Tinker, J. L., Conroy, C., and Bosch, F. C. van den (Apr. 2013). Galaxy evolution in groups and clusters: satellite star formation histories and quenching time-scales in a hierarchical Universe. *Monthly Notices of the Royal Astronomical Society* 432(1), 336–358. ISSN: 0035-8711.

Whitaker, K. E., Dokkum, P. G. van, Brammer, G., and Franx, M. (July 2012). THE STAR FORMATION MASS SEQUENCE OUT TO $z = 2.5$. *The Astrophysical Journal* 754(2), L29. ISSN: 2041-8213.

White, S. D. M. and Rees, M. J. (May 1978). Core condensation in heavy halos: a two-stage theory for galaxy formation and clustering. 183, 341–358.

Wilcots, E. (Dec. 2004). SKA observations of the cosmic web. 48(11-12), 1281–1287.

Young, J. and Scoville, N. (1991). Molecular gas in galaxies. *Annual review of astronomy and astrophysics* 29(1), 581–625.

Zel'Dovich, Y. B. (Mar. 1970). Reprint of 1970A&A.....5...84Z. Gravitational instability: an approximate theory for large density perturbations. 500, 13–18.

Zinger, E., Dekel, A., Birnboim, Y., Kravtsov, A., and Nagai, D. (May 2016). The role of penetrating gas streams in setting the dynamical state of galaxy clusters. *Monthly Notices of the Royal Astronomical Society* 461(1), 412–432. ISSN: 1365-2966.

Zinger, E., Dekel, A., Birnboim, Y., Nagai, D., Lau, E., and Kravtsov, A. V. (Jan. 2018). Cold fronts and shocks formed by gas streams in galaxy clusters. *Monthly Notices of the Royal Astronomical Society* 476(1), 56–70. ISSN: 1365-2966.

Zwicky, F. (Jan. 1933). Die Rotverschiebung von extragalaktischen Nebeln. *Helvetica Physica Acta* 6, 110–127.

Zwicky, F. (Oct. 1937). On the Masses of Nebulae and of Clusters of Nebulae. 86, 217.